

Discriminating the HTM and MLRSM models in collider studies via doubly charged Higgs boson pair production and the subsequent leptonic decays

Janusz Gluza,^{a,b} Magdalena Kordiaczyńska,^a Tripurari Srivastava^c

^a*Institute of Physics, University of Silesia, Katowice, Poland*

^b*Faculty of Science, University of Hradec Králové, Czech Republic*

^c*Theoretical Physics Division, Physical Research Laboratory, Ahmedabad-380009, India*

E-mail: janusz.gluza@us.edu.pl, mkordiaczynska@us.edu.pl,
tripurari@prl.res.in

ABSTRACT: We present a case study for the doubly charged Higgs bosons $H^{\pm\pm}$ pair production in e^+e^- and pp colliders with their subsequent decays to four charged leptons. We consider the Higgs Triplet Model (HTM) not restricted by the custodial symmetry and the Minimal Left-Right Symmetric Model (MLRSM). The models include scalar triplets with different complexity of scalar potentials and, due to experimental restrictions, completely different scales of non-standard triplet vacuum expectation values. In both models, a doubly charged Higgs boson $H^{\pm\pm}$ can acquire a mass of hundreds of gigaelectronvolts, which can be probed at HL-LHC, future e^+e^- , and hadron colliders. We take into account a comprehensive set of constraints on the parameters of both models coming from neutrino oscillations, LHC, e^+e^- and low-energy lepton flavour violating data and assume the same mass of $H^{\pm\pm}$. Our finding is that the $H^{\pm\pm}$ pair production in lepton and hadron colliders is comparable in both models, though more pronounced in MLRSM. We show that the decay branching ratios can be different within both models, leading to distinguishable four lepton signals and that the strongest are 4μ events yielded by MLRSM. Typically we find that MLRSM signals are one order of magnitude larger than in HTM. For example, the $pp \rightarrow 4\mu$ MLRSM signal for 1 TeV $H^{\pm\pm}$ mass results in a clearly detectable significance of $S \simeq 11$ for HL-LHC and $S \simeq 290$ for FCC-hh. Finally we provide quantitative predictions for the dilepton invariant mass distributions and lepton separations which help to identify non-standard signals.

Contents

1	Introduction	2
1.1	Discovery of the first Higgs scalar boson at LHC and the Standard Model	2
1.2	Searching for new scalar bosons at future colliders and a choice of tested models	2
2	Doubly charged Higgs bosons and neutrinos in the considered triplet BSM scenarios	4
3	The HTM model and the relevant experimental parameter constraints	7
3.1	Neutrino mixing matrix and mass hierarchies within HTM	11
3.2	The triplet VEV v_Δ and the ρ -parameter	12
3.3	Relation between v_Δ and doubly charged scalar particles parameters in the light of low and high energy experimental limits	12
4	The MLRSM model and relevant experimental constraints on its parameters	14
4.1	Constraints on MLRSM model parameters and the triplet VEV v_R	14
5	Collider signals, the results	16
5.1	The $H^{\pm\pm}$ pair production at e^+e^- and pp colliders	16
5.2	HTM, a choice of benchmark parameters and $H^{\pm\pm}$ decay scenarios	21
5.3	MLRSM, a choice of benchmark parameters and $H_{1,2}^{\pm\pm}$ decay scenarios	25
5.4	The four leptons background in pp and e^+e^- collisions	27
5.5	Final four lepton signals within the HTM and MLRSM models, a comparison	28
6	Conclusions and outlook	32
7	Appendix.	33
7.1	The HTM scalar potential and fields	33
7.2	The MLRSM scalar potential and fields	35
7.3	$H_1^{\pm\pm}$ and $H_2^{\pm\pm}$ couplings with leptons in MLRSM	37
7.4	Supplemental material for phenomenological studies of $H^{\pm\pm}$ scalar particles	39

1 Introduction

1.1 Discovery of the first Higgs scalar boson at LHC and the Standard Model

The spectacular discovery of the chargeless Higgs particle (H^0) at the LHC [1–3] is consistent with the prediction of the Standard Model (SM), confirming the basic concept of the spontaneous symmetry breaking mechanism and elementary particle mass generation. Observed H^0 decays into gauge boson particles W^+W^- and ZZ [4–6] fits beautifully into this picture. Similarly, determination of $t\bar{t}H^0$ couplings in gluon fusion [7–9] and $t\bar{t}H^0$ production [10] confirm Higgs boson role in fermion mass generation. With gathered statistics, we know more and more about this particle, namely its decay rate to $\gamma\gamma$ [11, 12], spin-parity which is dominantly $J^P = 0^+$ [4, 5, 13–15]. Also mass suppressed decay rate to muon pairs when comparing to top pairs is evident [12, 16]. Yet another spectacular success of the LHC physics is a clear discovery that the Higgs boson decays to the third generation of fermions, namely to the pairs of τ leptons and b-quarks. Especially determination of the Yukawa Higgs boson coupling to b-quarks is tricky, as though this channel amounts to about 60% of Higgs boson decays, the QCD b-quark background is overwhelming [17]. The story of the Higgs boson studies continues. Very recently the measurements of the Higgs boson’s properties have reached a new stage in precision through detection of a rare decay mode where the Higgs boson decays into two muons [18, 19]. Aiming at sub-percent precision for Higgs boson decays, quantitative tests of the SM for Higgs boson couplings need further scrutinization in studies at HL-LHC and future Higgs factories. These also include the investigation of the Higgs boson self-coupling [20].

1.2 Searching for new scalar bosons at future colliders and a choice of tested models

Detection of the Standard Model scalar particle does not preclude validity of more elaborated physical scenarios with extended scalar sectors. The simplest extensions beyond the SM doublet scalar multiplet include their copies, like the two Higgs doublet model [21], supersymmetric extensions of the SM [22, 23] or, stepping up in this construction, scenarios with triplet scalar representations either in their supersymmetric [24, 25] or non-supersymmetric versions [26–28]. Here we will consider the latter. There are many possibilities for triplet representations, depending on the hypercharge $Y \equiv 2(Q - T_3)$ [29–32]. We will explore the simplest one which involves doubly charged Higgs fields in the triplet representation with hypercharge $Y = 2$, the Higgs Triplet Model (HTM) [33]. For that, we will not assume any special symmetries or constructions [34, 35], so that v_Δ , the triplet vacuum expectation value (VEV) will be extremely tiny, at the scale of electronvolts which makes experiments more challenging. We will also consider a much more complex model where the Standard Model $SU(2) \times U(1)$ gauge symmetry is extended by an additional $SU(2)$ group, the so-called minimal left-right symmetric model (MLRSM) [28, 36–40]. Thus we consider a setting where both the HTM and the MLRSM models include doubly charged Higgs bosons.

HTM received a considerable amount of attention recently [41–54]. This model when confronted with experimental data, features a strong restriction in which v_Δ is very small, $\mathcal{O}(1)$ (GeV), or below. Here, in particular, we concentrate on the cases where v_Δ is of the order of neutrino masses. Then the triplet Yukawa couplings will be of the $\mathcal{O}(1)$ order and $H^{\pm\pm}$ decays dominantly into the same-sign dilepton channel. In this case, the LHC direct search bound on the doubly charged scalar mass, $m_{H^{\pm\pm}} \gtrsim 850$ GeV [55] applies. At the same time, the constraints from different lepton flavor violating (LFV) processes and non-universality of leptonic couplings start to weigh in. There is thus a direct relationship among the triplet VEV v_Δ , neutrino masses, their mixing and doubly charged Higgs couplings. That is why the production and decays of $H^{\pm\pm}$ scalars at high energies depend substantially on the oscillation data and limits on LFV processes in HTM.

On the other hand, in MLRSM the dominating non-standard effects in phenomenological studies are connected with the right-handed breaking scale v_R which affects the couplings and masses of a wide set of non-standard heavy particles of spin 0,1,1/2 present in the model. Low-energy precision

SM and rare processes, as well as high-energy collider studies, limit the possible values of v_R from below. The scale of relevance for v_R starts from the $\mathcal{O}(1)$ TeV level up [56].

Consequently in both models we have two completely different VEV scales, v_Δ and v_R .

How to discriminate such two distinct models experimentally? Indeed it is not easy as any non-standard effect considered or thought of so far in phenomenological studies in search for BSM models failed to show unambiguous excess rates (reported excesses were vanishing with higher statistic).

One of the most appealing rare process capable of exposing BSM signals involving doubly charged Higgs bosons at high energy colliders would be the $H^{\pm\pm}$ pair production and the subsequent decays to four charged leptons. Here the same charge sign dileptons appear from parent's $H^{\pm\pm}$, $H^{\pm\pm} \rightarrow l^\pm l^\pm$, which is distinguishable from the SM background. On top of that, we compare the $H^{\pm\pm}$ production and decay signals in the two considered BSM models taking into account all relevant experimental limits. In this work we investigate this scenario in detail.

The HTM model which we discuss is the simplest theoretical scenario with the triplet scalar representation, without ad-hoc symmetries put in. On the opposite side of the theoretical complexity stands the MLRSM model. This model poses a broad spectrum of non-standard features: additional gauge group, so other gauge bosons and right-handed currents, heavy neutral leptons, a plethora of Higgs scalars, including two doubly charged Higgs bosons $H_{(1,2)}^{\pm\pm}$. Details on scalar potentials and fields are given in the Appendix. On top of that, as already mentioned, the process of the $H^{\pm\pm}$ pair production at colliders is peculiar because it exhibits a small background. We assume a scenario that the excess signal of four charged leptons $e^+e^-(pp) \rightarrow H^{++}H^{--} \rightarrow 4l$ over the background is identified. In case when no other non-standard signals appear (e.g. connected with right-handed currents), the question is how to find to which non-standard model does the signal belong? In practice, such identification will be not trivial. In our opinion the problem of distinguishing two models based on rare processes where particles with the same masses play a crucial role is an important topic as needless to say such statements are essential for future post-LHC studies. Usually, in phenomenological analysis any specific models are considered. The exception is the effective field theory approach where non-standard interactions and energy scales are probed. However, to say anything about specific models, if positive signals and deviations from the SM signals will be found, comparative studies as given here based on particular models will be crucial. Apart from these general statements, other exciting subtleties can be probed in these studies connected with the neutrino sector. We will come to this topic in a moment.

To get reliable predictions for BSM processes, essential restrictions on the BSM model parameters coming from rare and so far not observed LFV processes must be considered. As even a single unambiguous LFV event detection would be a signal of beyond SM physics, there are many efforts to upgrade or create new experimental setups for that, see e.g. [57, 58]. Present bounds for low energy LFV signals, such as nuclear μ to e conversion will become more stringent through the so-called intensity frontier experiments [59, 60]. The same is true for $(\beta\beta)_{0\nu}$ experiments, see e.g. [61, 62]. In this work, we consider these processes to predict reliable BSM $H^{\pm\pm}$ collider signals.

Concerning high energy colliders, there are presently several options considered internationally for future electron colliders [63], namely, FCC (Future Circular Collider) [64, 65], CLIC (Compact Linear Collider) [66, 67] – both at CERN, the ILC (International Linear Collider¹) [69, 70]. The CEPC (Chinese Electron Positron Collider) [71, 72] in China is of the circular type and similarly to FCC is expected to collide electrons with positrons at 90-365 GeV center of mass energies. The ILC collider could potentially be positioned in Japan, and its centre of mass collision energies would reach 1 TeV while CLIC would cover the energies between 380 GeV and 3 TeV. In the future, extreme energies may become possible in Plasma Wakefield Linear Colliders [73]. In case of FCC-ee, four running stages are considered [64, 74, 75], with focus on Z,W,H and top quark

¹Recently ILC and CLIC unite to advance the global development work for the next-generation linear collider [68].

production. This means that the maximal energy will be not enough to search for direct $H^{\pm\pm}$ pair production signals. What remains is the high luminosity LHC (HL-LHC) [63, 76], and the FCC-hh proton-proton option with center of mass energies of collided protons reaching 100 TeV [77, 78].

A significant part of calculations done in this paper was performed using the MadGraph [79] and Pythia [80, 81] programs. The UFO files were generated using FeynRules [82] and built on our model file, based on the default Standard Model implementation.

2 Doubly charged Higgs bosons and neutrinos in the considered triplet BSM scenarios

Regarding the scalar particle masses, we have constructed a mass spectrum in which $M_{H^{\pm\pm}} = 700$ GeV. Corresponding parameters of scalar potentials in both models are given in Table 1.

HTM	$\mu = 1.7 \times 10^{-7}, \quad \lambda = 0.519, \quad \lambda_1 = 0.519, \quad \lambda_2 = 0, \quad \lambda_3 = -1, \quad \lambda_4 = 0.$ $M_h = 125.3 \text{ GeV}, \quad M_H = 700 \text{ GeV}, \quad M_{H^\pm} = 700 \text{ GeV}, \quad M_{H^{\pm\pm}} = 700 \text{ GeV}.$
MLRSM	$\lambda_1 = 0.129, \quad \rho_1 = 0.0037, \quad \rho_2 = 0.0037, \quad \rho_3 - 2\rho_1 = 0.015, \quad \alpha_3 = 4.0816, \quad 2\lambda_2 - \lambda_3 = 0.$ $M_{H_0^0} = 125.3 \text{ GeV}, \quad M_{H_1^0} = 10 \text{ TeV}, \quad M_{H_2^0} = 600 \text{ GeV}, \quad M_{H_3^0} = 605.4 \text{ GeV},$ $M_{H_1^{\pm\pm}} = 700 \text{ GeV}, \quad M_{H_2^{\pm\pm}} = 700 \text{ GeV}, \quad M_{H_1^\pm} = 654.4 \text{ GeV}, \quad M_{H_2^\pm} = 10\,003.1 \text{ GeV}.$

Table 1: Benchmark points and corresponding potential parameters for HTM and LRSM with $M_{H^{\pm\pm}} = M_{H_{1,2}^{\pm\pm}} = 700$ GeV. The scalar potential parameters, fields and relations for masses are defined in the Appendix, Eq. 7.1 and Eq. 7.18. We identify h and H_0^0 as the SM Higgs boson (H^0).

The mass benchmark points are constructed in order to satisfy several theoretical conditions like potential stability, unitarity and the T-parameter restriction and bounds from $h \rightarrow \gamma\gamma$ [56, 83–87], see also sections 3 and 4.

As we can see in Tab. 1, there are more scalar fields in MLRSM than in HTM. Then any detectable signal connected with a neutral, singly or doubly charged Higgs bosons which are present in MLRSM but are not present in HTM would be in favour of MLRSM. However, we should note that though MLRSM is very rich in particle content and non-standard interactions, despite enormous theoretical and experimental efforts over last several decades, what we get so far are exclusion limits on the parameters of this model. All experimental data considered so far gives no indication for neutral, singly or doubly charged scalars, extra neutral heavy leptons, extra gauge bosons. So, the starting point is actually the same: we do not know if and which BSM model is realized in nature and we are still looking for a first experimental indication towards any non-standard signals in one or another model. As the models' parameters are already severely constrained, we have to consider very rare processes and hence faint signals. We focus on the cleanest BSM colliders signal connected with

doubly charged scalars: their pair production and subsequent decays (correlations between the same-sign leptons in the final state originated from $H^{\pm\pm}$ decays). To leave no stone unturned, we will focus especially on the case in which two doubly charged Higgs bosons in MLRSM have the same masses as otherwise the second scalar $H_2^{\pm\pm}$ connected with right-handed triplet in MLRSM (see Appendix for fields definitions) would help to discriminate between both models in favor of MLRSM. A case with different $H_1^{\pm\pm}$ and $H_2^{\pm\pm}$ masses in e^+e^- CLIC center of mass energies will be shortly discussed in Section 5.5, non-degenerate mass cases for hadron colliders have been discussed already in [88]. For the same masses of $H_1^{\pm\pm}$ and $H_2^{\pm\pm}$, the production rates are higher in MLRSM than in HTM. We will see what is the contribution of $H_2^{\pm\pm}$ against $H_1^{\pm\pm}$ in production processes at lepton and hadron colliders, in case of the same doubly charged boson masses and how these contributions change with center of mass energy. As we will see, there are scenarios with model parameters where the difference of signals in both models can be further enhanced by studying leptonic branching ratios of doubly charged Higgs bosons and kinematic cuts.

Fixing the scalar mass spectrum lets us take a first look at the production processes $e^+e^- \rightarrow H_{(1,2)}^{++} H_{(1,2)}^{--}$ and $pp \rightarrow H_{(1,2)}^{++} H_{(1,2)}^{--}$ for HTM and MLRSM. This will bring us to the discussion of the importance of the neutrino sector. Fig. 1 and Fig. 2 show classes of Feynman diagrams for the $H^{\pm\pm}$ pair production in e^+e^- collisions in both models. There are s-channel diagrams mediated by neutral gauge bosons Z and γ and Higgs bosons, and the t-channel diagram. Due to experimental restrictions discussed in the next two sections, the contributions coming from the s-channel diagrams are comparable to the off-resonance regions, and the resonance regions for the considered center of mass energies and masses lie away from the allowed region of parameters (see Figs. 7, 8). It gives possibility to discuss how the t-channel diagrams in Fig. 1 and Fig. 2 affects the process.

As schematically depicted in the figures the relevant $H^{\pm\pm} - l^\mp - l'^\mp$ vertices come from Yukawa couplings.

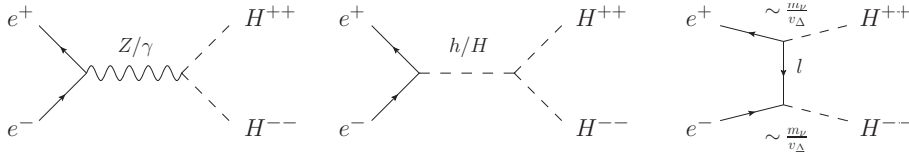


Figure 1: Pair production of doubly charged Higgs bosons $e^+e^- \rightarrow H^{++}H^{--}$ in the HTM model. For the t-channel the couplings depend on neutrino parameters and v_Δ . The exact form of the coupling is given by Eq. (2.3).

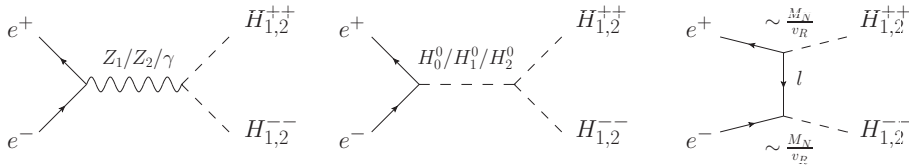


Figure 2: Feynman diagrams at the tree level for pair production of doubly charged Higgs bosons $e^+e^- \rightarrow H^{++}H^{--}$ in the MLRSM model. For the t-channel the couplings depend on the heavy neutrino masses and v_R . The exact form of the coupling is given by Eq. (2.4).

In HTM the Yukawa term (7.5) with neutrino fields generates Majorana masses

$$\mathcal{L}_Y^\Delta \rightarrow \mathcal{L}_\nu^\Delta = \frac{1}{2} \bar{\nu}_\ell \frac{v_\Delta}{\sqrt{2}} \mathcal{Y}_{\ell\ell'} \nu_{\ell'} \equiv \frac{1}{2} \bar{\nu}_\ell (M_\nu)_{\ell\ell'} \nu_{\ell'}. \quad (2.1)$$

This term also contains the $H^{\pm\pm} - l^\mp - l'^\mp$ vertex which leads to lepton flavor violation. We can diagonalize the neutrino mass matrix by U as follows [89]

$$U^\dagger M_\nu U^* = \frac{1}{2} D_\nu = \frac{1}{2} \text{diag}\{m_1, m_2, m_3\}. \quad (2.2)$$

The matrix U relates the mass eigenstates $|\nu_i\rangle$ through a superposition of the flavor states $|\nu_\ell\rangle$: $|\nu_i\rangle = U^T |\nu_\ell\rangle$, so it is directly connected with the PMNS matrix (3.7) and the exact relation between them is $U^* = V_{PMNS}$. Now we can write the Yukawa couplings as a function of the PMNS matrix and the masses of neutrinos. From Eq. (2.2), $\mathcal{Y}_{\ell\ell'}$ can be written in the following form

$$\mathcal{Y}_{\ell\ell'} = \frac{1}{\sqrt{2}v_\Delta} V_{PMNS}^* D_\nu V_{PMNS}^\dagger. \quad (2.3)$$

We discuss the parametrization of V_{PMNS} and the employed range of the oscillation parameters in Section 3.1.

The $\mathcal{Y}_{\ell\ell'}$ coupling depends on v_Δ , neutrino masses and oscillation parameters. From perturbativity, $\mathcal{Y}_{\ell\ell'}^2 \leq 4\pi$. Apart from this restriction, there are stringent limits on $\mathcal{Y}_{\ell\ell'}$ coming from various experimental data discussed in the next section.

In MLRSM the t-channel with the $H^{\pm\pm} - l_i - l_j$ vertex is inversely proportional to v_R . We assume, see section 7.3, vanishing off-diagonal couplings. In this case the vertex is

$$H^{\pm\pm} - l_i - l_j = \frac{\sqrt{2}}{v_R} M_{N_i}. \quad (2.4)$$

As we can see, the coupling Eq. (2.3) in HTM can be enhanced in the case of small values of $v_\Delta \rightarrow 0$. However, it is at the same time proportional to the light neutrino masses. The analogous coupling $H^{\pm\pm} - l_i - l_j$ in MLRSM is related to the heavy neutrino masses and v_R , which are limited by, e.g. bounds on heavy gauge boson masses, see section 4. In the next two sections, we will consider details of the considered models to find the allowed space of the models' physical parameters, including the neutrino sector, which as seen enters the considered processes with very different light and heavy masses.

In general, it would be tempting to find a way to show when the processes of doubly charged Higgs boson pair production decouple from the neutrino masses. Though such relations are a feature of considered models, if the signals which we predict in both models would not fit experimental data, this would be a sign for another mechanism that takes place. For MLRSM and HTM the basic neutrino mass mechanisms are the seesaw type-I and type-II, respectively.

The $H^{\pm\pm}$ pair can be produced in the proton-proton collider via photon, Z boson and neutral scalar particles in the s-channel, see Fig. 3. As will be discussed in section 5.1, due to existing experimental constraints, also here the production process is very similar in both models. What will bring the difference are doubly charged Higgs boson decays which lead to the four charged lepton final signals. To discuss it properly, in the next two sections we will present relevant experimental constraints on the models' parameters.

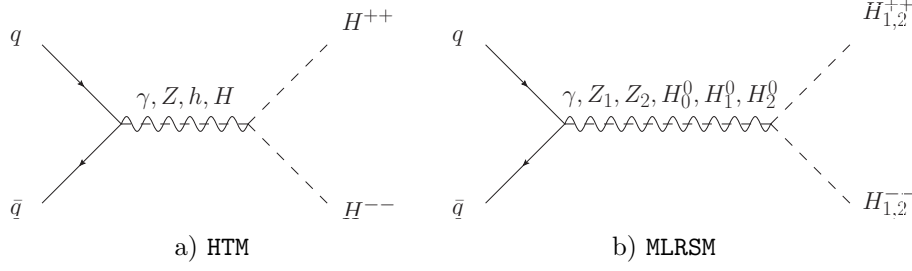


Figure 3: Feynman diagrams for the doubly charged scalar particles' pair production in proton-proton colliders within (a) HTM and (b) MLRSM models.

3 The HTM model and the relevant experimental parameter constraints

The Yukawa term (7.5) includes the $H^\pm - l - \nu$ and considered in the last section $H^{\pm\pm} - l - l$ vertices. They can contribute to several LFV processes like radiative decay of charged leptons $l_i \rightarrow l_j \gamma$, three body decay of charged leptons $l_i \rightarrow l_j l_k l_l$, μ -to- e conversion in nuclei $\mu N \rightarrow e N^*$. We show the contributing diagrams for HTM in Fig. 4(a)-(e). In Fig. 4(f) we include the muonium-antimuonium conversion $\mu^- e^+ \rightarrow \mu^+ e^-$. Corresponding limits on the $H^{\pm\pm}$ parameters are gathered in Tab. 2. Tab. 3 gathers relevant SM processes: Møller scattering $e^- e^- \rightarrow e^- e^-$, Bhabha scattering $e^+ e^- \rightarrow e^+ e^-$, the anomalous magnetic moment of the muon $(g-2)_\mu$ from which also useful limits on the $H^{\pm\pm}$ parameters are derived. These processes have been discussed in the context of HTM in many works [33, 90–96]). The branching ratios (BR) in Table 2 depend on the charged scalar masses and the Yukawa couplings $\mathcal{Y}_{\ell\ell'}$, defining the allowed space of mass and coupling parameters for charged scalars.

The radiative decays $l_i \rightarrow l_j \gamma$ and the μ -to- e conversion process mediated by doubly and singly charged scalar bosons originate from the following Lagrangian [97]

$$\mathcal{L} \subset -\frac{4eG_F}{\sqrt{2}} m_l A_R(q^2) \bar{l}' \sigma^{\nu\mu} P_R l F_{\mu\nu} - \frac{e^2 G_F}{\sqrt{2}} A_L(q^2) \bar{l}' \gamma^\nu P_L l \sum_{q=u,d} q_Q \bar{Q} \gamma_\nu Q + h.c. \quad (3.1)$$

Branching ratios depend on the form factors A_L and A_R , which actual form depends on Higgs scalar contributions to the considered processes. For the doubly charged scalar there are four relevant diagrams as shown in Fig. 4 (a) and (b). The amplitude for $H^{\pm\pm}$ for the first two diagrams Fig. 4 (a), at the leading order of the doubly charged scalar mass is

$$\begin{aligned} \mathcal{M}_{M_{H^{\pm\pm}}}^I \subset & -\frac{(\mathcal{Y}^*)_{ei}(\mathcal{Y})_{\mu i} \gamma_\mu P_L}{128\pi^2} \left(\frac{2}{\epsilon} + \log \frac{4\pi\mu^2}{M_{H^{\pm\pm}}^2} \right) \\ & + \frac{(\mathcal{Y}^*)_{ei}(\mathcal{Y})_{\mu i} \gamma_\mu P_L}{64\pi^2} \left(-\frac{1}{4} - \frac{r}{36} + \frac{s_i}{2} + \frac{r}{6} f(r, s_i) \right) \\ & + \frac{(\mathcal{Y}^*)_{ei}(\mathcal{Y})_{\mu i} P_L}{384\pi^2 M_{H^{\pm\pm}}^2} \left[\left(-\frac{5}{6} + f(r, s_i) \right) (\not{p}_1 \gamma_\mu \not{p}_1 + \not{p}_2 \gamma_\mu \not{p}_2) \right. \\ & \left. + \left(\frac{1}{6} + f(r, s_i) \right) (\not{p}_1 \gamma_\mu \not{p}_2) + \left(\frac{17}{6} - f(r, s_i) \right) (\not{p}_2 \gamma_\mu \not{p}_1) \right] \\ & - \frac{(\mathcal{Y}^*)_{ei}(\mathcal{Y})_{\mu i} P_R}{1152\pi^2 M_{H^{\pm\pm}}^2} \left(\not{p}_1 p_{1\mu} + 5\not{p}_1 p_{2\mu} + 5\not{p}_2 p_{1\mu} + \not{p}_2 p_{2\mu} \right), \end{aligned} \quad (3.2)$$

where $f(r, s_i) = \frac{4s_i}{r} + \log(s_i) + \left(1 - \frac{2s_i}{r} \right) \sqrt{1 + \frac{4s_i}{r}} \log \left(\frac{\sqrt{r} + \sqrt{r+4s_i}}{\sqrt{r} - \sqrt{r+4s_i}} \right)$, $r = \frac{-q^2}{m_{H^{\pm\pm}}^2}$, $s_i = \frac{m_i^2}{m_{H^{\pm\pm}}^2}$. μ is a mass parameter introduced in dimensional regularization, $\epsilon = 4 - D$ and D is dimension.

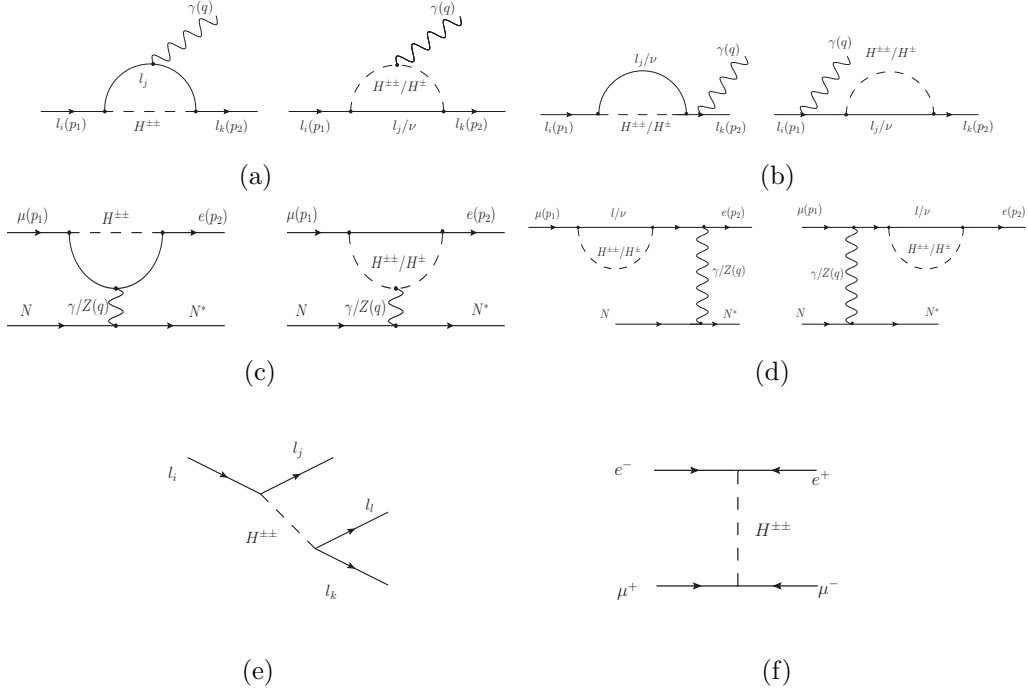


Figure 4: Feynman diagrams representing the contributions to various Lepton flavour violating processes mediated by charged scalar in the HTM. (a) and (b) are representing the radiative decay $l_i \rightarrow l_j \gamma$, (c) and (d) corresponds to μ to e conversion. Three body decay of lepton contribution is shown by diagram (e) and diagram (f) represents muonium-antimuonium conversion.

The contribution from other two diagrams Fig. 4(b) mediated by the doubly charged scalar boson is

$$\begin{aligned}
 \mathcal{M}_{M_{H^{\pm\pm}}}^{II} \subset & \frac{(\mathcal{Y}^*)_{ei}(\mathcal{Y})_{\mu i} \gamma_\mu P_L}{128\pi^2} \left(\frac{2}{\epsilon} + \log \frac{4\pi\mu^2}{M_{H^{\pm\pm}}^2} \right) \\
 & + \frac{(\mathcal{Y}^*)_{ei}(\mathcal{Y})_{\mu i} \gamma_\mu P_L}{128\pi^2} \left(\frac{1}{2} + \frac{s_e + s_\mu}{3} - s_i \right) \\
 & + \frac{(\mathcal{Y}^*)_{ei}(\mathcal{Y})_{\mu i} P_R}{384\pi^2 M_{H^{\pm\pm}}^2} (\not{p}_2 \gamma_\mu \not{p}_1). \tag{3.3}
 \end{aligned}$$

By adding (3.2) and (3.3) we can see that the final contribution is finite and after doing some algebra the contribution of the doubly charged scalar form factors can be written in a compact way

$$\begin{aligned}
 \mathcal{M}_{M_{H^{\pm\pm}}} \subset & -\frac{(\mathcal{Y}^*)_{ei}(\mathcal{Y})_{\mu i}}{192\pi^2 M_{H^{\pm\pm}}^2} f(r, s_i) (q^2 \gamma_\mu - q_\mu q_\nu \gamma^\nu) P_L - \\
 & \frac{(\mathcal{Y}^*)_{ei}(\mathcal{Y})_{\mu i}}{192\pi^2 M_{H^{\pm\pm}}^2} (m_e P_L i\sigma_{\mu\nu} q^\nu + m_\mu P_R i\sigma_{\mu\nu} q^\nu). \tag{3.4}
 \end{aligned}$$

In a similar way one can compute the contributions from diagrams mediated by singly charged scalar bosons and the total amplitude in HTM can be written as

$$\begin{aligned}
 \mathcal{M}_{HTM} \subset & -\frac{(\mathcal{Y}^*)_{ei}(\mathcal{Y})_{\mu i}}{192\pi^2} \left(\frac{1}{12M_{H^\pm}^2} + \frac{f(r, s_i)}{M_{H^{\pm\pm}}^2} \right) (q^2 \gamma_\mu - q_\mu q_\nu \gamma^\nu) P_L - \\
 & \frac{(\mathcal{Y}^*)_{ei}(\mathcal{Y})_{\mu i}}{192\pi^2} \left(\frac{1}{8M_{H^\pm}^2} + \frac{1}{M_{H^{\pm\pm}}^2} \right) (m_e P_L i\sigma_{\mu\nu} q^\nu + m_\mu P_R i\sigma_{\mu\nu} q^\nu). \tag{3.5}
 \end{aligned}$$

Matching Eq. (3.5) to Eq. (3.1), we can extract the form of the $A_L(A_R)$ form factors and compute the analytic formulas for the radiative decays and μ -to- e conversion processes. The final analytic formula for considered LFV processes are gathered in the Appendix.

If the massive neutrinos couple to leptons and are of Majorana type, the lepton number can be violated by two units, $\Delta L = 2$. This leads to the neutrinoless double beta decay $\beta\beta 0\nu$ process [98, 99] and as it has not been observed so far, it puts a constraint on the model parameters. This process has been analyzed within HTM in [100], the non-standard contribution is negligibly small.

Above we have discussed LFV processes which have not been observed so far, leading to stringent bounds on BSM physics and parameters. Useful information about limits on the BSM physics can be also obtained by exploring observed SM processes and analysing experimental results and SM predictions. One of such finite processes is the Bhabha scattering present in electron-positron collisions. It serves as a calibration method for colliders as it is a QED dominated t-channel process, see Section II and Figs. 1-2 in [101]. The LEP data [102] sets a lower limit on $H^{\pm\pm}$, namely $\mathcal{Y}_{\ell\ell'} \geq 10^{-7}$ (to ensure $H^{\pm\pm}$ decay before entering the detector).

Another SM experiment which seems to provide a promising signature of the BSM physics is the observed excess in the anomalous magnetic moment of the muon $(g-2)_\mu$. There is a lasting discrepancy of more than 3σ in the measurement of $(g-2)_\mu$ with the corresponding SM value [103]. At present the deviation, as given by PDG, is [104]:

$$\Delta a_{(g-2)_\mu} \equiv a_\mu^{\text{exp}} - a_\mu^{\text{SM}} = 268(63)(43) \times 10^{-11}. \quad (3.6)$$

The experimental limits for Bhabha, Møller and $(g-2)_\mu$ SM processes are collected in Tab. 3. Charged scalars can contribute to the $(g-2)_\mu$ at the one-loop level. There are many studies of BSM contribution to $(g-2)_\mu$ in the literature. The contribution from a doubly charged Higgs boson to $(g-2)_\mu$ is discussed in [105] and in the context of HTM in [91]. The diagrams mediated by singly and doubly charged scalars contributions to $(g-2)_\mu$ are given by Fig. 4 (a) and (b) where both l_i, l_j are μ (muons). Contributions of singly and doubly charged scalar bosons to $(g-2)_\mu$ amounts a negative number [57] and $(g-2)_\mu$ anomaly is hard to explain by $H^{\pm\pm}$. However, it is worth mentioning that the observed anomaly is an open problem as still some discrepancies among different low-energy experiments exist [103].

	Process	Present limits	Future limits
LFV processes	$\text{BR}(\mu \rightarrow e\gamma)$	4.2×10^{-13} [106]	6.0×10^{-14} [107]
	$\text{BR}(\tau \rightarrow e\gamma)$	3.3×10^{-8} [108]	1.0×10^{-8} [109]
	$\text{BR}(\tau \rightarrow \mu\gamma)$	4.4×10^{-8} [108]	3.0×10^{-9} [110]
	$\text{BR}(\mu \rightarrow eee)$	1.0×10^{-12} [111]	$\sim 10^{-16}$ [112]
	$\text{BR}(\tau \rightarrow eee)$	2.7×10^{-8} [113]	5.0×10^{-10} [109]
	$\text{BR}(\tau \rightarrow \mu\mu\mu)$	2.1×10^{-8} [113]	4.0×10^{-10} [109]
	$\text{BR}(\tau^- \rightarrow \mu^+ e^- \mu^-)$	2.7×10^{-8} [113]	5.0×10^{-10} [109]
	$\text{BR}(\tau^- \rightarrow \mu^+ e^- e^-)$	1.5×10^{-8} [113]	3.0×10^{-10} [109]
	$\text{BR}(\tau^- \rightarrow e^+ \mu^- \mu^-)$	1.7×10^{-8} [113]	3.0×10^{-10} [109]
	$\text{BR}(\tau^- \rightarrow e^+ e^- \mu^-)$	1.8×10^{-8} [113]	3.0×10^{-10} [109]
	$\text{R}(\mu N \rightarrow e N^*)$	7.0×10^{-13} (for Au)	2.87×10^{-17} (for Al)
	$\mu^+ e^- \rightarrow \mu^- e^+$	$\sqrt{\mathcal{Y}_{ee} \cdot \mathcal{Y}_{\mu\mu}} < \frac{0.44 \cdot M_{H^{\pm\pm}}}{10^3 \text{ GeV}}$ [116]	

Table 2: Current and future limits on the processes with doubly charged scalar contributions, LFV processes (90% CL).

	Process	Present limits
SM processes		$ \mathcal{Y}_{ee} \leq \frac{\sqrt{4\pi} M_{H^{\pm\pm}}}{8.7 \times 10^3 \text{ GeV}}$ [117]
	$e^+ e^- \rightarrow l^+ l^-$ (LEP)	$ \mathcal{Y}_{e\mu} \leq \frac{1}{\sqrt{2}} \frac{\sqrt{4\pi} M_{H^{\pm\pm}}}{12.2 \times 10^3 \text{ GeV}}$ [117]
		$ \mathcal{Y}_{e\tau} \leq \frac{1}{\sqrt{2}} \frac{\sqrt{4\pi} M_{H^{\pm\pm}}}{9.1 \times 10^3 \text{ GeV}}$ [117]
	$e^- e^- \rightarrow e^- e^-$ (MØLLER)	$ \mathcal{Y}_{ee} \leq \frac{M_{H^{\pm\pm}}}{3.7 \times 10^3 \text{ GeV}}$ [118]
	$(g-2)_\mu$	$\Delta a_\mu = (29.3 \pm 9.0) \times 10^{-10}$ [119]

Table 3: Current limits on the Standard Model processes with doubly charged scalar contributions (95% CL).

3.1 Neutrino mixing matrix and mass hierarchies within HTM

From Eq. (2.3) we can see that the $H^{\pm\pm} - l - l'$ couplings depend on the neutrino oscillation parameters, neutrinos hierarchy and the lightest neutrino mass. Details of studies for the HTM model are thus very sensitive to the neutrino oscillation data, as discussed already in [33] and [54, 86, 120]. In our analysis the following, standard parametrization of the V_{PMNS} matrix is used:

$$V_{\text{PMNS}} = \begin{bmatrix} c_{12}c_{13}e^{i\alpha_1} & s_{12}c_{13}e^{i\alpha_2} & s_{13}e^{-i\delta_{CP}} \\ (-s_{12}c_{23} - c_{12}s_{23}s_{13}e^{i\delta_{CP}})e^{i\alpha_1} & (c_{12}c_{23} - s_{12}s_{23}s_{13}e^{i\delta_{CP}})e^{i\alpha_2} & s_{23}c_{13} \\ (s_{12}s_{23} - c_{12}c_{23}s_{13}e^{i\delta_{CP}})e^{i\alpha_1} & (-c_{12}s_{23} - s_{12}c_{23}s_{13}e^{i\delta_{CP}})e^{i\alpha_2} & c_{23}c_{13} \end{bmatrix}, \quad (3.7)$$

where s_{ij} and c_{ij} denotes $\sin(\theta_{ij})$ and $\cos(\theta_{ij})$, respectively. Tab. 4 shows global neutrino fits at the 2σ C.L. for neutrino parameters which are used in present analysis for two mass orderings, defined as:

$$\begin{aligned} \text{Normal mass hierarchy:} \quad & \text{Inverted mass hierarchy:} \\ m_{\nu_1} = m_{\nu_0}, \quad & m_{\nu_1} = \sqrt{m_{\nu_0}^2 - \Delta m_{21}^2 - \Delta m_{32}^2}, \\ m_{\nu_2} = \sqrt{m_{\nu_0}^2 + \Delta m_{21}^2}, \quad & m_{\nu_2} = \sqrt{m_{\nu_0}^2 - \Delta m_{32}^2}, \\ m_{\nu_3} = \sqrt{m_{\nu_0}^2 + \Delta m_{31}^2}, \quad & m_{\nu_3} = m_{\nu_0}, \end{aligned} \quad (3.8)$$

where $\Delta m_{ij}^2 = m_i^2 - m_j^2$.

	Normal hierarchy (NH)				Inverted hierarchy (IH)			
	Best fit (bf):	σ	bf $\pm 1\sigma$	bf $\pm 2\sigma$	Best fit (bf):	σ	bf $\pm 1\sigma$	bf $\pm 2\sigma$
$\sin^2 \theta_{12}$	0.310	+0.013 -0.012	0.298 ÷ 0.323	0.286 ÷ 0.336	0.310	+0.013 -0.012	0.298 ÷ 0.323	0.286 ÷ 0.336
$\sin^2 \theta_{23}$	0.558	+0.020 -0.033	0.525 ÷ 0.578	0.492 ÷ 0.598	0.563	+0.019 -0.026	0.537 ÷ 0.582	0.511 ÷ 0.601
$\sin^2 \theta_{13}$	0.02241	+0.00066 -0.00065	0.02176 ÷ 0.02307	0.02111 ÷ 0.02373	0.02261	+0.00067 -0.00064	0.02197 ÷ 0.02328	0.02133 ÷ 0.02395
$\delta_{CP} [^\circ]$	222	+38 -28	194 ÷ 260	166 ÷ 298	285	+24 -26	259 ÷ 309	233 ÷ 333
$\frac{\Delta m_{21}^2}{10^{-5} \text{ eV}^2}$	7.39	+0.21 -0.20	7.19 ÷ 7.60	6.99 ÷ 7.81	7.39	+0.21 -0.20	7.19 ÷ 7.60	6.99 ÷ 7.81
$\frac{\Delta m_{3l}^2}{10^{-3} \text{ eV}^2}$	+2.523	+0.032 -0.030	2.463 ÷ 2.527	2.463 ÷ 2.587	-2.509	+0.032 -0.030	-2.539 ÷ -2.477	-2.569 ÷ -2.445

Table 4: Neutrino oscillation data, notations as in [121]. $\Delta m_{ij}^2 = m_i^2 - m_j^2$. Depending on the hierarchy, for atmospheric neutrino oscillations either $\Delta m_{3l}^2 = \Delta m_{31}^2 > 0$ (NH) or $\Delta m_{3l}^2 = \Delta m_{32}^2 < 0$ (IH).

Concerning the Dirac CP-phase δ_{CP} , the global fits indicate preference for its non-zero values. Recent T2K results confirm this tendency and considered by us 2σ range of the Dirac phase covers well the best fit values given in [122]. In analysis we are choosing δ_{CP} data as given in Tab.4. There is no direct limit on the Majorana phases α_1, α_2 . However, in some studies there are predictions using the neutrinoless double beta decay, e.g., see [123]. There is no bound on the individual masses of neutrinos from the oscillation data. Therefore, the lightest neutrino mass m_{ν_0} is a free parameter and other two masses are determined through (3.8). Also, there are limits on the sum of three neutrino masses from different experiments: from the tritium decay [124] or neutrinoless double beta decay [125], the sharpest limit comes from astrophysics and cosmology [126]

$$\Sigma \equiv \sum_{i=1}^3 m_{\nu_i} \leq 0.23 \text{ eV}. \quad (3.9)$$

These limits set the upper bound on the lightest neutrino mass [127, 128], present experimental data gives

$$m_{\nu_0} = \begin{cases} 0.071 \text{ eV, NH,} \\ 0.066 \text{ eV, IH.} \end{cases} \quad (3.10)$$

3.2 The triplet VEV v_Δ and the ρ -parameter

As we mentioned in the introduction, the additional scalar triplet contributes to the ρ parameter. It can be defined either through a relation among massive SM gauge bosons Z and W and Weinberg mixing angle or relations among gauge couplings [129]. In HTM, at the tree level, ρ can be written as [130]:

$$\rho = \frac{1 + 2\frac{v_\Delta^2}{v_\Phi^2}}{1 + 4\frac{v_\Delta^2}{v_\Phi^2}}. \quad (3.11)$$

The experimental limit on the ρ parameter [131]:

$$\rho^{exp} = 1.00037 \pm 0.00023, \quad (3.12)$$

put the upper bound on the triplet VEV v_Δ .

Taking $\sqrt{v_\Phi^2 + 2v_\Delta^2} = v = (\sqrt{2}G_F)^{-\frac{1}{2}}$ [132, 133] where G_F is Fermi coupling constant $1.1663787(6) \times 10^{-5} \text{ GeV}^{-2}$ [134], we get

$$v_\Delta \leq 1.7 \text{ GeV}, \quad (3.13)$$

for ρ^{exp} , within 2σ deviations. Let us note that the limit on v_Δ can not be obtained for ρ^{exp} within 2σ deviation. It is connected with the fact that relation (3.12) has sense only for $\rho^{exp} \leq 1$, otherwise v_Δ comes out to be a complex number. We will see in the following section that other low experimental data are more important, lowering down the scale of v_Δ in an unambiguous way to the (sub)electronvolt level.

3.3 Relation between v_Δ and doubly charged scalar particles parameters in the light of low and high energy experimental limits

In this section, we analyze bounds on the triplet VEV v_Δ from low and high energy experiments discussed earlier (see Tables 2 and 3). Fig. 5 shows excluded regions in the plane of v_Δ and $M_{H^{\pm\pm}}$ parameters' space based on current limits on branching ratios (for both NH and IH scenarios) for

various LFV processes and $(g-2)_\mu$. The analytic formulas for the relevant quantities are collected in the Appendix. In analysis we consider 2σ range of neutrino oscillation parameters, Tab. 4, Majorana phases α_1 and α_2 are varied in the full range $(0, 2\pi)$. We vary lightest neutrino mass m_{ν_0} keeping the Σ (sum of neutrino masses) limit (3.9) for both inverted and normal hierarchies. We assume degenerate mass for charged scalar bosons, $M_{H^{\pm\pm}} = M_{H^\pm}$, and vary them from ~ 500 GeV to 1000 GeV ($M_{H^{\pm\pm}} \lesssim 470$ is already excluded by the LHC, see section 5 and a discussion around Tab. 9). The shaded regions in Fig. 5 are excluded from LFV and muon $(g-2)_\mu$ limits.

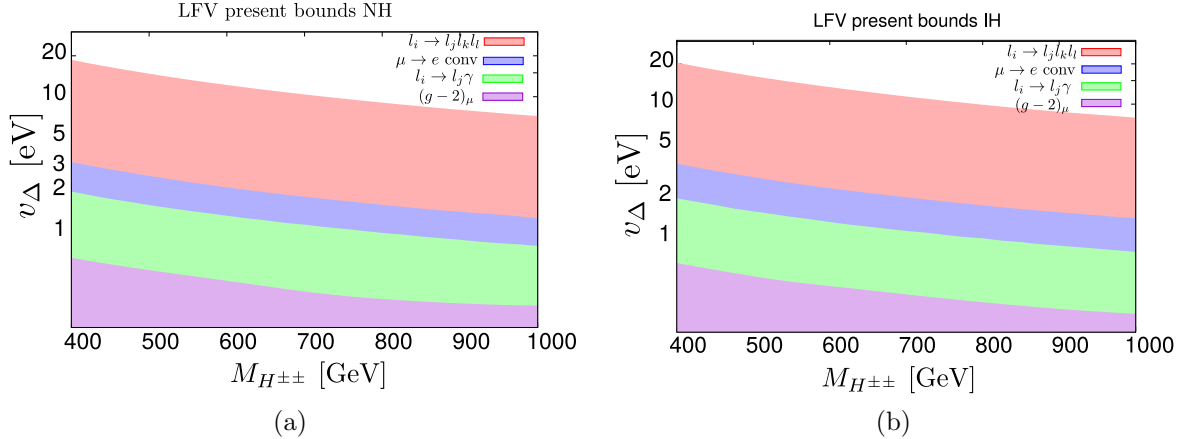


Figure 5: Plots for v_Δ vs $m_{H^{\pm\pm}}$ using normal and inverted hierarchy data. Shaded regions correspond to the exclusion limits coming from LFV bounds for current data and future sensitivity expectations. The neutrino oscillation data are taken in the 2σ range. In general, precision of future experiments (see Tab. 2) will allow to get one order of magnitude better limits on v_Δ .

We use different colors to show the exclusion from individual LFV processes: radiative decay of leptons (green), three body decay of leptons (red), μ -to- e conversion (blue), and $(g-2)_\mu$ (violet). We can see that the most stringent limit is due to three body decays $l_i \rightarrow l_j l_k l_l$ specifically the $\mu \rightarrow eee$ process. We do not find any significant difference between two neutrino mass hierarchy scenarios, but for low neutrino masses the radiative decay $\mu \rightarrow e\gamma$ starts to play an important role in normal hierarchy case (see Tab. 5). Bounds coming from scattering processes or muonium to antimuonium conversion are at least one order of magnitude smaller than those obtain through $(g-2)_\mu$ calculation and are not included in the above plots.

In Table 5, we collect the lower limits of v_Δ in eV for different values of Majorana phases and lightest neutrino mass assuming $m_{H^{\pm\pm}} = 700$ GeV. The process which put the strongest limit is written below the numerical values. For our further analysis and the HTM benchmark point we take $v_\Delta = 15$ eV.

		NH			IH		
α_1	α_2	$m_{\nu_0} = 0$	$m_{\nu_0} = 0.01$	$m_{\nu_0} = 0.071$	$m_{\nu_0} = 0$	$m_{\nu_0} = 0.01$	$m_{\nu_0} = 0.066$
0	0	1.04 $\mu \rightarrow e\gamma$	1.60 $\mu \rightarrow eee$	6.45 $\mu \rightarrow eee$	3.36 $\mu \rightarrow eee$	3.74 $\mu \rightarrow eee$	7.47 $\mu \rightarrow eee$
0	$\frac{\pi}{2}$	1.04 $\mu \rightarrow e\gamma$	1.15 $\mu \rightarrow eee$	7.48 $\mu \rightarrow eee$	4.92 $\mu \rightarrow eee$	4.99 $\mu \rightarrow eee$	8.09 $\mu \rightarrow eee$
$\frac{\pi}{2}$	0	1.04 $\mu \rightarrow e\gamma$	1.04 $\mu \rightarrow e\gamma$	6.68 $\mu \rightarrow eee$	4.92 $\mu \rightarrow eee$	5.06 $\mu \rightarrow eee$	8.56 $\mu \rightarrow eee$
$\frac{\pi}{2}$	$\frac{\pi}{2}$	1.04 $\mu \rightarrow e\gamma$	1.71 $\mu \rightarrow eee$	5.61 $\mu \rightarrow eee$	3.36 $\mu \rightarrow eee$	3.09 $\mu \rightarrow eee$	3.15 $\mu \rightarrow eee$
Oscillations $\pm 2\sigma$		0.93 ÷ 10.31			1.07 ÷ 11.38		

Table 5: Lower bounds on the triplet vacuum expectation value v_Δ (in eV) for different values of Majorana phases and doubly charged scalar mass $M_{H^{\pm\pm}} = 700$ GeV. The most strict limit is coming from the LFV processes named under the numerical value. As we can see, the triplet VEV v_Δ is mainly bounded by experimental limits on $\mu \rightarrow eee$ and $\mu \rightarrow e\gamma$ decays. First four rows present results for best fit of neutrino oscillation data. The last row shows range of the lowest possible v_Δ for oscillation parameters within $\pm 2\sigma$ range and Majorana phases within the entire 2π angle. All values in the table are in eV.

4 The MLRSM model and relevant experimental constraints on its parameters

We consider a left-right symmetric model based on the $SU(2)_L \otimes SU(2)_R \otimes U(1)_{B-L}$ gauge group [28, 36–38, 40] in its most restricted form, so-called Minimal Left-Right Symmetric Model (MLRSM) which contains a bidoublet Φ and two (left and right) triplets $\Delta_{L,R}$ [29, 38, 39, 88] see the Appendix for details.

4.1 Constraints on MLRSM model parameters and the triplet VEV v_R

The heavy sector of the model is triggered by VEV v_R connected with the Higgs triplet Δ_R . All new gauge and scalar bosons are proportional to v_R , and $v_R \gg \kappa$, where κ is a VEV related to the scale of the SM spontaneous symmetry breaking and to the SM gauge bosons W_1, Z_1 , $\kappa \simeq 246$ GeV, see Eq. (7.17).

Using the relation between the heavy charged gauge boson mass and the $SU(2)_R$ triplet VEV v_R

$$M_{W_2}^2 \simeq \frac{g^2 v_R^2}{2} \quad \Rightarrow \quad M_{W_2} \simeq 0.47 v_R, \quad (4.1)$$

we can find the parameter space for v_R and heavy neutrino masses. In the last few years the LHC has constrained the possible v_R scale very much by exploiting different channels where W_2 plays a crucial role, e.g., W_2 decays to two jets [135], two jets and two leptons [136] and top-bottom quarks [137]. Altogether, the following bounds on M_{W_2} have been obtained: (i) ATLAS - 3.6 TeV (2017) [135]; 4.8 TeV (e -channel), 5 TeV (μ -channel) for $M_N \in [0.4, 0.5]$ TeV (2019) [138]; (ii) CMS - 4.4 TeV (2018) [136], assuming that $SU(2)_R$ gauge coupling g_L equals the $SU(2)_L$ coupling g_R . These bounds can be relaxed without such an assumption [139–142]. The CMS experimental data based on the $pp \rightarrow lljj$ process are presented as the $M_{W_2} - M_N$ exclusion plots, see Fig. 6 in [136] and Fig. 7 in [143]. For convenience we repeat them here in Fig. 6. We use these data,

and analogous data from the ATLAS collaboration [144], leading to restrictions on the t-channel in Fig. 8 and final signals presented in Section 5.5.

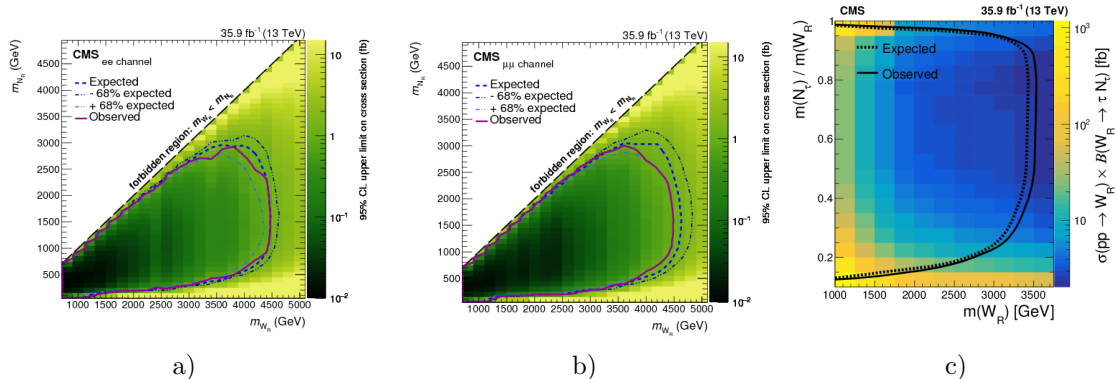


Figure 6: Upper limit on the $pp \rightarrow lljj$ cross section for different $M_{W_R} \equiv M_{W_2}$ and $M_{N_R} \equiv M_N$ mass hypotheses, for the electron (a), muon (b) and taon (c) channels. The thin-dotted (blue) curves in the Fig. a) and b) indicate the region in (M_{W_2}, M_{N_i}) parameter space that is expected to be excluded at 68% CL [136, 143].

As assumed in Fig. 6 we take $M_{W_2} \geq M_N$ and a correlation between the masses which are proportional to v_R [56, 145]. By passing, let us note that most of the experimental LHC analyses are based on simplified scenarios where heavy neutrinos are mass degenerate with diagonal mixings and where CP-violating effects are not taken into account. However, CP-parities of neutrinos can be different leading to destructive interference effects, relaxing limits on the v_R scale, see [146–148].

A simultaneous fit to the SM low energy charged and neutral currents set a rather weak bound on M_{W_2} , so v_R , namely $M_{W_2} > 715$ GeV [104, 146]. However, there are additional restrictions for model’s parameters coming from radiative corrections. As far as one loop corrections are concerned and additional precision constraints on MLRSM parameters, there are very few studies based on LR models, i.e., [39, 129, 146, 149] (MLRSM model), the other papers are: [150, 151] (limits on W_2 mass coming from the $K_L - K_S$ process (finite box diagrams, renormalization not required)), [152] (LEP physics), [153–157] (process $b \rightarrow s\gamma$). Some interesting results are discussed also in papers [158, 159] where the problem of decoupling of heavy scalar particles in low energy processes has been discussed. In [160] it has been shown that low-energy radiative corrections shrink non-standard parameters to very small regions, due to correlations among gauge bosons, scalars and heavy neutrino masses, though still there is a freedom connected among others with unknown scale v_R . We assume v_R and windows of possible masses of heavy MLRSM particles allowed by low energy analysis [160–164].

Apart from experimental limits, due to tree-unitarity and flavor changing neutral currents (FCNC) constraints, the scalar potential parameter α_3 in Eq. (7.18) is restricted and masses of neutral Higgs bosons H_0^0, A^0 should be greater than 10 TeV. The lowest limit on v_R scale is $1.3 \div 6.5$ TeV [56], depending on the mass scale of FCNC Higgs bosons [165]. Such a relatively low (TeV) scale of the heavy sector is theoretically possible, even if gauge unification (GUT) is demanded, for a discussion, see [166] and [167].

5 Collider signals, the results

5.1 The $H^{\pm\pm}$ pair production at e^+e^- and pp colliders

As discussed in previous sections, we assume $M_{H_{(1,2)}^{\pm\pm}} = 700$ GeV. This value will be further justified when the $H^{\pm\pm}$ decay branching ratios are discussed in next sections. Therefore, for substantial $H^{\pm\pm}$ pair production in e^+e^- collisions, we need the centre mass energy \sqrt{s} above 1 TeV. As discussed in Introduction such energies for e^+e^- colliders are planned presently only at CLIC. Numerical results for $\sqrt{s} = 1.5$ TeV are gathered in Fig. 7 and Fig. 8 for HTM and MLRSM, respectively.

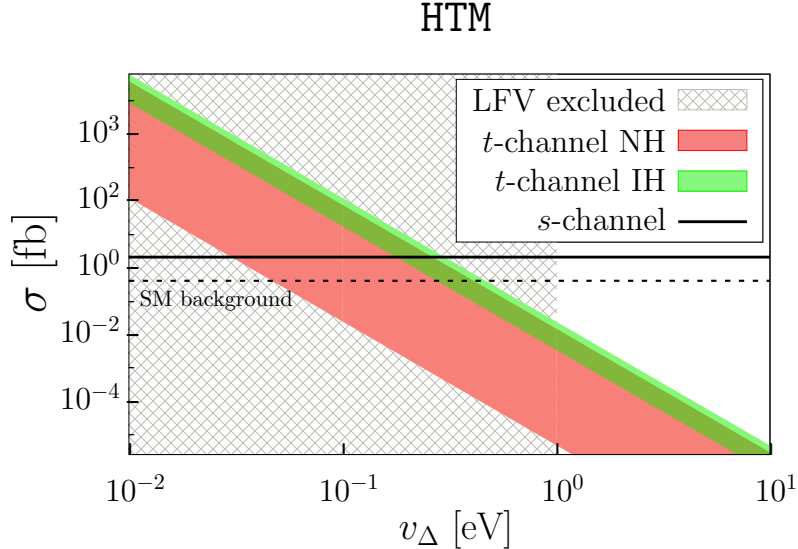


Figure 7: Doubly charged Higgs boson pair production $e^+e^- \rightarrow H^{++}H^{--}$ for $M_{H^{\pm\pm}} = 700$ GeV and CM energy 1.5 TeV in the HTM model. The crossed area is excluded by the low energy data (Tab. 5). We took the neutrino oscillation parameters within the $\pm 2\sigma$ range (Tab. 4), that is why the t -channel is smeared. With a dashed line, we have marked the SM background for four leptons production (electrons and muons) which is $\sigma = 0.415$ fb, see section 5.4.

A contribution from scalar particles in Fig. 1 and Fig. 2 (middle diagrams) are negligible in comparison to the diagrams with the intermediate photon and Z bosons, see Tab. 7. Within HTM the contribution from the heavy neutral scalar H^0 in the s -channel is negligible as both $l-l-H^0$ and $H^{++}-H^{--}-H^0$ vertices are proportional to $\sin \alpha$, see Eq. (7.9), which is very small [168]. Also, the contribution from the Standard Model Higgs boson in the s -channel is small, a few orders of magnitude lower than the contribution from the gauge bosons, because of small Yukawa $e^+ - e^- - h$ coupling and heavy boson mass in the propagator. We have a similar situation in MLRSM. Even though there are some additional possible intermediating particles in the s channel (scalars and the Z_2 gauge boson, see Fig. 2), they are heavy, and the couplings are small. Large Higgs boson masses in the propagators are proportional to v_R (see the Appendix). We assume that masses of both $H_1^{\pm\pm}$ and $H_2^{\pm\pm}$ are equal. H_0^3 does not contribute to the process, because the $H_0^3 - H_{1,2}^{\pm\pm} - H_{1,2}^{\pm\pm}$ vertex is proportional to the left-handed triplet VEV v_L which is set to zero to preserve the ρ -parameter [169].

As discussed in Section 2, the t -channel in HTM contains the $e - l' - H^{\pm\pm}$ vertex inversely proportional to v_Δ in Eq. (2.3), this diagram becomes dominant for small v_Δ . However, it appears

MLRSM

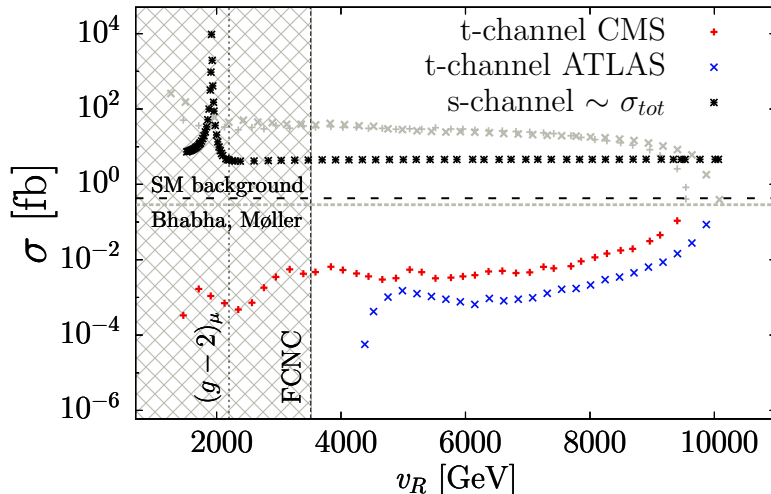


Figure 8: Doubly charged Higgs boson pair production $e^+e^- \rightarrow H_1^{++}H_1^{--} + H_2^{++}H_2^{--}$ for $M_{H_{(1,2)}^{\pm\pm}} = 700$ GeV and CM energy 1.5 TeV in MLRSM. For the t -channel the choice $M_{W_2} - M_N$ space is restricted by LHC results best fit expected values, see Fig. 6. The crossed area on the left is excluded by $(g-2)_\mu$ and FCNC. The maximum for $v_R = 1900$ GeV comes from the Z_2 resonance, $M_{Z_2} = 1.9$ TeV. The horizontal gray dashed line "Bhabha, Møller" separates the t -channel contribution to the cross section which is still allowed by the CMS and ATLAS exclusion analysis from constraints by the Bhabha and Møller processes (Tab. 2 and Tab. 3). The t -channel contribution above this line is forbidden. The SM background (black dashed horizontal line) after applying kinematic cuts is $\sigma = 0.415$ fb, see section 5.4.

that the region where the t -channel can dominate is ruled out by the low energy data and Tab. 5. The allowed t -channel cross section for $e^+e^- \rightarrow H^{++}H^{--}$ is a few orders of magnitude lower than the s -channel, which is equal to 2.4 fb, see a solid horizontal line in Fig. 7. As it is shown, regardless of the choice of the neutrino parameters, the whole region where the t -channel is not negligible is excluded.

The $e^+e^- \rightarrow H_1^{++}H_1^{--} + H_2^{++}H_2^{--}$ cross section in MLRSM, see Fig. 2 depends on the right-handed triplet VEV v_R and heavy neutrino masses. The allowed space for $M_{W_2} - M_N$ parameters has been considered in section 4.1 and is based on limits on the heavy neutrino masses taken from the LHC CMS and ATLAS data for the $pp \rightarrow lljj$ process [136, 143, 144]. This process is a collider analogue of the neutrinoless double beta decay mediated by a heavy charged boson, heavy Majorana neutrinos, and cross-sections depend strongly on masses and CP-parities of heavy neutrinos [147]. As we have in disposal CMS and ATLAS results, in calculations we assume $M_{W_2} > M_N$ with the same CP-parities of heavy neutrinos. In Fig. 8 we vary the M_{W_2} mass from 600 GeV to 5.5 TeV and the heavy neutrino mass up to 4.8 TeV and take the best fit expected values for the LHC exclusion data.

The production through the t -channel is constrained by the Yukawa coupling, Eq. Y_{ee} (2.4). We assume perturbativity of the coupling $Y_{ee} \sim \mathcal{O}(1)$. From $M_N = \sqrt{2}h_M v_R$, Eq. (7.39), with $h_M \lesssim 1$ we get the relation between v_R and heavy neutrino masses. Since the LHC exclusion plots assume $M_N < M_{W_2}$, this condition is fulfilled automatically for the considered parameter space.

The most strict limits comes from the Bhabha and Møller processes, see Fig. 9, the doubly charged scalar particles can contribute there. In Tab. 6 we gathered region of physical masses for heavy neutrinos which arise from the discussed low energy LFV constraints.

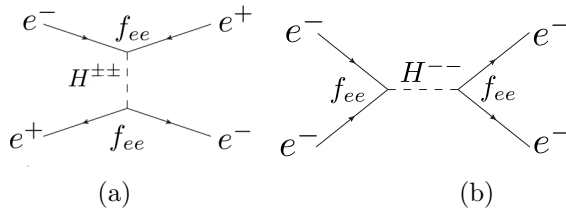


Figure 9: The $e^+e^- \rightarrow e^+e^-$ (Bhabha) and $e^-e^- \rightarrow e^-e^-$ (Møller) processes at the lowest order with doubly charged Higgs bosons.

$M_{H_{1,2}^{\pm\pm}}$ [GeV]	$v_R = 6$ TeV	$v_R = 15$ TeV
700	$M_{N_1} < 803$ GeV	$M_{N_1} < 2007$ GeV
1000	$M_{N_1} < 1147$ GeV	$M_{N_1} < 2867$ GeV

Table 6: Upper limits on the heavy neutrino masses for different sets of doubly charged Higgs boson and the triplet VEV v_R , taking into account low energy LFV constraints in Tab. 2 and SM processes in Tab. 3.

As we can see in Fig. 8, the t -channel gray parts of the plotted lines above the long-dashed "Bhabha, Møller" line assigned with cross \times and plus $+$ symbols might dominate within the whole region of the v_R parameter tested by LHC. However, adding the discussed Yukawa constraints on $H^{\pm\pm}$ couplings gathered in Tab. 2 and Tab. 3, this region is eliminated (corresponding allowed t -channel contributions with red and blue parts of the plotted CMS and ATLAS lines are thickened in Fig. 8). As the Bhabha and Møller processes constraint the t -channel contribution to be below 0.3 fb, altogether with the LHC constraints, it results in a much smaller contribution than the s -channel contribution and the interference effect is small: The total cross section σ_{tot} practically corresponds with the s -channel. Even though the mass M_{Z_2} is a function of v_R ($M_{Z_2} \simeq 0.78 v_R$), the higher resonances are suppressed since the small center mass energy is too small to observe them. For larger v_R values, we are outside the s -resonance for $\sqrt{s} = 1.5$ TeV and s -channel contributions are flat and small. For instance, for $v_R = 6(15)$ TeV which will be used as reference values in next sections for four lepton final state analysis, and which correspond to $M_{Z_2} = 4.7(11.7)$ TeV, $\sigma_s \simeq 4.6$ fb. The limits from the muon $(g-2)$ and the $\mu^+e^- \rightarrow \mu^-e^+$ process are also taken into account, since the corresponding diagrams contain the f_{ee} and $f_{\mu\mu}$ couplings, but they play no significant role. The $(g-2)_\mu$ process restricts the $f_{\mu\mu}$ coupling, see the Appendix. It affects heavy neutrino mass bounds and for further calculations we assume that maximum $M_{N_2} = 5$ TeV, what is safe for considered values of v_R (6 and 15 TeV). Unlike in the HTM case, the LFV processes do not restrict further the results because we assume the LFV vertices to be negligible with no light-heavy neutrino mixings (see Section 7.3). Taking into account the above constraints, the maximal cross section at the t -channel is $\sigma_t \sim 0.3$ fb.

All non-standard heavy particle masses are related to the vacuum expectation value of the right-handed triplet, see Appendix 7.2 and Eqs. (7.21)-(7.29). As discussed in [56], the combined effects

of relevant Higgs potential parameters and Higgs bosons responsible for FCNC limits regulate the lower limits of heavy gauge boson masses. In Fig. 8 we put only low-energy limits on v_R coming from $(g-2)_\mu$ and FCNC. We indicate $v_R \sim 3.5$ TeV, which by considering the Higgs boson mass spectrum Eqs. (7.21)-(7.27) is the minimal v_R for FCNC Higgs masses of A_1^0, H_1^0 scalars at the level of $\mathcal{O}(10)$ TeV, and the minimal allowed $M_{H_3^0}$ for α_3 scalar parameter to be less than 16. The mass limit for A_1^0, H_1^0 at the level of 10 TeV is the lowest limit on FCNC Higgs boson masses [165], one of the strongest limits has been obtained in [154] ($M_{A_1^0, H_1^0} \geq 50$ TeV). We can see that there are various estimates of the v_R scale, see also Fig. 6. Apart from the dijet LHC strong limits, there are searches in the one jet and one lepton signal category [138, 170] as well as off-shell W_2 and Z_2 channels [171, 172]. All these studies confirm that it is not natural to expect v_R to scale below 3.5 TeV. For these reasons, as pp studies at HL-LHC or future FCC-hh or CEPC colliders offer investigation of heavy BSM states at higher scales, in next sections for pp phenomenological studies we assume v_R scale and MLRSM mass benchmarks corresponding to higher v_R values at the level of 6 and 15 TeV.

In Tab. 7 we show fractions of dominating s-channel individual contributions to the doubly charged pair production cross section in e^+e^- collisions. Individual doubly charged production cross sections are: $\sigma(e^+e^- \rightarrow H_1^{++}H_1^{--}) = 2.46$ fb, $\sigma(e^+e^- \rightarrow H_2^{++}H_2^{--}) = 2.15$ fb, which should be compared to $\sigma(e^+e^- \rightarrow H_2^{++}H_2^{--})_{HTM} = 2.4$ fb in HTM, see the solid horizontal line in Fig. 7.

		$\sqrt{s} = 1.5$ TeV			
Model	Process $e^+e^- \rightarrow$	γ	Z_1	Z_2	scalars
MLRSM	$H_1^{++}H_1^{--}$	87%	13%	$\ll 1\%$	$\ll 1\%$
	$H_2^{++}H_2^{--}$	90%	10%	$\ll 1\%$	$\ll 1\%$
HTM	$H^{++}H^{--}$	88%	12%	—	$\ll 1\%$

Table 7: Individual s-channel contributions to the doubly charged pair production in electron-positron collision for $\sqrt{s} = 1.5$ TeV c.m. energy (CLIC) in the HTM and MLRSM models.

Let us proceed to the hadron colliders and pair production of $H^{\pm\pm}$ Higgs bosons. Basic tree-level diagrams for considered models are given in Fig. 3.

Fig. 10 shows the plot for the $pp \rightarrow H^{++}H^{--}$ cross sections both in the HTM and the MLRSM models. The cross sections are comparable in both models with slightly larger values for MLRSM. Typically, for $M_{H_1^{++}} = M_{H_2^{++}} = 1000$ GeV:

$$\sigma(pp \rightarrow (H_1^{++}H_1^{--} + H_2^{++}H_2^{--}) \rightarrow \ell_i^+ \ell_i^+ \ell_j^- \ell_j^-) = 0.063 \text{ (13.02) } fb, \quad (5.1)$$

for $\sqrt{s} = 14(100)$ TeV. The individual $H_1^{\pm\pm}$ and $H_2^{\pm\pm}$ contributions to the cross section for $\sqrt{s} = 14(100)$ TeV are:

$$\sigma(pp \rightarrow H_1^{++}H_1^{--}) = 0.046 \text{ (7.64) } fb, \quad (5.2)$$

$$\sigma(pp \rightarrow H_2^{++}H_2^{--}) = 0.017 \text{ (5.38) } fb, \quad (5.3)$$

$$\sigma(pp \rightarrow H^{++}H^{--})_{HTM} = 0.044 \text{ (5.13) } fb. \quad (5.4)$$

The HTM production process is about 70% (40%) of that in MLRSM for $\sqrt{s} = 14(100)$ TeV, respectively. We can see that $\sigma(pp \rightarrow H^{++}H^{--})_{HTM} \simeq \sigma(pp \rightarrow H_1^{++}H_1^{--})$, especially for the HL-LHC case. In Tab. 8 we sum up fractions of particle contributions to the process coming from individual channels. As we can see from Eqs. (5.2)-(5.4) and Tab. 8: (i) production of the $H_2^{\pm\pm}$ is

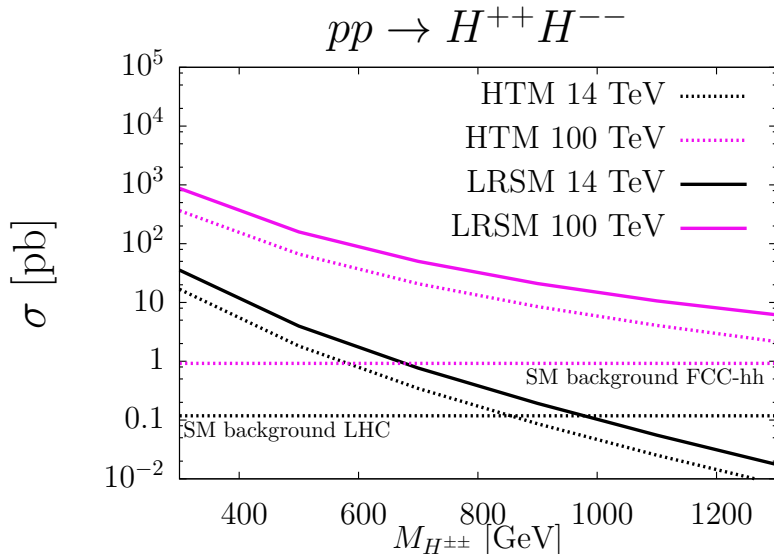


Figure 10: The $H^{\pm\pm}$ pair production $pp \rightarrow H^{\pm\pm}H^{\pm\pm}$ within the HTM and MLRSM models for LHC and FCC-hh center-of-mass energies. Horizontal dashed lines give the SM background for the process $pp \rightarrow 4l$, Tab. 14, with kinematic cuts defined in section 5.4. The QCD NLO $H^{\pm\pm}$ pair production k-factors are taken into account, see the main text.

Model	Process $pp \rightarrow$	14 TeV				100 TeV			
		γ	Z_1	Z_2	scalars	γ	Z_1	Z_2	scalars
MLRSM	$H_1^{++}H_1^{--}$	63%	36%	$< 1\%$	$\ll 1\%$	43%	27%	30%	$\ll 1\%$
	$H_2^{++}H_2^{--}$	74%	25%	$\sim 1\%$	$\ll 1\%$	68%	9%	23%	$\ll 1\%$
HTM	$H^{++}H^{--}$	65%	35%	—	$\ll 1\%$	62%	38%	—	$\ll 1\%$

Table 8: Individual channel contributions to the doubly charged pair production $\sqrt{s} = 14$ TeV c.m. energy (HL-LHC) and $\sqrt{s} = 100$ TeV c.m. energy (FCC-hh/CEPC) hadron colliders in HTM and the MLRSM models.

smaller than the $H_1^{\pm\pm}$ one, its contribution increases with c.m. energy; (ii) the γ channel dominates for both $H_1^{\pm\pm}$ and $H_2^{\pm\pm}$ pair production at HL-LHC c.m. energies while for FCC-hh/CEPC option, Z_2 -channel starts to be important. Due to the shown differences between MLRSM and HTM models we can expect a higher number of events for 4-lepton final states in MLRSM when masses of doubly charged Higgs bosons are the same. However, it does not have to be the case as the final results depend strongly on branching ratios which we will consider in the next section.

The QCD contributions to the doubly charged Higgs boson pair production increase the cross section at the NLO level. The role of the QCD effects in the hadronic processes of $H^{\pm\pm}$ pair production has been considered in [54]. A similar situation with positive contribution of QCD at the NLO and higher levels has been observed also for other processes in models which include triplet Higgs bosons and heavy neutral leptons [54, 173–176]. The corresponding k-factors (which measure ratios of higher order QCD effects to the tree level cross section) do not change considerably with

the $H^{\pm\pm}$ mass and centre of mass energies, k-factor $\in (1.15 \div 1.20)$. Due to different ratios of H_1^{++} and H_2^{++} pair production processes (see Eqs.(5.2)-(5.4) and Tab. 8), for $m_{H^{\pm\pm}} = 1$ TeV, the k-factor in HTM is 1.15 and is smaller than k-factors in MLRSM, which are $\simeq 1.6$ (1.85) for HL-LHC (FCC-hh/CEPC) centre of mass energies, respectively. There are various QCD contributions at the NLO level to the considered process, in which the s-channels $\gamma/Z_1/Z_2$ dominate over the gluon and photon fusion mechanisms, both for HL-LHC and FCC-hh/CEPC. Concerning potential contributions beyond NLO, the N^3LL terms are found to be about three times larger than NLO terms. However, this is connected mainly with gluon fusion which is subdominant for the considered H_1^{++} masses in the s-channel [54]. As the doubly charged pair production signals are dominated by the exchange of the SM particles in e^+e^- collisions (see Tab. 7), differences between doubly charged pair production signals in both models are small. A better estimation of QCD corrections, evaluating the NNLO terms, would resolve expected signals better. In the pp collision case, the production difference between the models for the considered benchmark points is much larger. NLO QCD corrections seem to be enough to discriminate the models, though we should note that the production difference between both models will decrease above $v_R = 15$ TeV, which is the upper limit for the v_R value considered in the present work. In scenarios with $v_R > 15$ TeV a knowledge of NNLO QCD corrections will be also useful in the pp collisions. Anticipating final four-lepton results, the above conclusions do not change for the considered benchmark points and kinematic cuts. Namely, ratios of MLRSM ($v_R = 15$ TeV) to HTM four-lepton signals can be as large as 1.7 (34 and 43) at e^+e^- and pp (HL-LHC and CEPC/FCC-hh) colliders, respectively (see 4μ signals, Tab. 15 and Tab. 16). Then NLO QCD k-factors should be enough to distinguish the HTM and MLRSM signals in pp collisions, unless the v_R scale is too large and the Z_2 gauge boson contribution becomes at the NNLO QCD level.

To summarize, the QCD contributions to the considered production processes at the NLO level are substantial in both models and must be taken into account in the analysis. To discriminate both models, evaluation of higher order QCD terms may be needed for higher v_R scales.

5.2 HTM, a choice of benchmark parameters and $H^{\pm\pm}$ decay scenarios

In HTM the doubly charged scalar has nine possible decay channels, depending on the scalar boson mass

- (i) $H^{\pm\pm} \rightarrow l_i l_j, \quad i, j = e, \mu, \tau,$
- (ii) $H^{\pm\pm} \rightarrow W^\pm W^\pm,$
- (iii) $H^{\pm\pm} \rightarrow H^\pm W^\pm,$
- (iv) $H^{\pm\pm} \rightarrow H^\pm H^\pm.$

In this paper we focus on the first channel (i) and present a case study for pair production of a doubly charged scalar boson and its subsequent leptonic decays, considered also in [177]. It is a very clean channel which provides a unique signature for colliders signal with a pair of the same sign leptons [88]. Scenarios (iii) and (iv) require non-degenerate masses for charged scalar particles: $M_{H^{\pm\pm}} > M_{H^\pm} + M_W$ and $M_{H^{\pm\pm}} > 2M_{H^\pm}$, respectively.

In Fig. 11 we show a variety of branching ratios as a function of v_Δ for various $H^{\pm\pm}$ decay channels. On the left plot we show the following decay modes: leptonic (red), W^\pm gauge bosons (green) and $H^\pm W^\pm$ (blue). On right we give a variation of leptonic and pair of gauge boson decay branching ratios for a degenerate mass of $H^{\pm\pm}$. There are two cases there: the solid line is for $M_{H^{\pm\pm}} = M_{H^\pm} = 700$ GeV and the dashed line is for a charged scalar boson mass of 300 GeV (this mass is already excluded by LHC, we left it for comparison with previous work, see Fig. 4 in [178]). The shaded region is connected with the lightest neutrino mass and mass hierarchy, within 2σ

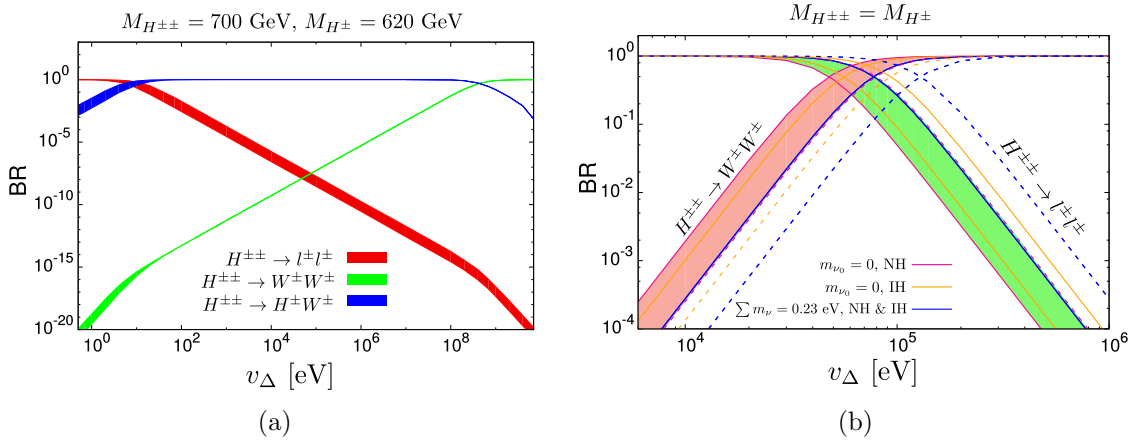


Figure 11: Branching ratios for $H^{\pm\pm}$ in HTM for a non-degenerated case (a) with $m_{H^{\pm\pm}} = 700$ GeV and $m_{H^{\pm}} = 620$ GeV and for a degenerate case (b) when $m_{H^{\pm\pm}} = m_{H^{\pm}} = 700$ and 300 GeV are assumed. The shaded regions correspond to IH and NH neutrino mass hierarchies with m_{ν_0} limited by Σ in (3.9) and $M_{H^{\pm\pm}} = 700$ GeV. Dashed lines in case (b) describes the branching ratios for $M_{H^{\pm\pm}} = M_{H^{\pm}} = 300$ GeV. The oscillation data are taken in the 2σ range.

oscillation parameter range. This region does not change the result substantially. We can see that the cross-cut point is shifting with charged scalar boson mass, but in the interesting mass region, the lepton channel dominates till v_{Δ} reaches values in range of $10^4 \div 10^5$ eV. In Fig. 11 (a) we take a mass gap $M_{H^{\pm\pm}} - M_{H^{\pm}} = 80$ GeV, in Fig. 11 (b) there is no mass gap and both $H^{\pm\pm} \rightarrow H^{\pm}W^{\pm}$ and $H^{\pm\pm} \rightarrow H^{\pm}H^{\pm}$ channels are suppressed. It has been shown in [86] and [87] that there are limits on the mass gap $|M_{H^{\pm\pm}} - M_{H^{\pm}}|$ in order to preserve the oblique T-parameter, unitarity and potential stability condition. For recent work on vacuum stability conditions of Higgs potentials in various variants of HTM models, see [179]. From electroweak precision data and limits from the $h \rightarrow \gamma\gamma$ process [83, 85] the dominant contributions are in the degenerate mass case. Therefore only leptonic and W gauge boson decay channels are possible. However, the $H^{\pm\pm} - W^{\mp} - W^{\mp}$ vertex is proportional to the triplet VEV v_{Δ} while the Yukawa coupling in the $H^{\pm\pm} - l^{\mp} - l^{\mp}$ vertex is proportional to $\frac{1}{v_{\Delta}}$, so the lepton channels dominate strongly over the scenario (ii) for the triplet VEV $v_{\Delta} < 10^5$ eV.

For VEV v_{Δ} in a range of eV, the cumulative leptonic channel dominates in that region regardless of the neutrino masses and oscillation parameters as well as doubly charged scalar boson masses. So, our final conclusion is that when $H^{\pm}W^{\pm}$ and $H^{\pm}H^{\pm}$ channels are suppressed, the leptonic decays dominate for low v_{Δ} .

The sharpest limit from ATLAS on $M_{H^{\pm\pm}}$ is that the $H^{\pm\pm}$ mass should be larger than 870 GeV for the left-handed triplet doubly charged scalar boson field, assuming the 100% branching ratio for the $H^{\pm\pm} \rightarrow l^{\pm}l^{\pm}$ decay ($l^{\pm} = e^{\pm}, \mu^{\pm}$). However, it is possible to lower down the limit to 450 GeV for a 10% leptonic decay branching ratio (see Fig. 13 d in [55]). On the other hand, the decays into a τ lepton are not considered in the above analysis. In Tab. 9 we present branching ratios for those channels and the result for the ee , $e\mu$ and $\mu\mu$ decays, within the $\pm 2\sigma$ range of the oscillation parameter space. For other channels including the τ we refer to [180]. The strength of lepton decay channels depends strongly on the neutrino masses, their hierarchies and oscillation parameters. It is possible to find the parameter space where the branching ratio for the particular lepton channel

BR	ll	ee	$e\mu$	$\mu\mu$
0.01	-	249.2	216.3	309.7
0.02	-	310.9	300.0	335.7
0.03	-	323.7	316.6	367.5
0.04	-	333.9	329.5	418.2
0.05	-	342.5	339.5	434.1
0.1	473.7	478.5	473.7	480.7
0.2	493.5	613.7	573.1	557.9
0.3	518.1	638.9	648.0	683.4
0.4	645.4	658.4	671.7	714.6
0.5	662.7	691.5	690.0	734.0
0.6	679.6	-	-	-
0.7	695.6	-	-	-

Table 9: Lowest limits on a mass of the doubly charged scalar boson $M_{H^{\pm\pm}}$ for different branching ratios [55]. We removed data which corresponds to the branching ratio region beyond what has been obtained in Fig. 12 within 2σ range of the neutrino oscillation parameters.

is small regardless v_Δ even if the cumulative lepton channel dominates over the W boson channel (the relative lepton decay contributions $\Gamma(H^{\pm\pm} \rightarrow l l') / \sum \Gamma(H^{\pm\pm} \rightarrow l_i l_j)$ do not depend on the triplet VEV v_Δ).

We combine the data both from the LHC limits [55] and neutrino parameters within the $\pm 2\sigma$ range given in Tab. 4 and compute the lowest limit on the doubly charged scalar boson mass². In Tab. 9 we removed the BR values that are forbidden due to the neutrino oscillation parameters. Another interesting conclusion from this table is that within the HTM the doubly charged scalar boson cannot be lighter than 473 GeV for the normal neutrino mass scenario (and 518 GeV for the inverted mass hierarchy), see Fig. 12 (a). Finally, the lowest mass limit on $M_{H^{\pm\pm}}$ within HTM is 473.7 GeV for NH and 645.4 GeV for IH with $\text{BR}(H^{\pm\pm} \rightarrow ll') = (\Gamma(H^{\pm\pm} \rightarrow e^\pm e^\pm + e^\pm \mu^\pm + \mu^\pm \mu^\pm)) / \Gamma(H^{\pm\pm} \rightarrow \sum_{i,j} l_i^\pm l_j^\pm) \geq 0.1$ and 0.4, respectively, where $l_{i,j} = e, \mu, \tau$. The most severe limit at 734 GeV comes from the same sign muon channel when BR is 50%.

In conclusion, when assuming the complete scenarios with $H^{\pm\pm}$ decays to all the leptons, still $M_{H^{\pm\pm}}$ can be relatively light.

Our main aim is to analyse the final four lepton ($4l$) signals which can be potentially seen at the colliders. The dominant signatures are $e^+e^+e^-e^-$ and $\mu^+\mu^+\mu^-\mu^-$ final states within both HTM and MLRSM models. In MLRSM they are not bounded by the neutrino oscillation parameters since the $H_{1,2}^{\pm\pm} - l - l$ vertex is related to the heavy right-handed neutrino masses and parameters, as discussed in section 7.3. Within the HTM model these $4l$ contributions are restricted by the light neutrino oscillation data. Using branching ratios shown in Fig. 12 we compute two parameter sets (for normal and inverted hierarchy) for which the branching ratio for $e^\pm e^\pm$ and $\mu^\pm \mu^\pm$ are the highest. We collect the chosen parameters in Tab. 10. We choose two benchmark masses for the collider analyses: $M_{H^{\pm\pm}} = 700$ GeV (which can be probed at very high energies in e^+e^- collision, when available, see section 5.1) and $M_{H^{\pm\pm}} = 1000$ GeV (this higher mass range can be probed without problems at the HL-LHC and FCC-hh, see Fig. 10). For the $e^\pm e^\pm$ decay channel we chose

²There is in principle a subtlety in the fact that the branching ratios are not directly measured. Instead, the rate for $4l$ production is measured. Here we rely on basic analysis and outcome given by the ATLAS collaboration.

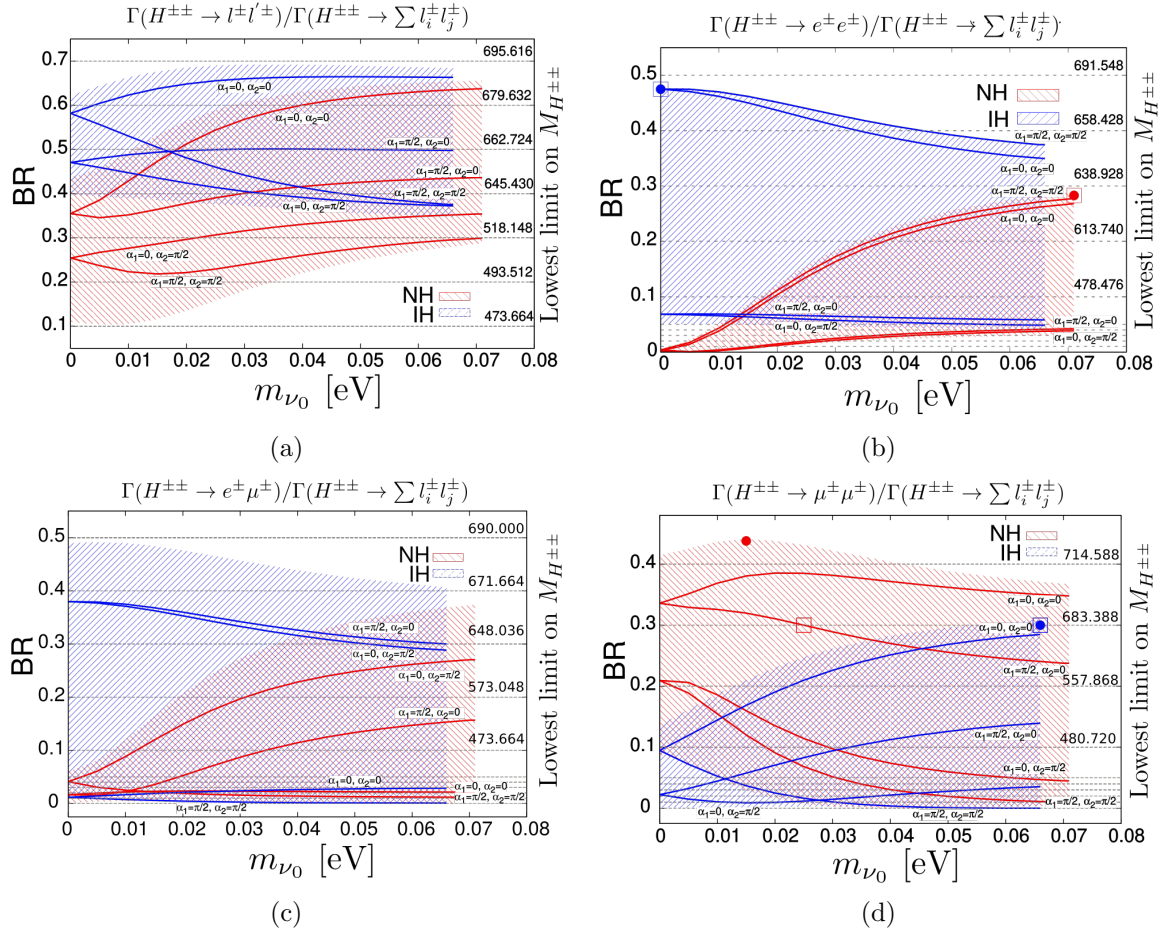


Figure 12: $H^{\pm\pm}$ decay branching ratios, $l, l' = e, \mu$ within the HTM model, with corresponding lower limits on the doubly charged scalar particle's masses [55]. Neutrino parameters are within the $\pm 2\sigma$ range, Tab. 4. Solid lines present the result for best fit of neutrino parameters and particular values of Majorana phases. We have marked the points used for further calculations with \square and \bullet which satisfy the following conditions: \bullet gives maximum possible BR for NH and IH cases with $M_{H^{\pm\pm}} = 1000$ GeV; \square gives lower BR values which allows for $M_{H^{\pm\pm}} = 700$ GeV.

the same neutrino parameters because within the whole neutrino parameter space $M_{H^{\pm\pm}} = 700$ GeV and $M_{H^{\pm\pm}} = 1000$ GeV are not excluded. For the $\mu^\pm \mu^\pm$ channel we chose the maximum possible BR for $M_{H^{\pm\pm}} = 1000$ GeV and BR=0.3 for $M_{H^{\pm\pm}} = 700$ GeV to keep the bound on the doubly charged scalar particle's mass lower than 700 GeV.

$M_{H^{\pm\pm}}$	$H^{\pm\pm} \rightarrow XX$	HTM			
		NH		IH	
700 GeV (\square)	ee_{\max} $BR < 0.5$	BR=0.283	$\alpha_1 = \frac{\pi}{2}$ $\alpha_2 = \frac{\pi}{2}$ $m_{\nu_0} = 0.071$ eV	BR=0.475	$\alpha_1 = \frac{\pi}{2}$ $\alpha_2 = \frac{\pi}{2}$ $m_{\nu_0} = 0$
	$\mu\mu_{\max}$ $BR < 0.3$	BR=0.3	$\alpha_1 = \frac{\pi}{2}$ $\alpha_2 = 0$ $m_{\nu_0} = 0.025$ eV	BR=0.3	$\alpha_1 = 0$ $\alpha_2 = 0$ $m_{\nu_0} = 0.066$ eV
1000 GeV (\bullet)	ee_{\max}	BR=0.283	$\alpha_1 = \frac{\pi}{2}$ $\alpha_2 = \frac{\pi}{2}$ $m_{\nu_0} = 0.071$ eV	BR=0.475	$\alpha_1 = \frac{\pi}{2}$ $\alpha_2 = \frac{\pi}{2}$ $m_{\nu_0} = 0$
	$\mu\mu_{\max}$	BR=0.438	$\alpha_1 = 0$ $\alpha_2 = 0$ $m_{\nu_0} = 0.015$ eV	BR=0.3	$\alpha_1 = 0$ $\alpha_2 = 0$ $m_{\nu_0} = 0.066$ eV

Table 10: Chosen parameter set for maximum branching ratios $BR(H^{\pm\pm} \rightarrow ee)$ and $BR(H^{\pm\pm} \rightarrow \mu\mu)$ and for the best fit neutrino parameters in Tab. 4. Corresponding benchmark points are marked in Fig. 12 (b) and (d) with \square ($M_{H^{\pm\pm}} = 700$ GeV) and \bullet ($M_{H^{\pm\pm}} = 1000$ GeV).

5.3 MLRSM, a choice of benchmark parameters and $H_{1,2}^{\pm\pm}$ decay scenarios

Contributing vertices to the non-leptonic decay channels stem from the kinetic term and scalar potential (see Eqs. 19 and 25 in [39]). Relevant decay modes of doubly charged scalar bosons and respective strength of couplings are gathered in Tab. 11. The emboldened processes in the table dominate for $v_L = \rho_4 = 0$ and $\xi \rightarrow 0$ [56, 169, 181], see the Appendix for details. Apart from the values of vertices, we need to take into account the mass spectrum. To suppress the FCNC processes some of neutral scalar particles have to be heavier than 10 TeV. As a consequence, the mass of H_2^\pm should be above 10 TeV, (7.21) and (7.27). Therefore we can neglect the $H_2^{\pm\pm}$ decay to the H_2^\pm scalar boson for CLIC and LHC energies. From (7.21) it is easy to find that the triplet VEV should fulfil an inequality: $v_R > \sqrt{2} 10^3 / \sqrt{\alpha_3}$ [GeV]. Because α_3 is a quartic coupling (four-scalar interaction) it contributes to the $2 \rightarrow 2$ scattering and the unitarity condition requires $\alpha_3 < 8\pi$ [56]. The triplet VEV v_R has to be higher than ~ 2800 GeV that translate to $M_{W_2} > 1325$ GeV. So we can neglect the doubly charged scalar bosons pair production with the subsequent decay to the heavy gauge boson pair $H_2^{\pm\pm} \rightarrow W_2^\pm + W_2^\pm$ for energies lower than $2M_{W_2}$.

In Tab. 11 we present the other possible decay channels of $H_{1,2}^{\pm\pm}$ and corresponding vertices. Most of them are negligible due to model's consistency [56, 169], only the bold decay channels can be substantial. The $H_{1,2}^{\pm\pm}$ decay to H_2^\pm is not possible for CLIC and LHC energies because of the FCNC limits (7.27). Vertices contributing to the $H_{1,2}^{\pm\pm}$ decays to W_1, W_2 can be large and are included in analysis leading to final four lepton signals.

Regarding $H_1^{\pm\pm}$, its decay to $H_1^\pm + W_1^\pm$ is limited by Higgs potential parameters and, as proved analytically in [182], the allowed split $\Delta M_H = M_{H_1^{\pm\pm}} - M_{H_1^\pm}$ can not exceed value 65.3 GeV.

We choose the benchmark points for $v_R = 6$ TeV and 15 TeV. The first value falls in energy range of LHC with $pp \rightarrow W_2 \rightarrow lN_l \rightarrow llW_2^* \rightarrow llq\bar{q}'$, assuming that $M_{N_i} < M_{W_2}$. Corresponding experimental results can be found in [136, 143]. We assume that the doubly charged scalar masses are degenerate and choose two benchmark points: 700 GeV and 1000 GeV. For the $M_{H_{1,2}^{\pm\pm}} = 700$ GeV case we keep the leptonic branching ratio limits as given in Tab. 9, that means $BR(H_{1,2}^{\pm\pm} \rightarrow ee) < 0.5$ and $BR(H_{1,2}^{\pm\pm} \rightarrow \mu\mu) < 0.3$. Tab. 12 presents the maximum possible branching ratios for $M_{H_{1,2}^{\pm\pm}} = 700$ GeV. For doubly charged Higgs boson mass of 1000 GeV there is no relevant experimental limits and the maximum branching ratios for ee or $\mu\mu$ decays can reach

$H_1^{\pm\pm}$	\rightarrow	$W_1 + W_1$	$\sim \cos^2 \xi v_L$	$H_2^{\pm\pm}$	\rightarrow	$W_1 + W_1$	$\sim \sin^2 \xi v_R$
$H_1^{\pm\pm}$	\rightarrow	$W_1 + W_2$	$\sim \cos \xi \sin \xi v_L$	$H_2^{\pm\pm}$	\rightarrow	$W_1 + W_2$	$\sim \cos \xi \sin \xi v_R$
$H_1^{\pm\pm}$	\rightarrow	$W_2 + W_2$	$\sim \sin^2 \xi v_L$	$H_2^{\pm\pm}$	\rightarrow	$W_2 + W_2$	$\sim \cos^2 \xi v_R$
$H_1^{\pm\pm}$	\rightarrow	$H_1^\pm + W_1$	$\sim \cos \xi g_L$	$H_2^{\pm\pm}$	\rightarrow	$H_2^\pm + W_1$	$\sim \sin \xi g_R$
$H_1^{\pm\pm}$	\rightarrow	$H_1^\pm + W_2$	$\sim \sin \xi g_L$	$H_2^{\pm\pm}$	\rightarrow	$H_2^\pm + W_2$	$\sim \cos \xi g_R$
$H_1^{\pm\pm}$	\rightarrow	$H_1^\pm + H_1^\pm$	$\sim \rho_2 v_L$	$H_2^{\pm\pm}$	\rightarrow	$H_1^\pm + H_1^\pm$	$\sim \rho_4 v_R$
$H_1^{\pm\pm}$	\rightarrow	$H_2^\pm + H_2^\pm$	$\sim \rho_4 v_L$	$H_2^{\pm\pm}$	\rightarrow	$H_2^\pm + H_2^\pm$	$\sim \rho_2 v_R$
$H_1^{\pm\pm}$	\rightarrow	$H_1^\pm + H_2^\pm$	$\sim \kappa_2$	$H_{1,2}^{\pm\pm}$	\rightarrow	$H_{2,1}^{\pm\pm} + H_0^0$	$\sim \rho_4 v_L$
$H_{1,2}^{\pm\pm}$	\rightarrow	$H_{2,1}^{\pm\pm} + H_1^0$	$\sim \rho_4 v_L$	$H_{1,2}^{\pm\pm}$	\rightarrow	$H_{2,1}^{\pm\pm} + H_2^0$	$\sim \rho_4 v_L$
$H_{1,2}^{\pm\pm}$	\rightarrow	$H_{2,1}^{\pm\pm} + H_3^0$	$\sim \rho_4 v_R$	$H_{1,2}^{\pm\pm}$	\rightarrow	$H_{2,1}^{\pm\pm} + A_2^0$	$\sim \rho_4 v_R$

Table 11: Doubly charged scalar boson decay channels to scalar and gauge bosons in MLRSM. We have listed all possible vertices, thickening the dominating processes assuming that the left triplet VEV v_L is equal to zero and keeping in mind experimental limits on the $W_1 - W_2$ mixing angle $\xi < 10^{-2}$ [134, 146] and setting the ρ_4 parameter to zero [56, 169]. The leptonic decays are analysed separately.

100% also in a case of $H_1^{\pm\pm}$. Here the situation is different than in HTM where upper bounds for $H^{\pm\pm}$ branching ratios are given. As discussed in Sections 2 and 3, neutrino Yukawa couplings can be rewritten in terms of oscillation parameters and v_Δ and experimental data restricts possible branching ratios in a substantial way. In addition, depending on the branching ratios, the lowest limit on the mass of a doubly charged scalar can be obtained. However, in the context of MLRSM, leptonic branching ratios for $H^{\pm\pm}$ depend in addition on v_R scale and heavy neutrino masses and couplings. This freedom makes it possible to reach full leptonic decays for $M_{H^{\pm\pm}}$, as given in Tab. 12 and Tab. 13.

	ee	$\mu\mu$	$ee + \mu\mu$
$\text{BR}_{H_1^{\pm\pm}}$	0.5	0.3	0.7
$\text{BR}_{H_2^{\pm\pm}}$	1.0	0.8	1.0

Table 12: Maximum branching ratios for $H_{1,2}^{\pm\pm} \rightarrow XX$ and $M_{H_{1,2}^{\pm\pm}} = 700$ GeV. Results for $H_1^{\pm\pm}$ coincides with the HTM case in Tab. 9. Branching ratios for $H_2^{\pm\pm}$ are due to right-handed leptonic couplings as analysed in [55].

Tab. 13 shows chosen, allowed values of heavy neutrino masses for given maximal branching ratios. They are consistent with assumption $M_{W_2} \geq M_N$ discussed in section 4, and a correlation between the masses which are proportional to v_R [56, 145]. In section 5.2 we have obtained the lowest limits for $M_{H^{\pm\pm}}$ as a function of the lightest neutrino mass for a given $H^{\pm\pm}$ branching ratio, arguing that $M_{H^{\pm\pm}}$ at the level of 700 GeV is still possible within HTM. The lowest limits on masses of $H_{1,2}^{\pm\pm}$ Higgs bosons have been obtained in [169] by analyzing restrictions on the scalar potential. Before we present final results we will discuss the SM background for the considered leptonic final states.

$M_{H_{1,2}^{\pm\pm}}$	MLRSM				$H_{1,2}^{\pm\pm} \rightarrow$
	$v_R = 6 \text{ TeV}$		$v_R = 15 \text{ TeV}$		
700 GeV	$\text{BR}_{H_{1,2}^{\pm\pm}}^{ee,\mu\mu} = 0.123$	$M_{N_1} = 250$ $M_{N_2} = 250$ $M_{N_3} = 620$	$\text{BR}_{H_{1,2}^{\pm\pm}}^{ee} = 0.5$	$M_{N_1} = 1300$	$4e$
			$\text{BR}_{H_{1,2}^{\pm\pm}}^{\mu\mu} = 0.25$	$M_{N_{2,3}} = 918$	
1000 GeV	$\text{BR}_{H_{1,2}^{\pm\pm}}^{ee,\mu\mu} = 0.123$	$M_{N_1} = 250$ $M_{N_2} = 250$ $M_{N_3} = 620$	$\text{BR}_{H_{1,2}^{\pm\pm}}^{\mu\mu} = 0.3$	$M_{N_1} = 1300$	4μ
			$\text{BR}_{H_{1,2}^{\pm\pm}}^{ee} = 0.4$	$M_{N_{2,3}} = 1130$	
1000 GeV	$\text{BR}_{H_{1,2}^{\pm\pm}}^{ee,\mu\mu} = 0.123$	$M_{N_1} = 250$ $M_{N_2} = 250$ $M_{N_3} = 620$	$\text{BR}_{H_{1,2}^{\pm\pm}}^{ee} \sim 1$	$M_{N_1} = 2867$ $M_{N_{2,3}} = 300$	$4e$
			$\text{BR}_{H_{1,2}^{\pm\pm}}^{\mu\mu} \sim 1$	$M_{N_2} = 5000$ $M_{N_{1,3}} = 300$	

Table 13: MLRSM parameters which maximize separately the branching ratios $\text{BR}(H^{\pm\pm} \rightarrow ee)$ and $\text{BR}(H^{\pm\pm} \rightarrow \mu\mu)$ for $v_R = 6 \text{ TeV}$ and $v_R = 15 \text{ TeV}$. A scenario with $v_R = 6 \text{ TeV}$ has been covered already by the LHC analysis, and branching ratios are due to Tab. 12, based on [136, 143]. The heavy neutrino masses for $v_R = 6 \text{ TeV}$ fulfill the low energy constraints given in Tab. 6. M_{N_1} is mostly restricted by the Møller scattering, while M_{N_2} is bounded by $(g-2)_\mu$.

5.4 The four leptons background in pp and e^+e^- collisions

We are interested at estimation of the Standard Model background for $pp \rightarrow l^+l^-l^+l^-$ and $e^+e^- \rightarrow l^+l^-l^+l^-$ processes, where $l^\pm = e^\pm, \mu^\pm$. The four leptons production at LHC is discussed in [88, 183]. The most relevant processes which contribute to the background are $t\bar{t}(Z/\gamma^*)$ and $(Z/\gamma^*)(Z/\gamma^*)$ production. To optimize the collider non-standard effects (decreasing SM tri- and four- lepton SM background and reducing the efficiency of misidentification of b-jets as leptons), we use the following criteria and selection cuts

- C1. Lepton identification criteria: transverse momentum $p_T \geq 10 \text{ GeV}$, pseudorapidity $|\eta| < 2.5$.
- C2. Detector efficiency for electron (muon): 70% (90%).
- C3. Lepton-lepton separation: $\Delta R_{ll} \geq 0.2$.
- C4. Lepton-photon separation $\Delta R_{l\gamma} \geq 0.2$ with $p_{T_\gamma} > 10 \text{ GeV}$.
- C5. Lepton-jet separation $\Delta R_{lj} \geq 0.4$.
- C6. Hadronic activity cut - within the cone of radius 0.2 around the lepton the hadronic activity should fulfill the inequality: $\sum p_{T_{hadron}} \geq 0.2 \times p_{T_l}$.
- C7. Z-veto - the invariant mass of any same flavour and opposite charge lepton should satisfy the condition: $|m_{l_1 l_2} - M_{Z_1}| \geq 6 \Gamma_{Z_1}$.
- C8. Hard p_T cuts: $p_T(l_1) > 30 \text{ GeV}$, $p_T(l_2) > 30 \text{ GeV}$, $p_T(l_3) > 20 \text{ GeV}$, $p_T(l_4) > 20 \text{ GeV}$.
- C9. Parton Distribution Functions (PDFs): CTEQ6L1 [184, 185].

The results are gathered in Tab. 14. For the e^+e^- collision we consider scattering and annihilation channels with photon radiation, $(Z/\gamma^*)(Z/\gamma^*)$ production and multiperipheral processes in Fig. 13. The most relevant are diagrams b) and d). For $\sqrt{s} = 1500 \text{ GeV}$ we get $\sigma = 4.465 \text{ fb}$ before and $\sigma = 0.415 \text{ fb}$ after applying the cuts defined above.

Process	Energy	$t\bar{t}(Z/\gamma^*)$	$(Z/\gamma^*)(Z/\gamma^*)$	TOTAL
$\sigma(pp \rightarrow 4l)$ [fb]	14 TeV	0.060	0.054	0.114
	100 TeV	0.58	0.20	0.78

Table 14: Dominant Standard Model background contributions to four-lepton signals at the LHC with $\sqrt{s} = 14$ TeV and FCC-hh with $\sqrt{s} = 100$ TeV after applying cuts given in the text. For the inclusive $t\bar{t}$ process the QCD NLO k-factor is 2.2 [186], accordingly, for $t\bar{t}(Z/\gamma^*)$ it is $k = 1.6$ [187], for $(Z/\gamma^*)(Z/\gamma^*)$ it is $k = 1.5$ [188]. Cross section values are given in fb.



Figure 13: Four lepton background diagrams in electron-positron colliders: $e^+e^- \rightarrow e^+e^-$ with FSR e^+e^- pair emission (a) and (b); with Z/γ^* production (c) and with multiperipheral processes (d).

5.5 Final four lepton signals within the HTM and MLRSM models, a comparison

The final signals depends on subsequent $H^{\pm\pm}$ decays ($\rightarrow 4e, 4\mu, 2e2\mu$) and suitable kinematic cuts. In the HTM model we take benchmark points for the model connected with maximal $4e$ and 4μ signals as given in Fig. 12 (plots on right). Analogous parameters for MLRSM are given in Tab. 13.

SM background: $e^+e^- \rightarrow 4l$					
4e	No cuts: $\sigma = 2.1$ fb				
	After cuts: $\sigma = 0.13$ fb, N = 200				
4μ	No cuts: $\sigma = 0.07$ fb				
	After cuts: $\sigma = 0.005$ fb, N = 8				
BSM signal: $e^+e^- \rightarrow H^{++}H^{--} \rightarrow 4l$	HTM		MLRSM		
	NH	IH	$v_R = 6$ TeV	$v_R = 15$ TeV	
4e	No cuts:	0.19 fb	0.53 fb	0.06 fb	0.924 fb
	After cuts:	0.02 fb N= 30	0.06 fb N= 90	0.007 fb N= 10	0.113 fb N= 169
4μ	No cuts:	0.22 fb	0.19 fb	0.06 fb	0.33 fb
	After cuts:	0.08 fb N= 120	0.08 fb N= 120	0.03 fb N= 38	0.137 fb N= 205

Table 15: Four lepton signals at lepton colliders for the doubly charged scalar pair production with subsequent decays, $e^+e^- \rightarrow H^{++}H^{--} \rightarrow 4l$ for $M_{H^{\pm\pm}} = 700$ GeV and $\sqrt{s} = 1.5$ TeV. In order to maximize signals in electron and muon channels we have applied different parameter sets from Tab. 10 (for HTM) and Tab. 13 (for MLRSM), see the main text for details. "N" estimates a number of final events with the assumed luminosity $L = 1500$ fb^{-1} .

The 4-lepton signals obtained for the e^+e^- case are gathered in Tab. 15. In section 5.4 we

defined the kinematic cuts which maximise the 4-lepton signals. With assumed total luminosity, we can see that the SM background is comfortable small for muons and the maximal 4μ signal's prediction in HTM can be significant, which is not true in the case of electrons. The difference is enhanced by assumed detector efficiency for electrons (muons), see the cut C2 in section 5.4. For MLRSM chosen parameters in Tab. 13 and $v_R = 6$ TeV the signals are small when compared to the SM background, especially for electrons. For muons a signal is ~ 3 times smaller than in HTM. However, for $v_R = 15$ TeV the signals for muons detection can be larger in MLRSM, since for that value of v_R , M_N and M_{W_2} values of parameters lie outside the region examined by the LHC (Fig 6). In this case independent, maximal branching ratios for $H_{1,2}^{\pm\pm} \rightarrow e^\pm e^\pm$ and $H_{1,2}^{\pm\pm} \rightarrow \mu^\pm \mu^\pm$ can reach 100%, (Tab. 13), which is not possible for HTM (Tab.10).

It should be noted that the $e^+e^- \rightarrow 4l$ results in MLRSM depends strongly on interference effects and the chosen heavy neutrino parameters as the LHC exclusion data affects directly the t-channel contributions. In fact, comparing the HTM results with the MLRSM results for $v_R = 6$ TeV, we can see that the $4l$ signals can be larger in HTM where the t-channel is negligible for all allowed parameters space (Fig. 7), while in the MLRSM model the t-channel effects can still be large and comparable to the s-channel contributions (Fig. 8). However, in both models the signals are much below the SM background level.

The maximal significance value $S \equiv S'/\sqrt{S'+B}$ where S' and B are the total number of signal and background events is $S = 14$ for 4μ signals in MLRSM with $v_R=15$ TeV. For HTM, $S = 11$ for both NH and IH neutrino mass scenarios and the 4μ signal. The goal for HL-LHC is to deliver about $L = 0.25 ab^{-1} = 250 fb^{-1}$ per year with the aim of integrating a total luminosity in the range of 3 to $4.5 ab^{-1}$ by the late 2030s [63]. For the FCC-hh, defined by the target of 100 TeV proton-proton collisions, a total integrated luminosity of 20-30 ab^{-1} is considered [189].

In Tab. 16 the results are given for the final $4l$ signals. This time we consider higher $H^{\pm\pm}$ mass of 1 TeV. The kinematic cuts are defined in section 5.4.

For pp collisions the $4e$ channel gives comparable to the background signals in MLRSM with $v_R = 15$ TeV. In pp collision the lowest order t-channel is not present, so no destructive interference with the s-channel is possible. As given in Tab. 16, the maximal significance value is $S = 11$ [290] for 4μ in MLRSM with $v_R=15$ TeV for HL-LHC and FCC-hh, respectively. For HTM in the same 4μ channel $S < 1$ both in NH and IH neutrino mass scenarios. So a detection of 4μ signals above the background level at HL-LHC and FCC-hh would give a clear indication for the MLRSM model with high values of v_R .

So far, we have focused on comparisons of the two models looking for specific signals for the total four charged lepton production rates and compared it to the background processes. In this way, we can present clear differences in a prediction for the leptonic signals in both models. In particular, as shown in Tab. 15 and Tab. 16, there are cases where the SM background is comparable or exceeds the BSM signal for electrons and positrons in the finals state. The question is if in such cases, dilepton distributions can help to identify small BSM signals and discriminate further BSM models. In Fig. 14 the SM background and BSM dilepton distributions for $e^+e^- \rightarrow 4e$ are given. We consider distributions of pairs of electrons/positrons (the same charge leptons) and electron-positron pairs, assigned as SSDL and OSDL, respectively. As we can see, the SM invariant mass SSDL and OSDL distributions are quite uniform, in opposite to the BSM signals where clear peaks are present for SSDL signals. The reason is obviously that the same sign dileptons originate from the same doubly charged particle. As we can see, in this case, though $4e$ signals in Tab. 15 are below the SM background, both HTM and MLRSM dileptons can be identified. It is less visible for the lepton-lepton separation ΔR_{ee} though the SSDL (OSDL) signals are enhanced for higher (lower) values of ΔR_{ee} , respectively, in both considered models. Let us note that m_{ee} and ΔR_{ee} distributions are very similar. This conclusion does not change for dimuon distributions or hadron colliders. For non-degenerate doubly charged masses in MLRSM in Fig. 14, maximum number of same di-lepton

SM background: $pp \rightarrow 4l$					
$4e$	No cuts: $\sigma = 9.1$ [102.6] fb				
	After cuts: $\sigma = 0.0071$ [0.153] fb, N = 28 [3825]				
4μ	No cuts: $\sigma = 9.1$ [100.6] fb				
	After cuts: $\sigma = 0.022$ [0.62] fb, N = 88 [15 167]				
BSM signal: $pp \rightarrow H^{++}H^{--} \rightarrow 4l$		HTM		LRSM	
		NH	IH	$v_R = 6$ TeV	$v_R = 15$ TeV
$4e$	No cuts:	0.0038 fb [0.39 fb]	0.0109 fb [1.11 fb]	0.0029 fb [0.87 fb]	0.136 fb [19.6 fb]
	After cuts:	0.00032 fb N= 1.3 [0.020 fb] [N= 484]	0.00092 fb N= 3.7 [0.059 fb] [N= 1459]	0.00026 fb N= 1.1 [0.0407 fb] [N= 1032]	0.0116 fb N= 45 [0.98 fb] N=[24 492]
4μ	No cuts:	0.0092 [1.086 fb]	0.0039 fb [0.48 fb]	0.0029 fb [0.87 fb]	0.136 fb [19.6 fb]
	After cuts:	0.0031 N= 11.5 [0.202 fb] [N= 5057]	0.00132 fb N= 5.3 [0.090 fb] [N= 2262]	0.001 fb N= 4 [0.181 fb] [N= 4509]	0.048 fb N= 180 [3.9 fb] N=[97 199]

Table 16: Four lepton signals for doubly charged scalar pair production with subsequent decays $pp \rightarrow H^{++}H^{--} \rightarrow 4l$ for $M_{H^{\pm\pm}} = 1000$ GeV and $\sqrt{s} = 14$ [100] TeV. In order to maximize signals in electron and muon channels we have applied different parameter sets from Tab. 10 (for HTM) and Tab. 13 (MLRSM), see the main text for details. "N" estimates the number of final events with assumed luminosity $L = 4 \text{ ab}^{-1} = 4000 \text{ fb}^{-1}$ for HL-LHC [63] and $L = 25 \text{ ab}^{-1} = 25000 \text{ fb}^{-1}$ for FCC-hh [189].

events are with an invariant mass peak around $m_{H_2^{\pm\pm}} = 500$ GeV and that around $m_{H_1^{\pm\pm}} = 700$ GeV is much smaller, as expected. Comparing HTM plots (second row) with non-degenerate MLRSM plots (bottom row), we can see that SSDL signals are shifted between both cases for both m_{ee} and ΔR_{ee} distributions.

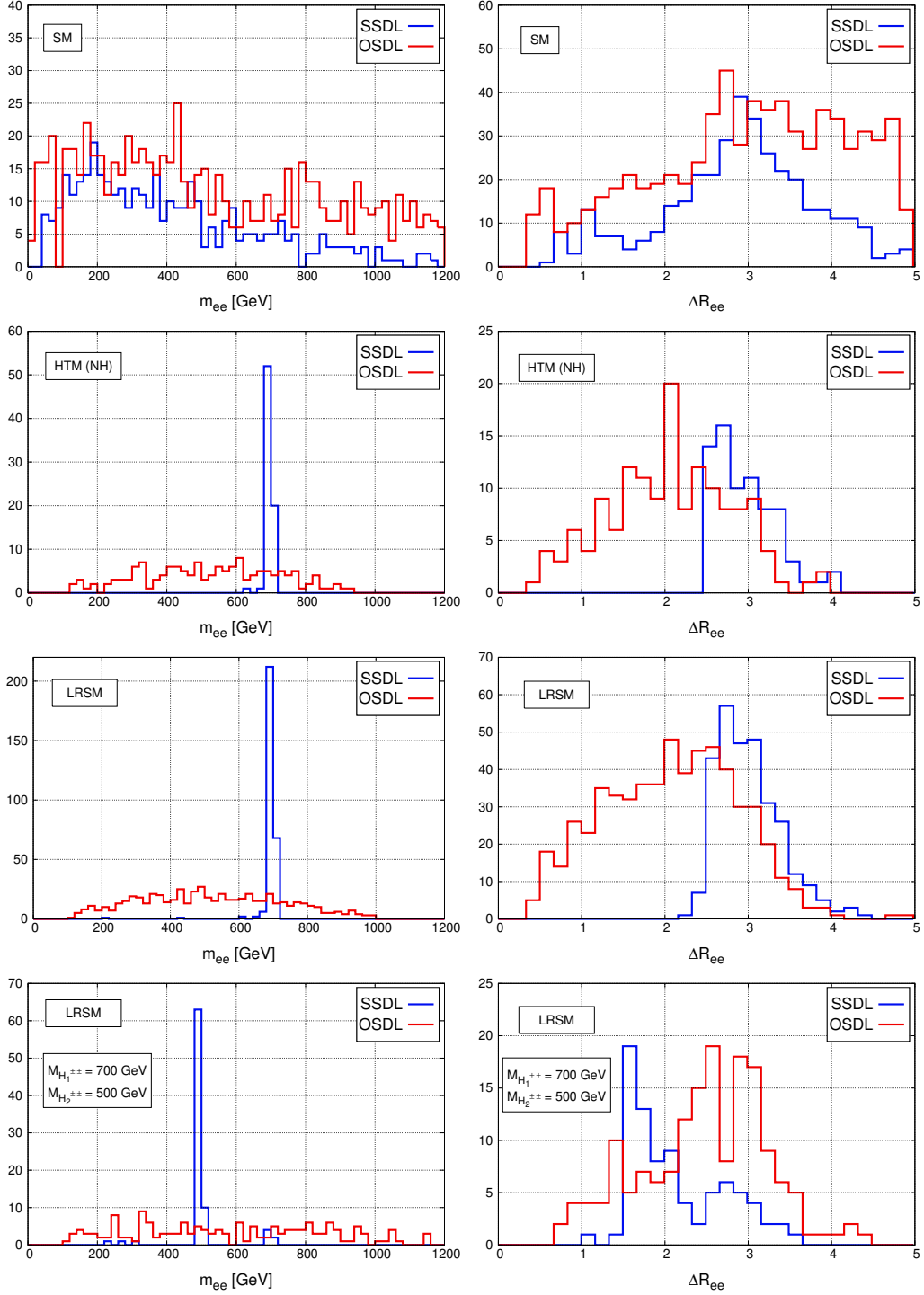


Figure 14: Dilepton distributions for $e^+e^- \rightarrow 4e$. In the left column m_{ee} distributions are shown for the SM background (top figure); HTM model with NH scenario and benchmark parameters as given in Tab.15 (second figure); MLRSM with benchmark parameters for $v_R = 6$ TeV as given in Tab.15 (third figure). The bottom, last row plots are for MLRSM with $m_{H_1^{\pm\pm}} = 700$ GeV and $m_{H_2^{\pm\pm}} = 500$ GeV. On right, analogous figures for the $e - e$ separation observable ΔR_{ee} are given.

6 Conclusions and outlook

The doubly charged Higgs bosons $H^{\pm\pm}$ pair production at e^+e^- and pp colliders, with their subsequent decays to four charged leptons can give a very clear signal when searching for non-standard scalar particles effects without missing energy. We discuss a relation between vacuum expectation value of the triplet v_Δ and $H^{\pm\pm}$ couplings with leptons, taking into account constraints on v_Δ coming from low energy studies connected with the ρ -parameter, muon $(g-2)_\mu$, lepton flavor violation, e^+e^- , LHC processes, and neutrino oscillations (normal and inverse mass scenarios). The low energy experiments rule out v_Δ below 10 eV (for $M_{H^{\pm\pm}} \sim 700$ GeV) both for normal and inverted hierarchy, the strongest limit for non-zero mass of the lightest neutrino comes from LFV $\mu \rightarrow 3e$, see Fig. 5 and Tab. 5. As the Yukawa $H^{\pm\pm} - l - l'$ couplings are inversely proportional to v_Δ , the t-channel $e^+e^- \rightarrow H^{++}H^{--}$ process could be enhanced, however, neutrino oscillation data makes it very small, and the s-channel dominates over allowed v_Δ , see Fig. 7. Similarly, Yukawa $H_{1,2}^{\pm\pm} - l - l'$ couplings in MLRSM could dominate the cross section for $e^+e^- \rightarrow H_{1,2}^{++}H_{1,2}^{--}$, however, e^+e^- Bhabha and Møller processes makes it below the s-channel contribution, see Fig. 8. These two cases show nicely how important are present SM and LFV experimental data, allowing to predict properly BSM signals in colliders studies. Altogether, $H^{\pm\pm}$ pair production processes in HTM and MLRSM are comparable, larger in MLRSM. The contributions of individual $H_1^{\pm\pm}$ and $H_2^{\pm\pm}$ pair production channels in MLRSM and $H^{\pm\pm}$ in HTM are discussed. The contributions change with HL-LHC and FCC-ee/CEPC center of mass energies. QCD NLO k-factors are discussed and taken into account in the $H^{\pm\pm}$ pair production and four lepton processes. Taking into account present bounds on MLRSM parameters, additional contributions from both the right-handed current and extra scalar particles within MLRSM do not make much difference.

Still, assuming non-universality of leptonic decays, and due to fields richness of MLRSM, branching ratios for the $H^{\pm\pm}$ decays can be very different in both models, leading to different final signals.

We discuss the same $H^{\pm\pm}$ masses in both models. Taking into account all leptonic decays, we show that LHC experimental data still allow for $H^{\pm\pm}$ mass as small as 700 GeV. We take it as the first scenario, the second is for $H^{\pm\pm}$ mass equal to 1 TeV.

We discuss carefully possible decay channels and finally, we make predictions for the complete process $pp \rightarrow H^{++}H^{--} \rightarrow 4l$. In both models, we optimised parameters to maximise separately $e^+e^-(pp) \rightarrow 4e$ and $e^+e^-(pp) \rightarrow 4\mu$ signals, at the same time being in agreement with all experimental constraints coming from other considered processes.

The results are gathered in Tab. 15 and Tab. 16. There are many interesting conclusions that we can draw from them, as discussed in section 5.5. In general, due to kinematic cuts and chosen parameters, 4μ signals dominate over $4e$. The latter signals are in most cases at best at the level of the SM background, both for lepton and hadron colliders. This situation gives a way to discriminate the two models. In fact, the most interesting situation in which v_R in MLRSM is relatively large, above sensitivity of LHC (we took $v_R = 15$ TeV) does not give too strict constraints on the model parameters, and the discovery signals can be large for $e^+e^-(pp) \rightarrow 4\mu$. In particular, for the HL-LHC and FCC-hh cases, detectable signals which would exceed the SM background are possible only for MLRSM. This conclusion is rather stable over changes of model parameters, for considered kinematic cuts. Though analysis of dilepton distributions can help further in detection of small BSM signals which are comparable or below the SM background, they are similar in patterns for both models and does not help in discrimination between HTM and MLRSM.

With the most straightforward setups, relying only on the production and decay total counting of events, we can discriminate models, and show in which channels we should look for that. We think that our work is an exemplary case study and from the minimal considerations, more sophisticated approaches can follow. As an outlook for further studies, a discussion of $e^\pm e^\pm \mu^\mp \mu^\mp$ and $e^\pm e^\mp \mu^\pm \mu^\mp$ channels might also be enjoyable, as well as four-lepton signal analysis with final state

polarisation. It will be also interesting to investigate for chosen benchmark points processes with single produced $H^{\pm\pm}$ or single charged Higgs scalars, and associated gauge bosons. For such cases the SM background will be much larger but it does not exclude positive BSM signals.

Acknowledgements

We thank Joydeep Chakraborty for useful discussions and Dipankar Das for his help with the FeynRules model. The research has been supported by the Polish National Science Center (NCN) under grant 2015/17/N/ST2/04067, COST (European Cooperation in Science and Technology) Action CA16201 PARTICLEFACE and the research activities co-financed by the funds granted under the Research Excellence Initiative of the University of Silesia in Katowice.

7 Appendix.

7.1 The HTM scalar potential and fields

The Higgs Triplet Model extends the Higgs sector of the SM by adding one scalar $SU(2)_L$ triplet (Δ) with hypercharge $Y = 2$ to the Standard Model doublet Φ (following the convention $Q = \frac{1}{2}Y + T_3$).

The most general scalar potential is given by [190]

$$V = -m_\Phi^2 (\Phi^\dagger \Phi) + \frac{\lambda}{4} (\Phi^\dagger \Phi)^2 + M_\Delta^2 \text{Tr} (\Delta^\dagger \Delta) + [\mu (\Phi^T i\sigma_2 \Delta^\dagger \Phi) + \text{h.c.}] \\ + \lambda_1 (\Phi^\dagger \Phi) \text{Tr} (\Delta^\dagger \Delta) + \lambda_2 [\text{Tr} (\Delta^\dagger \Delta)]^2 + \lambda_3 \text{Tr} [(\Delta^\dagger \Delta)^2] + \lambda_4 \Phi^\dagger \Delta \Delta^\dagger \Phi. \quad (7.1)$$

Without loss of generality we can take all the parameters to be real [191, 192]. Denoting by v_Δ and v_Φ the vacuum expectation values (VEV's) of the doublet and triplet

$$m_\Phi^2 = \frac{\lambda}{4} v_\Phi^2 + \frac{(\lambda_1 + \lambda_4)}{2} v_\Delta^2 - \sqrt{2}\mu v_\Delta, \quad (7.2a)$$

$$M_\Delta^2 = -(\lambda_2 + \lambda_3) v_\Delta^2 - \frac{(\lambda_1 + \lambda_4)}{2} v_\Phi^2 + \frac{\mu}{\sqrt{2}} \frac{v_\Phi^2}{v_\Delta}. \quad (7.2b)$$

We represent the scalar multiplets in the following way

$$\Phi = \frac{1}{\sqrt{2}} \begin{pmatrix} \sqrt{2}w_\Phi^+ \\ v_\Phi + h_\Phi + iz_\Phi \end{pmatrix}, \quad \Delta = \frac{1}{\sqrt{2}} \begin{pmatrix} w_\Delta^+ & \sqrt{2}\delta^{++} \\ v_\Delta + h_\Delta + iz_\Delta & -w_\Delta^+ \end{pmatrix}. \quad (7.3)$$

The triplet VEV v_Δ is expected to be at most at the order $\mathcal{O}(1)$ GeV to keep the electroweak ρ -parameter ~ 1 [178, 190, 193–195] (see section 3.2 for more details). The electroweak VEV is then given by

$$v = \sqrt{v_\Phi^2 + 2v_\Delta^2} \simeq 246 \text{ GeV}. \quad (7.4)$$

The Yukawa sector contains the complete SM Yukawa Lagrangian along with an extra part for the triplet

$$\mathcal{L}_Y^\Delta = \frac{1}{2} \mathcal{Y}_{\ell\ell'} L_\ell^T C^{-1} i\sigma_2 \Delta L_{\ell'} + \text{h.c.}, \quad (7.5)$$

where, C is the charged conjugation operator, $\mathcal{Y}_{\ell\ell'}$ is the symmetric Yukawa matrix and

$$L_\ell = \begin{pmatrix} \nu_\ell \\ \ell \end{pmatrix}_L, \quad [\ell = e, \mu, \tau], \quad (7.6)$$

are the left handed $SU(2)$ doublets for the three lepton generations. After spontaneous symmetry breaking (SSB), the Yukawa couplings in Eq. (7.5) will lead to the Majorana mass matrix for the left handed neutrinos. The same term in the Lagrangian is responsible for the interaction between doubly charged scalar particles and charged leptons. The $H^{\pm\pm} - l^\mp - l'^\mp$ vertex breaks the lepton number (see sections 2,3). The fields, $\delta^{\pm\pm} = H^{\pm\pm}$, represent the doubly charged scalar with the mass

$$M_{H^{\pm\pm}}^2 = \frac{\mu v_\Phi^2}{\sqrt{2}v_\Delta} - \frac{\lambda_4}{2}v_\Phi^2 - \lambda_3 v_\Delta^2. \quad (7.7)$$

To get physical states for neutral and singly charged particles, appropriate rotation of fields in the CP-odd and CP-even sectors must follow

$$\begin{pmatrix} G_0 \\ A \end{pmatrix} = \begin{pmatrix} \cos \beta' & \sin \beta' \\ -\sin \beta' & \cos \beta' \end{pmatrix} \begin{pmatrix} z_\Phi \\ z_\Delta \end{pmatrix}, \quad \text{with } \tan \beta' = \frac{2v_\Delta}{v_\Phi}, \quad (7.8)$$

$$\begin{pmatrix} h \\ H \end{pmatrix} = \begin{pmatrix} \cos \alpha & \sin \alpha \\ -\sin \alpha & \cos \alpha \end{pmatrix} \begin{pmatrix} h_\Phi \\ h_\Delta \end{pmatrix}, \quad \text{with } \tan 2\alpha = \frac{\sqrt{2}\mu v_\Phi - (\lambda_1 + \lambda_4)v_\Delta v_\Phi}{\frac{\mu v_\Phi^2}{2\sqrt{2}v_\Delta} + (\lambda_2 + \lambda_3)v_\Delta^2 - \frac{\lambda v_\Phi^2}{4}}. \quad (7.9)$$

Further, we use an approximation $\sin \alpha \sim \frac{2v_\Delta}{v_\Phi} \rightarrow 0$ [86], neutral scalar masses becomes

$$M_A^2 = \frac{\mu}{\sqrt{2}v_\Delta}(v_\Phi^2 + 4v_\Delta^2), \quad (7.10)$$

$$M_h^2 = \lambda v_\Phi^2 \cos^2 \alpha + \left(\frac{\mu v_\Phi^2}{\sqrt{2}v_\Delta} + 2v_\Delta^2(\lambda_2 + \lambda_3) \right) \sin^2 \alpha + 2 \left(v_\Phi v_\Delta(\lambda_1 + \lambda_4) - \sqrt{2}\mu v_\Phi \right) \cos \alpha \sin \alpha, \quad (7.11)$$

$$M_H^2 = \lambda v_\Phi^2 \sin^2 \alpha + \left(\frac{\mu v_\Phi^2}{\sqrt{2}v_\Delta} + 2v_\Delta^2(\lambda_2 + \lambda_3) \right) \cos^2 \alpha - 2 \left(v_\Phi v_\Delta(\lambda_1 + \lambda_4) - \sqrt{2}\mu v_\Phi \right) \cos \alpha \sin \alpha. \quad (7.12)$$

In the singly charged sector rotation of fields and masses are the following

$$\begin{pmatrix} G^\pm \\ H^\pm \end{pmatrix} = \begin{pmatrix} \cos \beta & \sin \beta \\ -\sin \beta & \cos \beta \end{pmatrix} \begin{pmatrix} w_\Phi^\pm \\ w_\Delta^\pm \end{pmatrix}, \quad \text{with } \tan \beta = \frac{\sqrt{2}v_\Delta}{v_\Phi}, \quad (7.13)$$

to obtain the charged Goldstone (G^\pm) along with a singly charged scalar (H^\pm) with mass

$$M_{H^\pm}^2 = \frac{(2\sqrt{2}\mu - \lambda_4 v_\Delta)}{4v_\Delta}(v_\Phi^2 + 2v_\Delta^2). \quad (7.14)$$

The H^\pm and $H^{\pm\pm}$ scalar's squared masses (7.14) and (7.7) contain terms proportional to v_Φ^2 and are inversely proportional to the triplet VEV v_Δ , which should be less than $\mathcal{O}(1 \text{ GeV})$ (see section 3.2). That means that M_{H^\pm} , $M_{H^{\pm\pm}}$ can be at the level of a few hundred GeV or higher. Latest LHC bounds on the doubly charged scalar masses vary from 450 to 870 GeV, depending on the decay modes, assuming that $\text{BR}(H^{\pm\pm} \rightarrow l^\pm l^\pm) \geq 10\%$ [55]. Photon-photon fusion studies [196] set a bound on $M_{H^{\pm\pm}}$ at the level of 748 GeV. Limits coming from e^+e^- colliders are significantly lower, from L3 Collaboration (LEP) it is about 100 GeV [102]. This bound comes with assumption that the t-channel is negligible (Fig. 1) as suppressed by the low $H^{\pm\pm} - l - l$ coupling. For singly charged scalar masses the mass bound is even lower, $M_{H^\pm} = 80 \text{ GeV}$ [124].

In this paper we assume that the neutral and charged scalars' masses are degenerated³, that means $M_{H^{\pm\pm}} = M_{H^\pm} = M_H = M_A$. That choice protects proper ranges of the T-parameter and potential unitarity for $v_\Delta \lesssim 1 \text{ GeV}$ [86, 87].

³Even though the mass split $M_H \equiv M_{H^{\pm\pm}} - M_{H^\pm}$ is proportional to v_Φ^2 , the electroweak precision data ($h \rightarrow \gamma\gamma$) gives a limit $|M_{H^{\pm\pm}} - M_{H^\pm}| \leq 40 \text{ GeV}$ [83–85].

7.2 The MLRSM scalar potential and fields

The spontaneous symmetry breaking occurs in two steps: $SU(2)_R \otimes U(1)_{B-L} \rightarrow U(1)_Y$, and $SU(2)_L \otimes U(1)_Y \rightarrow U(1)_{em}$. To achieve this symmetry breaking we choose a traditional spectrum of Higgs sector multiplets with a bidoublet and two triplets [29, 38, 39, 88, 197, 198].

$$\phi = \begin{pmatrix} \phi_1^0 & \phi_1^+ \\ \phi_2^- & \phi_2^0 \end{pmatrix} \equiv [2, 2, 0], \quad (7.15)$$

$$\Delta_{L(R)} = \begin{pmatrix} \delta_{L(R)}^+/\sqrt{2} & \delta_{L(R)}^{++} \\ \delta_{L(R)}^0 & -\delta_{L(R)}^+/\sqrt{2} \end{pmatrix} \equiv [3(1), 1(3), 2], \quad (7.16)$$

where the quantum numbers in square brackets are given for $SU(2)_L$, $SU(2)_R$ and $U(1)_{B-L}$ groups, respectively.

The vacuum expectation values (VEVs) of the scalar fields can be recast in the following form:

$$\langle \phi \rangle = \begin{pmatrix} \kappa_1/\sqrt{2} & 0 \\ 0 & \kappa_2/\sqrt{2} \end{pmatrix}, \quad \langle \Delta_{L,R} \rangle = \begin{pmatrix} 0 & 0 \\ v_{L,R}/\sqrt{2} & 0 \end{pmatrix}. \quad (7.17)$$

VEVs of the right-handed triplet (Δ_R) and the bi-doublet (ϕ), propel the respective symmetry breaking: $SU(2)_R \otimes U(1)_{B-L} \rightarrow U(1)_Y$, and $SU(2)_L \otimes U(1)_Y \rightarrow U(1)_{em}$. As $v_L \ll \kappa_{1,2} \ll v_R$, we take safely $v_L = 0$.

The full scalar potential includes left and right-handed triplets [39, 198, 199]:

$$\begin{aligned} V(\phi, \Delta_L, \Delta_R) = & \\ & + \lambda_1 \left\{ \left(\text{Tr} [\phi^\dagger \phi] \right)^2 \right\} + \lambda_2 \left\{ \left(\text{Tr} [\tilde{\phi} \phi^\dagger] \right)^2 + \left(\text{Tr} [\tilde{\phi}^\dagger \phi] \right)^2 \right\} \\ & + \lambda_3 \left\{ \text{Tr} [\tilde{\phi} \phi^\dagger] \text{Tr} [\tilde{\phi}^\dagger \phi] \right\} \\ & + \lambda_4 \left\{ \text{Tr} [\phi^\dagger \phi] \left(\text{Tr} [\tilde{\phi} \phi^\dagger] + \text{Tr} [\tilde{\phi}^\dagger \phi] \right) \right\} \\ & + \rho_1 \left\{ \left(\text{Tr} [\Delta_L \Delta_L^\dagger] \right)^2 + \left(\text{Tr} [\Delta_R \Delta_R^\dagger] \right)^2 \right\} \\ & + \rho_2 \left\{ \text{Tr} [\Delta_L \Delta_L] \text{Tr} [\Delta_L^\dagger \Delta_L^\dagger] + \text{Tr} [\Delta_R \Delta_R] \text{Tr} [\Delta_R^\dagger \Delta_R^\dagger] \right\} \\ & + \rho_3 \left\{ \text{Tr} [\Delta_L \Delta_L^\dagger] \text{Tr} [\Delta_R \Delta_R^\dagger] \right\} \\ & + \rho_4 \left\{ \text{Tr} [\Delta_L \Delta_L] \text{Tr} [\Delta_R^\dagger \Delta_R^\dagger] + \text{Tr} [\Delta_L^\dagger \Delta_L^\dagger] \text{Tr} [\Delta_R \Delta_R] \right\} \\ & + \alpha_1 \left\{ \text{Tr} [\phi^\dagger \phi] \left(\text{Tr} [\Delta_L \Delta_L^\dagger] + \text{Tr} [\Delta_R \Delta_R^\dagger] \right) \right\} \\ & + \alpha_2 \left\{ \text{Tr} [\phi \tilde{\phi}^\dagger] \text{Tr} [\Delta_R \Delta_R^\dagger] + \text{Tr} [\phi^\dagger \tilde{\phi}] \text{Tr} [\Delta_L \Delta_L^\dagger] \right\} \\ & + \alpha_2^* \left\{ \text{Tr} [\phi^\dagger \tilde{\phi}] \text{Tr} [\Delta_R \Delta_R^\dagger] + \text{Tr} [\tilde{\phi}^\dagger \phi] \text{Tr} [\Delta_L \Delta_L^\dagger] \right\} \\ & + \alpha_3 \left\{ \text{Tr} [\phi \phi^\dagger \Delta_L \Delta_L^\dagger] + \text{Tr} [\phi^\dagger \phi \Delta_R \Delta_R^\dagger] \right\} \\ & - \mu_1^2 \text{Tr} [\phi^\dagger \phi] - \mu_2^2 (\text{Tr} [\tilde{\phi} \phi^\dagger] + \text{Tr} [\tilde{\phi}^\dagger \phi]) \\ & - \mu_3^2 (\text{Tr} [\Delta_L \Delta_L^\dagger] + \text{Tr} [\Delta_R \Delta_R^\dagger]). \end{aligned} \quad (7.18)$$

Though in HTM and MLRSM we have left-handed triplets, HTM is not a simple subset of MLRSM as the scalar potentials, SSB mechanism, VEVs and underlying physics which follows are different. The scalar potential (7.18) in MLRSM is much more complicated than its counterpart in HTM: in MLRSM the triplet Δ_L is intertwined with right-handed multiplet Δ_R and bidoublet ϕ . It makes relations among physical and unphysical Higgs boson fields rather complex in MLRSM. Here significant are relations between the α_3 scalar potential parameter (which includes a mixture of a bidoublet and triplet fields) and ρ_1, ρ_3 scalar potential parameters for doubly charged Higgs boson masses given in Eq. (7.28) and Eq. (7.29) below. In correlation with experimental constraints for singly charged and neutral scalar fields, these parameters give the lowest limits for doubly charged Higgs masses, as discussed in [169]. Moreover, due to Yukawa couplings of left- and right-handed leptons with bidoublet in Eq. (7.38), the doubly charged Higgs bosons in both models couple differently to leptons. Consequently, both model neutrino mass relations are different, in HTM restricted directly by neutrino oscillation data, as discussed in the main text.

After spontaneous symmetry breaking of the potential Eq. (7.18), the mass matrix which includes $M_{H_0^0}$ can be written in the following form (for details, see [198])

$$M = \begin{pmatrix} 2\epsilon^2\lambda_1 & 2\epsilon^2\lambda_4 & \alpha_1\epsilon \\ 2\epsilon^2\lambda_4 & \frac{1}{2}[4(2\lambda_2 + \lambda_3)\epsilon^2 + \alpha_3] & 2\alpha_2\epsilon \\ \alpha_1\epsilon & 2\alpha_2\epsilon & 2\rho_1 \end{pmatrix}. \quad (7.19)$$

Expanding eigenvalues of this matrix in a small $\epsilon = \sqrt{\kappa_1^2 + \kappa_2^2}/v_R$ parameter we get

$$M_{H_0^0}^2 = 2 \left(\lambda_1 - \frac{\alpha_1^2}{4\rho_1} \right) (\kappa_1^2 + \kappa_2^2) \simeq (125 \text{ GeV})^2, \quad (7.20)$$

The analytic mass formulas for other scalar bosons in MLRSM as a function of quartic couplings and v_R can be written as [56]

$$M_{H_1^0}^2 = \frac{1}{2}\alpha_3 v_R^2 > (10 \text{ TeV})^2, \quad (7.21)$$

$$M_{H_2^0}^2 = 2\rho_1 v_R^2, \quad (7.22)$$

$$M_{H_3^0}^2 = \frac{1}{2}(\rho_3 - 2\rho_1)v_R^2 > (55.4 \text{ GeV})^2, \quad (7.23)$$

$$M_{A_1^0}^2 = \frac{1}{2}\alpha_3 v_R^2 - 2(\kappa_1^2 + \kappa_2^2)(2\lambda_2 - \lambda_3) > (10 \text{ TeV})^2, \quad (7.24)$$

$$M_{A_2^0}^2 = \frac{1}{2}(\rho_3 - 2\rho_1)v_R^2 \quad (7.25)$$

$$M_{H_1^\pm}^2 = \frac{1}{2}(\rho_3 - 2\rho_1)v_R^2 + \frac{1}{4}\alpha_3(\kappa_1^2 + \kappa_2^2), \quad (7.26)$$

$$M_{H_2^\pm}^2 = \frac{1}{2}\alpha_3 v_R^2 + \frac{1}{4}\alpha_3(\kappa_1^2 + \kappa_2^2) > (10 \text{ TeV})^2, \quad (7.27)$$

$$M_{H_1^{\pm\pm}}^2 = \frac{1}{2}(\rho_3 - 2\rho_1)v_R^2 + \frac{1}{2}\alpha_3(\kappa_1^2 + \kappa_2^2), \quad (7.28)$$

$$M_{H_2^{\pm\pm}}^2 = 2\rho_2 v_R^2 + \frac{1}{2}\alpha_3(\kappa_1^2 + \kappa_2^2), \quad (7.29)$$

where κ_1, κ_2 are VEVs of the bidoublet and $\sqrt{\kappa_1^2 + \kappa_2^2}$ has to be equal to the electroweak symmetry breaking scale v , see (7.4). We assume that $\kappa_1 = v = 246 \text{ GeV}$ and $\kappa_2 \rightarrow 0$. Some explicit masses of Higgs bosons relevant for $H^{\pm\pm}$ branching ratios in section 5.3 comes from restrictions discussed in [56].

In MLRSM relations among physical and unphysical fields (“G” stands for Goldstone modes) are

$$\phi_1^0 \simeq \frac{1}{\sqrt{2}} [H_0^0 + i\tilde{G}_1^0], \quad (7.30)$$

$$\phi_2^0 \simeq \frac{1}{\sqrt{2}} [H_1^0 - iA_1^0], \quad (7.31)$$

$$\delta_R^0 = \frac{1}{\sqrt{2}} (H_2^0 + iG_2^0), \quad \delta_L^0 = \frac{1}{\sqrt{2}} (H_3^0 + iA_2^0), \quad (7.32)$$

$$\delta_L^+ = H_1^+, \quad \delta_R^+ \simeq G_R^+, \quad (7.33)$$

$$\phi_1^+ \simeq H_2^+, \quad \phi_2^+ \simeq G_L^+, \quad (7.34)$$

$$\delta_R^{\pm\pm} = H_1^{\pm\pm}, \quad \delta_L^{\pm\pm} = H_2^{\pm\pm}. \quad (7.35)$$

The structure of Higgs potential in a general framework of left-right symmetric models has been discussed in details in [198, 199]. We adopted it in our studies. In particular, to retain the invariant Majorana Yukawa couplings of the leptons to the Higgs triplet, the potential does not include the terms with all multiplets (bidoublet, two triplets) present simultaneously, e.g. $Tr[\phi\Delta_R\phi^\dagger\Delta_L^\dagger] + h.c.$ (in [198, 199] denoted as the β_i -type terms). In the limit of vanishing β_i terms the doubly charged Higgs scalar 2×2 mass matrix is diagonal and does not include the mixed mass terms $\delta_L^{\pm\pm}\delta_R^{\mp\mp}$. These restrictions simplify a form of doubly charged mass terms, as given in the manuscript, Eqs. (7.28) and (7.29). It means that in MLRSM (and other extensions when gauge couplings $g_L \neq g_R$), doubly charged Higgs triplets in $\Delta_{L,R}$ are physical fields. There is no mixing angle between two doubly charged Higgs bosons in MLRSM and the mass matrix which appears there for unphysical fields is diagonal from the very beginning. This no-mixing feature is also true in general where the β_i -type terms are allowed, in the limit $v_R \gg \kappa_{1,2}$.

7.3 $H_1^{\pm\pm}$ and $H_2^{\pm\pm}$ couplings with leptons in MLRSM

In MLRSM due to additional heavy states the neutrino sector and Yukawa couplings are more complicated than in HTM. Here we argue that due an energy scales difference between v_R and the low-energy bidoublet VEV $\kappa \equiv \sqrt{\kappa_1^2 + \kappa_2^2}$, $\kappa \ll v_R$, the see-saw mechanism is possible and low energy LFV signals are suppressed due to high v_R and heavy neutrino masses. To see, this, the most general doubly charged couplings to leptons, which takes into account mixing matrices, reads [39]

$$\begin{aligned} \delta_R^{++}\bar{l}_L^c h_M l'_R + h.c. &= \frac{1}{\sqrt{2}v_R} \sum_{l,k} \left\{ \delta_R^{++} \left[l_l^T C \left(K_R^T (M_\nu)_{diag} K_R \right)_{lk} P_R l_k \right] \right. \\ &\quad \left. + \delta_R^{--} \left[\bar{l}_l \left(K_R^\dagger (M_\nu)_{diag} K_R^* \right)_{lk} P_L C \bar{l}_k^T \right] \right\}, \end{aligned} \quad (7.36)$$

$$\begin{aligned} \delta_L^{++}\bar{l}_R^c h_M l'_L + h.c. &= \frac{1}{\sqrt{2}v_R} \sum_{l,k} \left\{ \delta_L^{++} \left[l_k^T C \left(K_L^T X K_L^* \right)_{kl} P_L l_l \right] \right. \\ &\quad \left. + \delta_L^{--} \left[\bar{l}_k \left(K_L^T X^* K_L^* \right)_{kl} P_R C \bar{l}_l^T \right] \right\} \end{aligned} \quad (7.37)$$

where $X = (K_L^* K_R^T) (M_\nu)_{diag} (K_R K_L^\dagger)$.

These couplings originate from the Yukawa part of the Lagrangian for additional scalar triplets and a bidoublet ϕ :

$$- \bar{L}_L \left[h_l \phi + \tilde{h}_l \tilde{\phi} \right] L_R - i \bar{L}_R^c \sigma_2 \Delta_L h_M L_L - i \bar{L}_L^c \sigma_2 \Delta_R h_M L_R + h.c. \quad (7.38)$$

Uniqueness of left- and right-handed couplings for positively and negatively charged doubly charged Higgs bosons to leptons in Eq. (7.36) and Eq. (7.37) is due to the Feynman rules and flow of the charged currents in vertices, as explained in length in [200]. The relations between

physical and unphysical scalar, gauge and fermion fields are embedded in our FeynRules package to calculate branching ratios and cross sections. We also mentioned that for neutral scalars, due to the bidoublet coupling in Eq. (7.38) to both left- and right-handed leptons, there is a mixture of scalar fields coming from left and right triplets, however, as given in Eqs. (7.30)-(7.35), for $v_R \gg \kappa_{1,2}$, most of the mixings are negligible.

Diagonalization of the resulting neutrino mass matrix

$$M_\nu = \begin{pmatrix} 0 & M_D \\ M_D^T & M_R \end{pmatrix}, \quad M_R = \sqrt{2}h_M v_R, \quad (7.39)$$

goes with the help of a unitary 6×6 matrix U

$$U^T M_\nu U = (M_\nu)_{diag}, \quad U = \begin{pmatrix} K_L^* \\ K_R \end{pmatrix}.$$

This procedure leads to the introduction of the K_L and K_R submatrices in Eq. (7.36) and Eq. (7.37) [145, 201].

The charged lepton mass matrix is diagonalised by $V_{L,R}^l$

$$V_L^{l\dagger} M_l V_R^l = (M_l)_{diag}.$$

Apart from charged lepton and neutrino mass terms, Lagrangian Eq. (7.38) contains scalar-lepton interactions too.

$(M_\nu)_{diag}$ contains 3 light neutrinos, their contribution to the couplings Eq. (7.37) and Eq. (7.36) are negligible. To see amount of heavy neutrinos contributions to Eq. (7.37) and Eq. (7.36), we note that structure of K_L and K_R mixing matrices are the following [145, 201]

$$(K_L)_{l_i \nu_j} = \begin{pmatrix} e & \mu & \tau \\ \left. \begin{pmatrix} \dots \\ \dots \\ \dots \end{pmatrix} \right\} \text{light neutrinos} \\ \left. \begin{pmatrix} \dots \\ \dots \\ \dots \end{pmatrix} \right\} \text{heavy neutrinos} \end{pmatrix} \sim \begin{pmatrix} \mathcal{O}(1) \\ \mathcal{O}\left(\frac{1}{m_N}\right) \end{pmatrix}, \quad (7.40)$$

$$(K_R)_{l_i \nu_j} = \begin{pmatrix} e & \mu & \tau \\ \left. \begin{pmatrix} \dots \\ \dots \\ \dots \end{pmatrix} \right\} \text{light neutrinos} \\ \left. \begin{pmatrix} \dots \\ \dots \\ \dots \end{pmatrix} \right\} \text{heavy neutrinos} \end{pmatrix} \sim \begin{pmatrix} \mathcal{O}\left(\frac{1}{m_N}\right) \\ \mathcal{O}(1) \end{pmatrix}. \quad (7.41)$$

Off-diagonal elements for heavy neutrinos couplings in K_R are typically also of the order of inverse heavy neutrino mass scale, that is why LFV couplings of leptons with doubly charged Higgs bosons are strongly suppressed, $\delta_{L,R} - l - l$ off-diagonal lepton couplings are suppressed by $1/m_N^2$ when comparing to diagonal cases.

For reasons discussed in [149] and more extensively in [202], we take seesaw diagonal light-heavy neutrino mixings. It means that W_1 couples mainly to light neutrinos, while W_2 couples to the heavy ones.

To summarize, unlike in the HTM case, the $H^{\pm\pm} - l^\mp - l^\mp$ vertex does not depend on the light neutrino mixing. With $v_L = 0$ the MLRSM realizes the seesaw type-I mechanism and the light neutrino mass is due to the existence of additional heavy neutrino states and v_R scale.

We should note that it is not natural and very hard to create non-decoupling mixings for non-diagonal K_L and K_R matrix elements, even when some symmetries are considered in type-I seesaw models [202].

7.4 Supplemental material for phenomenological studies of $H^{\pm\pm}$ scalar particles

Diagrams in Fig. 4 present the contribution from the singly and doubly charged scalar particles to lepton flavour violating processes and to muon $(g-2)_\mu$. Those diagrams contain vertices $H^{\pm\pm} - l_i - l_j$ and $H^\pm - l_i - \nu_j$ which origin from the Yukawa part of the Lagrangian, combining the Standard Model Yukawa term with the triplet part Eq. (7.5)

$$\mathcal{L}_Y = \mathcal{L}_Y^\Phi + \mathcal{L}_Y^\Delta = -y_{ij} \overline{L}_L^i \Phi l_R^j + \mathcal{Y}_{ij} \overline{L}_L^{i c} i\sigma_2 \Delta L_L^j + \text{h.c.} \quad (7.42)$$

From Eq. (7.42) we obtain the interaction between charged leptons and a doubly charged scalar and the interaction of a singly charged scalar with a charged lepton and neutrino. Taking into account Eq. (7.13) and Eq. (7.4) and keeping in mind that $y_{ij} \propto \frac{1}{v_\Phi}$ is a SM diagonal matrix

$$\mathcal{V}^{\pm\pm} = \begin{cases} l_i^+ - l_j^+ - H^{--} = i (\mathcal{Y}_{ij} + \mathcal{Y}_{ji}) \\ l_i^- - l_j^- - H^{++} = i (\mathcal{Y}_{ij}^* + \mathcal{Y}_{ji}^*) \end{cases}, \quad (7.43)$$

$$\mathcal{V}_\Delta^\pm = \begin{cases} \tilde{\nu}_i - l_j^+ - H^- = \frac{i}{\sqrt{2}} \cos \beta (\mathcal{Y}_{ij} + \mathcal{Y}_{ji}) \\ \nu_i - l_j^- - H^+ = \frac{i}{\sqrt{2}} \cos \beta (\mathcal{Y}_{ij}^* + \mathcal{Y}_{ji}^*) \end{cases} \propto \frac{\sqrt{v_\Phi^2 - 2v_\Delta^2}}{v_\Phi \cdot v_\Delta}, \quad (7.44)$$

$$\mathcal{V}_\Phi^\pm = \begin{cases} \tilde{\nu}_i - l_i^- - H^+ = i \sin \beta y_i \\ \nu_i - l_i^+ - H^- = i \sin \beta y_i \end{cases} \propto \frac{\sqrt{2}v_\Delta}{v_\Phi \sqrt{v_\Phi^2 - 2v_\Delta^2}}. \quad (7.45)$$

Vertices \mathcal{V}_Δ^\pm and $\mathcal{V}_\Delta^{\pm\pm}$ comes from the same part of the Lagrangian and they break the lepton flavour. Vertex \mathcal{V}_Φ^\pm is proportional to v_Δ while vertex \mathcal{V}_Δ^\pm is inversely proportional to the triplet VEV and dominates up to $v_\Delta \sim 10^6$ eV. Since we are interested in lower regions of v_Δ values, its effect is negligible. So, with a good approximation for low values of v_Δ

$$\mathcal{V}_\Delta^\pm \equiv \mathcal{V}^\pm \simeq \frac{1}{\sqrt{2}} \mathcal{V}^{\pm\pm}. \quad (7.46)$$

As we discussed in section 3, the branching ratios of the radiative and μ -to- e conversion depends on the one-loop form factors. From Eq. (3.5), we can read them explicitly

$$\begin{aligned} A_L(q^2) &= -\frac{(\mathcal{Y}^*)_{ei}(\mathcal{Y})_{\mu i}}{24\sqrt{2}G_F\pi^2} \left(\frac{1}{12M_{H^\pm}^2} + \frac{f(r, s_i)}{M_{H^{\pm\pm}}^2} \right), \\ A_R &= -\frac{(\mathcal{Y}^*\mathcal{Y})_{e\mu}}{192\sqrt{2}G_F\pi^2} \left(\frac{1}{8M_{H^\pm}^2} + \frac{1}{M_{H^{\pm\pm}}^2} \right), \end{aligned} \quad (7.47)$$

where $f(r, s_i)$ is given by:

$$f(r, s_i) = \frac{4s_i}{r} + \log(s_i) + \left(1 - \frac{2s_i}{r}\right) \sqrt{1 + \frac{4s_i}{r}} \log \left(\frac{\sqrt{r} + \sqrt{r + 4s_i}}{\sqrt{r} - \sqrt{r + 4s_i}} \right), \quad (7.48)$$

$$r = \frac{-q^2}{m_{H^{\pm\pm}}^2}, \quad s_i = \frac{m_i^2}{m_{H^{\pm\pm}}^2}. \quad (7.49)$$

We have checked with earlier literature and the analytic forms for the CLFV processes are given as [33, 92, 93, 105, 203]:

Radiative lepton decay $l_i \rightarrow l_j \gamma$:

The branching ratios of radiative decay processes can be given by:

$$\text{BR}(l_i \rightarrow l_j \gamma) = 384\pi^2 (4\pi\alpha_{em}) |A_R|^2 \text{BR}(l_i \rightarrow l_j \nu_i \bar{\nu}_j).$$

Therefore the BRs for various radiative decays can be written as:

$$\begin{aligned} \text{BR}(\mu \rightarrow e \gamma) &= \frac{\alpha_{em}}{192\pi} \frac{|(\mathcal{V}^\dagger \mathcal{V})_{e\mu}|^2}{G_F^2} \left(\frac{1}{M_{H^\pm}^2} + \frac{8}{M_{H^{\pm\pm}}^2} \right)^2 \text{BR}(\mu \rightarrow e \bar{\nu}_e \nu_\mu), & \text{BR}(\mu \rightarrow e \bar{\nu}_e \nu_e) &= 100\%, \\ \text{BR}(\tau \rightarrow e \gamma) &= \frac{\alpha_{em}}{192\pi} \frac{|(\mathcal{V}^\dagger \mathcal{V})_{e\tau}|^2}{G_F^2} \left(\frac{1}{M_{H^\pm}^2} + \frac{8}{M_{H^{\pm\pm}}^2} \right)^2 \text{BR}(\tau \rightarrow e \bar{\nu}_e \nu_\tau), & \text{BR}(\tau \rightarrow e \bar{\nu}_e \nu_\tau) &= 17.83\%, \\ \text{BR}(\tau \rightarrow \mu \gamma) &= \frac{\alpha_{em}}{192\pi} \frac{|(\mathcal{V}^\dagger \mathcal{V})_{\mu\tau}|^2}{G_F^2} \left(\frac{1}{M_{H^\pm}^2} + \frac{8}{M_{H^{\pm\pm}}^2} \right)^2 \text{BR}(\tau \rightarrow \mu \bar{\nu}_\mu \nu_\tau), & \text{BR}(\tau \rightarrow \mu \bar{\nu}_\mu \nu_\tau) &= 17.41\%. \end{aligned}$$

The contribution of $H^{\pm\pm}$ to the branching ratios is eight times larger than by H^\pm because of the difference in a magnitude of couplings between \mathcal{V}^\pm and $\mathcal{V}^{\pm\pm}$ in Eq. (7.46), in addition the amplitude is proportional to the particles charge (which gives an additional factor of 4).

Three body decays $l \rightarrow l_i l_j l_k$:

$$\begin{aligned} \text{BR}(\mu \rightarrow eee) &= \frac{1}{4G_F^2} \frac{|(\mathcal{V}^\dagger)_{ee}(\mathcal{V})_{\mu e}|^2}{M_{H^{\pm\pm}}^4} \text{BR}(\mu \rightarrow e \bar{\nu} \nu), \\ \text{BR}(\tau \rightarrow l_i l_j l_k) &= \frac{S}{4G_F^2} \frac{|(\mathcal{V}^\dagger)_{\tau i}(\mathcal{V})_{jk}|^2}{M_{H^{\pm\pm}}^4} \text{BR}(\tau \rightarrow \mu \bar{\nu} \nu), \quad S = \begin{cases} 1 & \text{if } j = k \\ 2 & \text{if } j \neq k \end{cases}. \end{aligned}$$

μ -to- e conversion

In the computation of conversion rate μ to e , both form factors contribute and the analytic form can be written as

$$\text{CR}(\mu \mathcal{N} \rightarrow e \mathcal{N}^*) = \frac{\Gamma_{conv}}{\Gamma_{capt}} \cong \frac{2\alpha_{em}^5 G_F^2 m_\mu^5 Z_{eff}^4 Z |F(q^2)|^2}{\Gamma_{capt}} \left| 8A_R + \frac{2}{3}A_L \right|^2. \quad (7.50)$$

Therefore, the μ -to- e conversion ratio in the nuclei field can be given as [93, 105]:

$$\begin{aligned} \text{CR}(\mu \mathcal{N} \rightarrow e \mathcal{N}^*) &= \frac{\Gamma_{conv}}{\Gamma_{capt}} \cong \frac{\alpha_{em}^5}{36\pi^4} \frac{m_\mu^5}{\Gamma_{capt}} Z_{eff}^4 Z |F(q^2 = -m_\mu^2)|^2 \times \\ &\quad \left| \frac{(M_\nu^\dagger M_\nu)_{e\mu}}{2v_\Delta^2} \left[\frac{5}{24m_{H^\pm}^2} + \frac{1}{m_{H^{\pm\pm}}^2} \right] + \frac{1}{2v_\Delta^2 m_{H^{\pm\pm}}^2} \sum_{l=e,\mu,\tau} (M_\nu)_{el}^\dagger f(r, s_i) (M_\nu)_{l\mu} \right|^2, \end{aligned} \quad (7.51)$$

where: Γ_{capt} – total muon capture rate (see Tab. 17),

Z_{eff} – effective charge for the muon in the 1s state,

	$\Gamma_{capt} [\text{s}^{-1}]$	$\Gamma_{capt} [\text{eV}]$	Z_{eff}
$^{197}_{79}\text{Au}$	13.07×10^6	8.60×10^{-9}	33.5
$^{48}_{22}\text{Ti}$	2.59×10^6	1.71×10^{-9}	17.5
$^{27}_{13}\text{Al}$	0.7054×10^6	0.4643×10^{-9}	11.5

Table 17: Total muon capture rate and effective charge for ^{197}Au , ^{48}Ti and ^{27}Al [204].

Muon $(g-2)_\mu$

In case of doubly charged scalars, cumulative effects of muon $(g-2)_\mu$ and lepton flavor violation have been discussed in details in [105, 205, 206] and for a triplet scalar it has been discussed in [91].

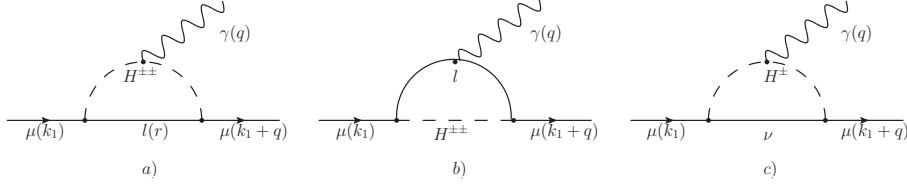


Figure 15: Feynman diagrams represent the contribution to $(g-2)_\mu$ within HTM

Contribution to muon $(g-2)$ from doubly and singly charged scalar are shown in Fig. 15. Final formulas for $H^{\pm\pm}$ and H^\pm reads

$$[\Delta a_\mu]_{H^{\pm\pm}} = -\sum_l f^l \times \left\{ \frac{2m_\mu^2 |\mathcal{V}_{\mu l}^{\pm\pm}|^2}{8\pi^2} \underbrace{\int_0^1 dx \left[\frac{\{x^3 - x^2 + \frac{m_l}{m_\mu}(x^2 - x)\}}{(m_\mu^2 x^2 + (M_{H^{\pm\pm}}^2 - m_\mu^2)x + (1-x)m_l^2)} \right]}_{C_1} \right\} \quad (7.52)$$

$$- \frac{m_\mu^2 |\mathcal{V}_{\mu l}^{\pm\pm}|^2}{8\pi^2} \underbrace{\int_0^1 dx \left[\frac{\{x^2 - x^3 + \frac{m_l}{m_\mu} x^2\}}{(m_\mu^2 x^2 + (m_l^2 - m_\mu^2)x + M_{H^{\pm\pm}}^2(1-x))} \right]}_{C_2} \right\}, \quad (7.53)$$

$$[\Delta a_\mu]_{H^\pm} = -\frac{1}{2} \sum_\nu \frac{m_\mu^2 |\mathcal{V}_{\mu\nu}^\pm|^2}{8\pi^2} \underbrace{\int_0^1 dx \left[\frac{(x^3 - x^2)}{(m_\mu^2 x^2 + (M_{H^\pm}^2 - m_\mu^2)x)} \right]}_{C_3}. \quad (7.54)$$

f^l is a symmetric factor equals to 4 for $l = \mu$ and 1 otherwise. The term proportional to the C_1 integral is connected with the diagram a) in Fig. 15, the term with the C_2 integral corresponds to Fig. 15 b). Equation (7.54) presents a contribution from a singly charged particle H^\pm (Fig. 15 c)) to $(g-2)_\mu$. Since both \mathcal{V}^\pm and $\mathcal{V}^{\pm\pm}$ vertices are comparable, see Eq. (7.46), the contributions from different diagrams depend mostly on C_1 , C_2 and C_3 integrals. Fig. 16 shows that the strongest contribution $(g-2)_\mu$ comes from the doubly charged scalar $H^{\pm\pm}$.

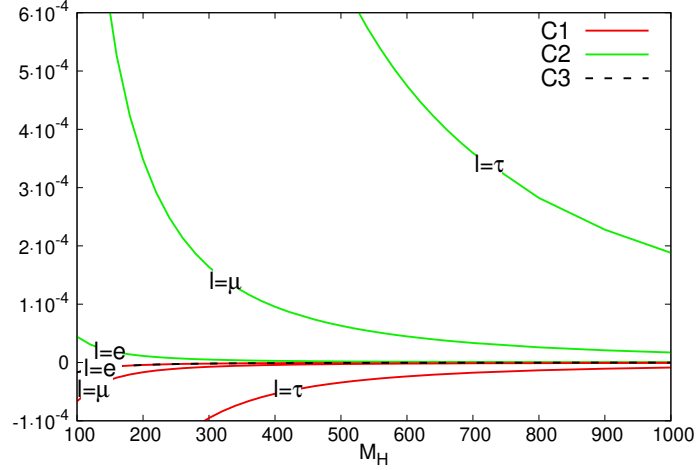


Figure 16: C_1 , C_2 and C_3 integrals Eqs. (7.52)-(7.54) as a function of charged scalars mass $M_{H^\pm} = M_{H^{\pm\pm}} \equiv M_H$.

References

- [1] **ATLAS** Collaboration, G. Aad et al., *Observation of a new particle in the search for the Standard Model Higgs boson with the ATLAS detector at the LHC*, *Phys. Lett.* **B716** (2012) 1–29, [[arXiv:1207.7214](#)].
- [2] **CMS** Collaboration, S. Chatrchyan et al., *Observation of a new boson at a mass of 125 GeV with the CMS experiment at the LHC*, *Phys. Lett.* **B716** (2012) 30–61, [[arXiv:1207.7235](#)].
- [3] G. Aad et al., *A Particle Consistent with the Higgs Boson Observed with the ATLAS Detector at the Large Hadron Collider*, *Science* **338** (2012), no. 6114 1576–1582.
- [4] **CMS** Collaboration, S. Chatrchyan et al., *Study of the Mass and Spin-Parity of the Higgs Boson Candidate Via Its Decays to Z Boson Pairs*, *Phys. Rev. Lett.* **110** (2013), no. 8 081803, [[arXiv:1212.6639](#)].
- [5] **ATLAS** Collaboration, G. Aad et al., *Evidence for the spin-0 nature of the Higgs boson using ATLAS data*, *Phys. Lett.* **B726** (2013) 120–144, [[arXiv:1307.1432](#)].
- [6] **CMS** Collaboration, S. Chatrchyan et al., *Measurement of W^+W^- production and search for the Higgs boson in pp collisions at $\sqrt{s} = 7$ TeV*, *Phys. Lett.* **B699** (2011) 25–47, [[arXiv:1102.5429](#)].
- [7] **CMS** Collaboration, V. Khachatryan et al., *Search for the associated production of the Higgs boson with a top-quark pair*, *JHEP* **09** (2014) 087, [[arXiv:1408.1682](#)]. [Erratum: *JHEP* 10, 106 (2014)].
- [8] **ATLAS** Collaboration, G. Aad et al., *Search for $H \rightarrow \gamma\gamma$ produced in association with top quarks and constraints on the Yukawa coupling between the top quark and the Higgs boson using data taken at 7 TeV and 8 TeV with the ATLAS detector*, *Phys. Lett.* **B740** (2015) 222–242, [[arXiv:1409.3122](#)].
- [9] **ATLAS, CMS** Collaboration, G. Aad et al., *Measurements of the Higgs boson production and decay rates and constraints on its couplings from a combined ATLAS and CMS analysis of the LHC pp collision data at $\sqrt{s} = 7$ and 8 TeV*, *JHEP* **08** (2016) 045, [[arXiv:1606.02266](#)].
- [10] **ATLAS** Collaboration, G. Aad et al., *Search for the associated production of the Higgs boson with a top quark pair in multilepton final states with the ATLAS detector*, *Phys. Lett.* **B749** (2015) 519–541, [[arXiv:1506.05988](#)].
- [11] A. Djouadi, M. Spira, and P. M. Zerwas, *Two photon decay widths of Higgs particles*, *Phys. Lett.* **B311** (1993) 255–260, [[hep-ph/9305335](#)].

- [12] **ATLAS** Collaboration, G. Aad et al., *Measurements of the Higgs boson production and decay rates and coupling strengths using pp collision data at $\sqrt{s} = 7$ and 8 TeV in the ATLAS experiment*, *Eur. Phys. J.* **C76** (2016), no. 1 6, [[arXiv:1507.04548](#)].
- [13] **ATLAS** Collaboration, G. Aad et al., *Study of the spin and parity of the Higgs boson in diboson decays with the ATLAS detector*, *Eur. Phys. J. C* **75** (2015), no. 10 476, [[arXiv:1506.05669](#)].
[Erratum: *Eur.Phys.J.C* 76, 152 (2016)].
- [14] **ATLAS** Collaboration, G. Aad et al., *Determination of spin and parity of the Higgs boson in the $WW^* \rightarrow e\nu\mu\nu$ decay channel with the ATLAS detector*, *Eur. Phys. J.* **C75** (2015), no. 5 231, [[arXiv:1503.03643](#)].
- [15] **CMS** Collaboration, E. Di Marco, *Studies of the Higgs boson spin and parity using the $\gamma\gamma$, ZZ, and WW decay channels with the CMS detector*, *Nucl. Part. Phys. Proc.* **273-275** (2016) 746–752.
- [16] **CMS** Collaboration, A. M. Sirunyan et al., *Observation of the Higgs boson decay to a pair of τ leptons with the CMS detector*, *Phys. Lett.* **B779** (2018) 283–316, [[arXiv:1708.00373](#)].
- [17] M. Aaboud et al., *Observation of $H \rightarrow b\bar{b}$ decays and VH production with the ATLAS detector*, *Physics Letters B* **786** (2018) 59 – 86.
- [18] **CMS Collaboration** Collaboration, *Measurement of Higgs boson decay to a pair of muons in proton-proton collisions at $\sqrt{s} = 13$ TeV*, Tech. Rep. CMS-PAS-HIG-19-006, CERN, Geneva, 2020.
- [19] **ATLAS** Collaboration, G. Aad et al., *A search for the dimuon decay of the Standard Model Higgs boson with the ATLAS detector*, , [[arXiv:2007.07830](#)].
- [20] A. Blondel and P. Janot, *Future strategies for the discovery and the precise measurement of the Higgs self coupling*, , [[arXiv:1809.10041](#)].
- [21] G. C. Branco, P. M. Ferreira, L. Lavoura, M. N. Rebelo, M. Sher, and J. P. Silva, *Theory and phenomenology of two-Higgs-doublet models*, *Phys. Rept.* **516** (2012) 1–102, [[arXiv:1106.0034](#)].
- [22] J. Gunion and H. E. Haber, *Higgs Bosons in Supersymmetric Models. 1.*, *Nucl. Phys. B* **272** (1986) 1. [Erratum: *Nucl.Phys.B* 402, 567–569 (1993)].
- [23] J. F. Gunion, H. E. Haber, G. L. Kane, and S. Dawson, *The Higgs Hunter’s Guide*, *Front. Phys.* **80** (2000) 1–404.
- [24] J. Espinosa and M. Quirós, *Higgs triplets in the supersymmetric standard model*, *Nuclear Physics B* **384** (1992), no. 1 113 – 146.
- [25] S. Di Chiara and K. Hsieh, *Triplet Extended Supersymmetric Standard Model*, *Phys. Rev.* **D78** (2008) 055016, [[arXiv:0805.2623](#)].
- [26] W. Konetschny and W. Kummer, *Nonconservation of total lepton number with scalar bosons*, *Physics Letters B* **70** (1977), no. 4 433 – 435.
- [27] G. Gelmini and M. Roncadelli, *Left-handed neutrino mass scale and spontaneously broken lepton number*, *Physics Letters B* **99** (1981), no. 5 411 – 415.
- [28] R. N. Mohapatra and G. Senjanović, *Neutrino mass and spontaneous parity nonconservation*, *Phys. Rev. Lett.* **44** (Apr, 1980) 912–915.
- [29] J. F. Gunion, J. Grifols, A. Mendez, B. Kayser, and F. Olness, *Higgs bosons in left-right-symmetric models*, *Phys. Rev. D* **40** (Sep, 1989) 1546–1561.
- [30] R. Vega and D. A. Dicus, *Doubly charged higgs and w^+w^+ production*, *Nuclear Physics B* **329** (1990), no. 3 533 – 546.
- [31] J. F. Gunion, R. Vega, and J. Wudka, *Higgs triplets in the standard model*, *Phys. Rev. D* **42** (Sep, 1990) 1673–1691.
- [32] K. Huitu, J. Maalampi, A. Pietila, and M. Raidal, *Doubly charged Higgs at LHC*, *Nucl. Phys.* **B487** (1997) 27–42, [[hep-ph/9606311](#)].

- [33] E. J. Chun, K. Y. Lee, and S. C. Park, *Testing Higgs triplet model and neutrino mass patterns*, *Phys. Lett.* **B566** (2003) 142–151, [[hep-ph/0304069](#)].
- [34] H. Georgi and M. Machacek, *Doubly charged Higgs bosons*, *Nucl. Phys.* **B262** (1985) 463–477.
- [35] C.-W. Chiang and K. Yagyu, *Testing the custodial symmetry in the Higgs sector of the Georgi-Machacek model*, *JHEP* **01** (2013) 026, [[arXiv:1211.2658](#)].
- [36] R. N. Mohapatra and J. C. Pati, *A Natural Left-Right Symmetry*, *Phys. Rev.* **D11** (1975) 2558.
- [37] G. Senjanovic and R. N. Mohapatra, *Exact Left-Right Symmetry and Spontaneous Violation of Parity*, *Phys. Rev.* **D12** (1975) 1502.
- [38] N. G. Deshpande, J. F. Gunion, B. Kayser, and F. Olness, *Left-right-symmetric electroweak models with triplet Higgs field*, *Phys. Rev. D* **44** (Aug, 1991) 837–858.
- [39] P. Duka, J. Gluza, and M. Zralek, *Quantization and renormalization of the manifest left-right symmetric model of electroweak interactions*, *Annals Phys.* **280** (2000) 336–408, [[hep-ph/9910279](#)].
- [40] G. Barenboim, M. Gorbahn, U. Nierste, and M. Raidal, *Higgs sector of the minimal left-right symmetric model*, *Phys. Rev.* **D65** (2002) 095003, [[hep-ph/0107121](#)].
- [41] A. Arhrib, R. Benbrik, M. Chabab, G. Moulhaka, M. C. Peyranère, L. Rahili, and J. Ramadan, *Higgs potential in the type II seesaw model*, *Phys. Rev. D* **84** (Nov, 2011) 095005.
- [42] A. Melfo, M. Nemevšek, F. Nesti, G. Senjanović, and Y. Zhang, *Type II neutrino seesaw mechanism at the LHC: The roadmap*, *Phys. Rev. D* **85** (Mar, 2012) 055018.
- [43] M. Aoki, S. Kanemura, and K. Yagyu, *Testing the Higgs triplet model with the mass difference at the LHC*, *Phys. Rev. D* **85** (Mar, 2012) 055007.
- [44] S. Kanemura and K. Yagyu, *Radiative corrections to electroweak parameters in the Higgs triplet model and implication with the recent Higgs boson searches*, *Phys. Rev. D* **85** (Jun, 2012) 115009.
- [45] A. G. Akeroyd and S. Moretti, *Enhancement of $H \rightarrow \gamma\gamma$ from doubly charged scalars in the Higgs triplet model*, *Phys. Rev. D* **86** (Aug, 2012) 035015.
- [46] K. Blum, R. T. D’Agnolo, and J. Fan, *Vacuum stability bounds on higgs coupling deviations in the absence of new bosons*, *Journal of High Energy Physics* **2015** (Mar, 2015) 166.
- [47] S. Blunier, G. Cottin, M. A. Díaz, and B. Koch, *Phenomenology of a Higgs triplet model at future e^+e^- colliders*, *Phys. Rev.* **D95** (2017), no. 7 075038, [[arXiv:1611.07896](#)].
- [48] P. S. B. Dev, C. M. Vila, and W. Rodejohann, *Naturalness in testable type II seesaw scenarios*, *Nucl. Phys.* **B921** (2017) 436–453, [[arXiv:1703.00828](#)].
- [49] A. Biswas, *All about $H^{\pm\pm}$ in Higgs Triplet Model.*, [[arXiv:1702.03847](#)].
- [50] Y. Du, A. Dunbrack, M. J. Ramsey-Musolf, and J.-H. Yu, *Type-II Seesaw Scalar Triplet Model at a 100 TeV pp Collider: Discovery and Higgs Portal Coupling Determination*, *JHEP* **01** (2019) 101, [[arXiv:1810.09450](#)].
- [51] T. B. de Melo, F. S. Queiroz, and Y. Villamizar, *Doubly Charged Scalar at the High-Luminosity and High-Energy LHC*, *Int. J. Mod. Phys. A* **34** (2019), no. 27 1950157, [[arXiv:1909.07429](#)].
- [52] R. Primulando, J. Julio, and P. Uttayarat, *Scalar phenomenology in type-II seesaw model*, *JHEP* **08** (2019) 024, [[arXiv:1903.02493](#)].
- [53] P. B. Dev, S. Khan, M. Mitra, and S. K. Rai, *Doubly-charged Higgs boson at a future electron-proton collider*, *Phys. Rev. D* **99** (2019), no. 11 115015, [[arXiv:1903.01431](#)].
- [54] B. Fuks, M. Nemevsek, and R. Ruiz, *Doubly Charged Higgs Boson Production at Hadron Colliders*, *Phys. Rev. D* **101** (2020), no. 7 075022, [[arXiv:1912.08975](#)].

- [55] **ATLAS** Collaboration, M. Aaboud et al., *Search for doubly charged Higgs boson production in multi-lepton final states with the ATLAS detector using proton–proton collisions at $\sqrt{s} = 13$ TeV*, *Eur. Phys. J. C* **78** (2018), no. 3 199, [[arXiv:1710.09748](#)].
- [56] J. Chakraborty, J. Gluza, T. Jelinski, and T. Srivastava, *Theoretical constraints on masses of heavy particles in Left-Right Symmetric Models*, *Phys. Lett.* **B759** (2016) 361–368, [[arXiv:1604.06987](#)].
- [57] M. Lindner, M. Platscher, and F. S. Queiroz, *A Call for New Physics : The Muon Anomalous Magnetic Moment and Lepton Flavor Violation*, *Phys. Rept.* **731** (2018) 1–82, [[arXiv:1610.06587](#)].
- [58] L. Calibbi and G. Signorelli, *Charged Lepton Flavour Violation: An Experimental and Theoretical Introduction*, *Riv. Nuovo Cim.* **41** (2018), no. 2 1, [[arXiv:1709.00294](#)].
- [59] **COMET** Collaboration, Y. Kuno, *A search for muon-to-electron conversion at J-PARC: The COMET experiment*, *PTEP* **2013** (2013) 022C01.
- [60] **Mu2e** Collaboration, D. Brown, *The Mu2e Experiment: Searching for Muon to Electron Conversion*, *Nucl. Part. Phys. Proc.* **260** (2015) 151–154.
- [61] **Majorana** Collaboration, N. Abgrall et al., *The Majorana Demonstrator Neutrinoless Double-Beta Decay Experiment*, *Adv. High Energy Phys.* **2014** (2014) 365432, [[arXiv:1308.1633](#)].
- [62] P. D. Bolton, F. F. Deppisch, and P. Bhupal Dev, *Neutrinoless double beta decay versus other probes of heavy sterile neutrinos*, *JHEP* **03** (2020) 170, [[arXiv:1912.03058](#)].
- [63] R. K. Ellis et al., *Physics Briefing Book: Input for the European Strategy for Particle Physics Update 2020.*, [[arXiv:1910.11775](#)].
- [64] **FCC** Collaboration, A. Abada et al., *FCC-ee: The Lepton Collider: Future Circular Collider Conceptual Design Report Volume 2*, *Eur. Phys. J. ST* **228** (2019), no. 2 261–623.
- [65] FCC – Future Circular Collider, Conceptual Design Report <https://fcc-cdr.web.cern.ch/>.
- [66] L. Linssen, A. Miyamoto, M. Stanitzki, and H. Weerts, *Physics and Detectors at CLIC: CLIC Conceptual Design Report*, [[arXiv:1202.5940](#)].
- [67] CLIC – Compact Linear International Collider Project, CERN, <http://clicdp.web.cern.ch/>.
- [68] The Linear Collider Collaboration, <http://www.linearcollider.org/>.
- [69] G. Aarons et al., *International Linear Collider Reference Design Report Volume 2: Physics at the ILC*, [[arXiv:0709.1893](#)].
- [70] A. Arbey et al., *Physics at the e^+e^- Linear Collider*, *Eur. Phys. J.* **C75** (2015), no. 8 371, [[arXiv:1504.01726](#)].
- [71] *CEPC Conceptual Design Report: Volume 1 - Accelerator.*, [[arXiv:1809.00285](#)].
- [72] CEPC – Circular Electron Positron Collider Project, China, <http://cepc.ihep.ac.cn/>.
- [73] E. Adli, *Plasma Wakefield Linear Colliders - Opportunities and Challenges.*, [[arXiv:1905.01879](#)].
- [74] A. Blondel et al., *Standard model theory for the FCC-ee Tera-Z stage*, *CERN Yellow Rep. Monogr.* **3** (2019) [[arXiv:1809.01830](#)].
- [75] A. Blondel, A. Freitas, J. Gluza, and T. e. a. Riemann, *Theory Requirements and Possibilities for the FCC-ee and other Future High Energy and Precision Frontier Lepton Colliders.*, [[arXiv:1901.02648](#)].
- [76] High-Luminosity LHC, CERN, <https://home.cern/science/accelerators/high-luminosity-lhc>.
- [77] R. Contino et al., *Physics at a 100 TeV pp collider: Higgs and EW symmetry breaking studies*, *CERN Yellow Report* (2017), no. 3 255–440, [[arXiv:1606.09408](#)].
- [78] T. Golling et al., *Physics at a 100 TeV pp collider: beyond the Standard Model phenomena*, *CERN Yellow Report* (2017), no. 3 441–634, [[arXiv:1606.00947](#)].

- [79] Alwall, J., Frederix, R., Frixione, S. et al., *The automated computation of tree-level and next-to-leading order differential cross section, and their matching to parton shower simulations*, *JHEP* **07** (2014) 079, [[arXiv:1405.0301](#)].
- [80] T. Sjostrand, S. Mrenna, and P. Z. Skands, *A Brief Introduction to PYTHIA 8.1*, *Comput. Phys. Commun.* **178** (2008) 852–867, [[arXiv:0710.3820](#)].
- [81] T. Sjostrand, S. Mrenna, and P. Z. Skands, *PYTHIA 6.4 Physics and Manual*, *JHEP* **05** (2006) 026, [[hep-ph/0603175](#)].
- [82] A. Alloul, N. D. Christensen, C. Degrange, C. Duhr, and B. Fuks, *Feynrules 2.0 - a complete toolbox for tree-level phenomenology*, *Comput. Phys. Commun.* **185** (2014) 2250–2300, [[arXiv:1310.1921](#)].
- [83] E. J. Chun, H. M. Lee, and P. Sharma, *Vacuum Stability, Perturbativity, EWPD and Higgs-to-diphoton rate in Type II Seesaw Models*, *JHEP* **11** (2012) 106, [[arXiv:1209.1303](#)].
- [84] A. G. Akeroyd and S. Moretti, *Enhancement of H to $\gamma\gamma$ from doubly charged scalars in the Higgs Triplet Model*, *Phys. Rev.* **D86** (2012) 035015, [[arXiv:1206.0535](#)].
- [85] J.-F. Shen, Y.-P. Bi, and Z.-X. Li, *Pair production of scalars at the ILC in the Higgs triplet model under the non-degenerate case*, *EPL* **112** (2015), no. 3 31002.
- [86] D. Das and A. Santamaria, *Updated scalar sector constraints in higgs triplet model*, *Phys. Rev.* **D94** (2016) 015015, [[arXiv:1604.08099](#)].
- [87] J. Gluza, M. Kordiaczyńska, and T. Srivastava, *Doubly Charged Higgs Bosons and Spontaneous Symmetry Breaking at eV and TeV Scales*, *Symmetry* **12** (2020), no. 1 153.
- [88] G. Bambhaniya, J. Chakraborty, J. Gluza, M. Kordiaczyńska, and R. Szafron, *Left-Right Symmetry and the Charged Higgs Bosons at the LHC*, *JHEP* **05** (2014) 033, [[arXiv:1311.4144](#)].
- [89] Z.-z. Xing and Y.-L. Zhou, *A Generic Diagonalization of the 3×3 Neutrino Mass Matrix and Its Implications on the μ - τ Flavor Symmetry and Maximal CP Violation*, *Phys. Lett.* **B696** (2010) 584–590, [[arXiv:1008.4906](#)].
- [90] E. Ma, M. Raidal, and U. Sarkar, *Phenomenology of the neutrino mass giving Higgs triplet and the low-energy seesaw violation of lepton number*, *Nucl. Phys.* **B615** (2001) 313–330, [[hep-ph/0012101](#)].
- [91] T. Fukuyama, H. Sugiyama, and K. Tsumura, *Constraints from LFV processes in the Higgs triplet model*, *JHEP* **03** (2010) 044, [[arXiv:0909.4943](#)].
- [92] A. G. Akeroyd, M. Aoki, and H. Sugiyama, *Lepton Flavour Violating Decays $\tau \rightarrow \bar{l}ll$ and $\mu \rightarrow e\gamma$ in the Higgs Triplet Model*, *Phys. Rev.* **D79** (2009) 113010, [[arXiv:0904.3640](#)].
- [93] D. Dinh, A. Ibarra, E. Molinaro, and S. Petcov, *The $\mu - e$ Conversion in Nuclei, $\mu \rightarrow e\gamma$, $\mu \rightarrow 3e$ Decays and TeV Scale See-Saw Scenarios of Neutrino Mass Generation*, *JHEP* **08** (2012) 125, [[arXiv:1205.4671](#)]. [Erratum: *JHEP* 09, 023 (2013)].
- [94] J. Chakraborty, P. Ghosh, and W. Rodejohann, *Lower Limits on $\mu \rightarrow e\gamma$ from New Measurements on U_{e3}* , *Phys. Rev.* **D86** (2012) 075020, [[arXiv:1204.1000](#)].
- [95] A. Crivellin, M. Ghezzi, L. Panizzi, G. M. Pruna, and A. Signer, *Low- and high-energy phenomenology of a doubly charged scalar*, *Phys. Rev. D* **99** (2019), no. 3 035004, [[arXiv:1807.10224](#)].
- [96] N. Chakrabarty, C.-W. Chiang, T. Ohata, and K. Tsumura, *Charged scalars confronting neutrino mass and muon $g - 2$ anomaly*, *JHEP* **12** (2018) 104, [[arXiv:1807.08167](#)].
- [97] N. D. Dinh, *Probing the Possible TeV Scale See-saw Origin of Neutrino Masses with Charged Lepton Flavour Violation Processes and Neutrino Mass Spectroscopy Using Atoms*. PhD thesis, SISSA, Trieste (2013).
<https://s3.cern.ch/inspire-prod-files-3/33d85e96ff45ced9c9fcc19bd8195233>.

- [98] J. Schechter and J. Valle, *Neutrinoless Double beta Decay in $SU(2) \times U(1)$ Theories*, *Phys. Rev. D* **25** (1982) 2951.
- [99] L. Wolfenstein, *Triplet Scalar Bosons and Double Beta Decay*, *Phys. Rev.* **D26** (1982) 2507.
- [100] S. T. Petcov, H. Sugiyama, and Y. Takanishi, *Neutrinoless Double Beta Decay and $H^{\pm\pm} \rightarrow l'^{\pm}l^{\pm}$ Decays in the Higgs Triplet Model*, *Phys. Rev.* **D80** (2009) 015005, [[arXiv:0904.0759](#)].
- [101] S. Actis, M. Czakon, J. Gluza, and T. Riemann, *Virtual hadronic and heavy-fermion $\mathcal{O}(\alpha^2)$ corrections to Bhabha scattering*, *Phys. Rev.* **D78** (2008) 085019, [[arXiv:0807.4691](#)].
- [102] **L3** Collaboration, P. Achard et al., *Search for doubly charged Higgs bosons at LEP*, *Phys. Lett.* **B576** (2003) 18–28, [[hep-ex/0309076](#)].
- [103] F. Campanario, H. Czyż, J. Gluza, T. Jeliński, G. Rodrigo, S. Tracz, and D. Zhuridov, *Standard model radiative corrections in the pion form factor measurements do not explain the a_{μ} anomaly*, *Phys. Rev. D* **100** (2019), no. 7 076004, [[arXiv:1903.10197](#)].
- [104] **Particle Data Group** Collaboration, M. Tanabashi et al., *Review of particle physics*, *Phys. Rev. D* **98** (Aug, 2018) 030001.
- [105] J. Chakraborty, P. Ghosh, S. Mondal, and T. Srivastava, *Reconciling $(g-2)_{\mu}$ and charged lepton flavor violating processes through a doubly charged scalar*, *Phys. Rev.* **D93** (2016), no. 11 115004, [[arXiv:1512.03581](#)].
- [106] **MEG** Collaboration, A. M. Baldini et al., *Search for the lepton flavour violating decay $\mu^+ \rightarrow e^+ \gamma$ with the full dataset of the MEG experiment*, *Eur. Phys. J.* **C76** (2016), no. 8 434, [[arXiv:1605.05081](#)].
- [107] A. M. Baldini et al., *MEG Upgrade Proposal*, , [[arXiv:1301.7225](#)].
- [108] **BaBar** Collaboration, B. Aubert et al., *Searches for Lepton Flavor Violation in the Decays $\tau^{\pm} \rightarrow e^{\pm} \gamma$ and $\tau^{\pm} \rightarrow \mu^{\pm} \gamma$* , *Phys. Rev. Lett.* **104** (2010) 021802, [[arXiv:0908.2381](#)].
- [109] B. Wang, *Searches for New Physics at the Belle II Experiment*, in *Meeting of the APS Division of Particles and Fields*, 11, 2015. [[arXiv:1511.00373](#)].
- [110] T. Aushev et al., *Physics at Super B Factory*, , [[arXiv:1002.5012](#)].
- [111] **SINDRUM** Collaboration, U. Bellgardt et al., *Search for the Decay $\mu^+ \rightarrow e^+ e^+ e^-$* , *Nucl. Phys.* **B299** (1988) 1–6.
- [112] A. Blondel et al., *Research Proposal for an Experiment to Search for the Decay $\mu \rightarrow eee$* , , [[arXiv:1301.6113](#)].
- [113] K. Hayasaka et al., *Search for Lepton Flavor Violating Tau Decays into Three Leptons with 719 Million Produced Tau+Tau- Pairs*, *Phys. Lett.* **B687** (2010) 139–143, [[arXiv:1001.3221](#)].
- [114] W. H. Bertl et al., *A Search for muon to electron conversion in muonic gold*, *Eur.Phys.J.* **C47** (2006) 337–346.
- [115] **Mu2e** Collaboration, L. Bartoszek et al., *Mu2e Technical Design Report*, , [[arXiv:1501.05241](#)].
- [116] J. Maalampi and N. Romanenko, *Single production of doubly charged Higgs bosons at hadron colliders*, *Phys. Lett.* **B532** (2002) 202–208, [[hep-ph/0201196](#)].
- [117] T. Nomura, H. Okada, and H. Yokoya, *Discriminating leptonic Yukawa interactions with doubly charged scalar at the ILC*, *Nucl. Phys. B* **929** (2018) 193–206, [[arXiv:1702.03396](#)].
- [118] P. B. Dev, M. J. Ramsey-Musolf, and Y. Zhang, *Doubly-Charged Scalars in the Type-II Seesaw Mechanism: Fundamental Symmetry Tests and High-Energy Searches*, *Phys. Rev. D* **98** (2018), no. 5 055013, [[arXiv:1806.08499](#)].
- [119] A. Nyffeler, *Status of hadronic light-by-light scattering in the muon $g-2$* , *Nuovo Cim.* **C037** (2014), no. 02 173–178, [[arXiv:1312.4804](#)]. [*Int. J. Mod. Phys. Conf. Ser.*35,1460456(2014)].

- [120] Y. Cai, T. Han, T. Li, and R. Ruiz, *Lepton Number Violation: Seesaw Models and Their Collider Tests*, *Front. in Phys.* **6** (2018) 40, [[arXiv:1711.02180](#)].
- [121] “NuFit 4.1.” <http://www.nu-fit.org/>, 2019.
- [122] **T2K** Collaboration, K. Abe et al., *Constraint on the matter–antimatter symmetry-violating phase in neutrino oscillations*, *Nature* **580** (2020), no. 7803 339–344, [[arXiv:1910.03887](#)].
- [123] I. Girardi, S. T. Petcov, and A. V. Titov, *Predictions for the Majorana CP Violation Phases in the Neutrino Mixing Matrix and Neutrinoless Double Beta Decay*, *Nucl. Phys.* **B911** (2016) 754–804, [[arXiv:1605.04172](#)].
- [124] **Particle Data Group** Collaboration, C. Patrignani et al., *Review of Particle Physics*, *Chin. Phys.* **C40** (2016), no. 10 100001.
- [125] W. Rodejohann, *Neutrino-less Double Beta Decay and Particle Physics*, *Int. J. Mod. Phys.* **E20** (2011) 1833–1930, [[arXiv:1106.1334](#)].
- [126] **Planck** Collaboration, P. A. R. Ade et al., *Planck 2013 results. XVI. Cosmological parameters*, *Astron. Astrophys.* **571** (2014) A16, [[arXiv:1303.5076](#)].
- [127] V. D. Barger and K. Whisnant, *Majorana neutrino masses from neutrinoless double beta decay and cosmology*, *Phys. Lett. B* **456** (1999) 194–200, [[hep-ph/9904281](#)].
- [128] M. Czakon, J. Gluza, J. Studnik, and M. Zralek, *In quest of neutrino masses at $O(eV)$ scale*, *Phys. Rev. D* **65** (2002) 053008, [[hep-ph/0110166](#)].
- [129] M. Czakon, J. Gluza, F. Jegerlehner, and M. Zralek, *Confronting electroweak precision measurements with new physics models*, *Eur. Phys. J.* **C13** (2000) 275–281, [[hep-ph/9909242](#)].
- [130] T. G. Rizzo, *Tests of the fermion and higgs multiplet structure of the $su(2) \times u(1)$ model*, *Phys. Rev. D* **21** (Mar, 1980) 1404–1409.
- [131] M. Aoki and S. Kanemura, *Unitarity bounds in the Higgs model including triplet fields with custodial symmetry*, *Phys. Rev. D* **77** (May, 2008) 095009.
- [132] V. Barger, T. Han, P. Langacker, B. McElrath, and P. Zerwas, *Effects of genuine dimension-six Higgs operators*, *Phys. Rev.* **D67** (2003) 115001, [[hep-ph/0301097](#)].
- [133] S. Kanemura, Y. Okada, E. Senaha, and C. P. Yuan, *Higgs coupling constants as a probe of new physics*, *Phys. Rev.* **D70** (2004) 115002, [[hep-ph/0408364](#)].
- [134] **Particle Data Group** Collaboration, M. Tanabashi et al., *Review of Particle Physics*, *Phys. Rev.* **D98** (2018), no. 3 030001.
- [135] **ATLAS** Collaboration, M. Aaboud et al., *Search for new phenomena in dijet events using 37 fb^{-1} of pp collision data collected at $\sqrt{s} = 13 \text{ TeV}$ with the ATLAS detector*, *Phys. Rev.* **D96** (2017), no. 5 052004, [[arXiv:1703.09127](#)].
- [136] **CMS** Collaboration, A. M. Sirunyan et al., *Search for a heavy right-handed W boson and a heavy neutrino in events with two same-flavor leptons and two jets at $\sqrt{s} = 13 \text{ TeV}$* , *JHEP* **05** (2018), no. 05 148, [[arXiv:1803.11116](#)].
- [137] **CMS** Collaboration, A. M. Sirunyan et al., *Searches for W' bosons decaying to a top quark and a bottom quark in proton-proton collisions at 13 TeV* , *JHEP* **08** (2017) 029, [[arXiv:1706.04260](#)].
- [138] **ATLAS** Collaboration, M. Aaboud et al., *Search for a right-handed gauge boson decaying into a high-momentum heavy neutrino and a charged lepton in pp collisions with the ATLAS detector at $\sqrt{s} = 13 \text{ TeV}$* , *Phys. Lett. B* **798** (2019) 134942, [[arXiv:1904.12679](#)].
- [139] J. Gluza and T. Jeliński, *Heavy neutrinos and the $pp \rightarrow lljj$ CMS data*, *Phys. Lett. B* **748** (2015) 125–131, [[arXiv:1504.05568](#)].
- [140] P. Bhupal Dev and R. Mohapatra, *Unified explanation of the $eejj$, diboson and dijet resonances at the LHC*, *Phys. Rev. Lett.* **115** (2015), no. 18 181803, [[arXiv:1508.02277](#)].

- [141] A. Das, P. S. B. Dev, and R. N. Mohapatra, *Same Sign versus Opposite Sign Dileptons as a Probe of Low Scale Seesaw Mechanisms*, *Phys. Rev. D* **97** (2018), no. 1 015018, [[arXiv:1709.06553](#)].
- [142] Frank, Mariana and Özdal, Özer and Poulou, Poulou, *Relaxing LHC constraints on the W_R mass*, *Phys. Rev.* **D99** (2019), no. 3 035001, [[arXiv:1812.05681](#)].
- [143] CMS Collaboration, A. M. Sirunyan et al., *Search for heavy neutrinos and third-generation leptoquarks in hadronic states of two τ leptons and two jets in proton-proton collisions at $\sqrt{s} = 13$ TeV*, *JHEP* **03** (2019) 170, [[arXiv:1811.00806](#)].
- [144] ATLAS Collaboration, M. Aaboud et al., *Search for heavy Majorana or Dirac neutrinos and right-handed W gauge bosons in final states with two charged leptons and two jets at $\sqrt{s} = 13$ TeV with the ATLAS detector*, *JHEP* **01** (2019) 016, [[arXiv:1809.11105](#)].
- [145] J. Gluza and M. Zralek, *Neutrino production in $e^+ e^-$ collisions in a left-right symmetric model*, *Phys. Rev.* **D48** (1993) 5093–5105.
- [146] M. Czakon, J. Gluza, and M. Zralek, *Low-energy physics and left-right symmetry: Bounds on the model parameters*, *Phys. Lett.* **B458** (1999) 355–360, [[hep-ph/9904216](#)].
- [147] J. Gluza, T. Jelinski, and R. Szafron, *Lepton number violation and ‘Diracness’ of massive neutrinos composed of Majorana states*, *Phys. Rev.* **D93** (2016), no. 11 113017, [[arXiv:1604.01388](#)].
- [148] P. Bhupal Dev, R. N. Mohapatra, and Y. Zhang, *CP Violating Effects in Heavy Neutrino Oscillations: Implications for Colliders and Leptogenesis*, *JHEP* **11** (2019) 137, [[arXiv:1904.04787](#)].
- [149] M. Czakon, J. Gluza, and J. Hejczyk, *Muon decay to one loop order in the left-right symmetric model*, *Nucl. Phys. B* **642** (2002) 157–172, [[hep-ph/0205303](#)].
- [150] G. Beall, M. Bander, and A. Soni, *Constraint on the Mass Scale of a Left-Right Symmetric Electroweak Theory from the $K(L) K(S)$ Mass Difference*, *Phys. Rev. Lett.* **48** (1982) 848.
- [151] Z. Gagyi-Palfy, A. Pilaftsis, and K. Schilcher, *Gauge independent analysis of $K_L \rightarrow e\mu$ in left-right models*, *Nucl. Phys.* **B513** (1998) 517–554, [[hep-ph/9707517](#)].
- [152] A. Pilaftsis, *Confronting left-right symmetric models with electroweak precision data at the Z peak*, *Phys. Rev.* **D52** (1995) 459–471, [[hep-ph/9502330](#)].
- [153] P. Ball, J. M. Frere, and J. Matias, *Anatomy of mixing induced CP asymmetries in left-right symmetric models with spontaneous CP violation*, *Nucl. Phys.* **B572** (2000) 3–35, [[hep-ph/9910211](#)].
- [154] M. E. Pospelov, *FCNC in left-right symmetric theories and constraints on the right-handed scale*, *Phys. Rev.* **D56** (1997) 259–264, [[hep-ph/9611422](#)].
- [155] K. Kiers, J. Kolb, J. Lee, A. Soni, and G.-H. Wu, *Ubiquitous CP violation in a top inspired left-right model*, *Phys. Rev.* **D66** (2002) 095002, [[hep-ph/0205082](#)].
- [156] T. G. Rizzo, *Constraints from $b \rightarrow s\gamma$ on the left-right symmetric model*, *Phys. Rev.* **D50** (1994) 3303–3309, [[hep-ph/9401319](#)].
- [157] P. L. Cho and M. Misiak, *$b \rightarrow s\gamma$ decay in $SU(2)_L \times SU(2)_R \times U(1)$ extensions of the standard model*, *Phys. Rev.* **D49** (1994) 5894–5903, [[hep-ph/9310332](#)].
- [158] G. Senjanovic and A. Sokorac, *Left-right Symmetric Gauge Theory and Its Prediction for Parity Violation in Atoms*, *Phys. Lett.* **76B** (1978) 610–614.
- [159] G. Senjanovic and A. Sokorac, *Effects of Heavy Higgs Scalars at Low-energies*, *Phys. Rev.* **D18** (1978) 2708.
- [160] J. Chakraborty, J. Gluza, R. Sevillano, and R. Szafron, *Left-Right Symmetry at LHC and Precise 1-Loop Low Energy Data*, *JHEP* **07** (2012) 038, [[arXiv:1204.0736](#)].
- [161] F. F. Deppisch, T. E. Gonzalo, S. Patra, N. Sahu, and U. Sarkar, *Double beta decay, lepton flavor violation, and collider signatures of left-right symmetric models with spontaneous D -parity breaking*, *Phys. Rev.* **D91** (2015), no. 1 015018, [[arXiv:1410.6427](#)].

- [162] D. Borah, A. Dasgupta, and S. Patra, *Neutrinoless double beta decay in minimal left–right symmetric model with universal seesaw*, *Int. J. Mod. Phys. A* **33** (2018), no. 35 1850198, [[arXiv:1706.02456](#)].
- [163] P. Fileviez Perez and C. Murgui, *Lepton Flavour Violation in Left-Right Theory*, *Phys. Rev.* **D95** (2017), no. 7 075010, [[arXiv:1701.06801](#)].
- [164] D. Borah and A. Dasgupta, *Charged lepton flavour violation and neutrinoless double beta decay in left-right symmetric models with type I+II seesaw*, *JHEP* **07** (2016) 022, [[arXiv:1606.00378](#)].
- [165] D. Guadagnoli and R. N. Mohapatra, *TeV Scale Left Right Symmetry and Flavor Changing Neutral Higgs Effects*, *Phys. Lett.* **B694** (2011) 386–392, [[arXiv:1008.1074](#)].
- [166] N. T. Shaban and W. J. Stirling, *Minimal left-right symmetry and $SO(10)$ grand unification using LEP coupling constant measurements*, *Phys. Lett.* **B291** (1992) 281–287.
- [167] M. Lindner and M. Weiser, *Gauge coupling unification in left-right symmetric models*, *Phys. Lett.* **B383** (1996) 405–414, [[hep-ph/9605353](#)].
- [168] D. Das and A. Santamaria, *Updated scalar sector constraints in the Higgs triplet model*, *Phys. Rev.* **D94** (2016), no. 1 015015, [[arXiv:1604.08099](#)].
- [169] G. Bambhaniya, J. Chakraborty, J. Gluza, T. Jeliński, and M. Kordiaczynska, *Lowest limits on the doubly charged Higgs boson masses in the minimal left-right symmetric model*, *Phys. Rev.* **D90** (2014), no. 9 095003, [[arXiv:1408.0774](#)].
- [170] M. Mitra, R. Ruiz, D. J. Scott, and M. Spannowsky, *Neutrino Jets from High-Mass W_R Gauge Bosons in TeV-Scale Left-Right Symmetric Models*, *Phys. Rev. D* **94** (2016), no. 9 095016, [[arXiv:1607.03504](#)].
- [171] R. Ruiz, *Lepton Number Violation at Colliders from Kinematically Inaccessible Gauge Bosons*, *Eur. Phys. J. C* **77** (2017), no. 6 375, [[arXiv:1703.04669](#)].
- [172] M. Nemešek, F. Nesti, and G. Popara, *Keung-Senjanović process at the LHC: From lepton number violation to displaced vertices to invisible decays*, *Phys. Rev. D* **97** (2018), no. 11 115018, [[arXiv:1801.05813](#)].
- [173] A. Das, *Pair production of heavy neutrinos in next-to-leading order QCD at the hadron colliders in the inverse seesaw framework*, , [[arXiv:1701.04946](#)].
- [174] R. Ruiz, *QCD Corrections to Pair Production of Type III Seesaw Leptons at Hadron Colliders*, *JHEP* **12** (2015) 165, [[arXiv:1509.05416](#)].
- [175] R. Padhan, D. Das, M. Mitra, and A. Kumar Nayak, *Probing doubly and singly charged Higgs bosons at the pp collider HE-LHC*, *Phys. Rev. D* **101** (2020), no. 7 075050, [[arXiv:1909.10495](#)].
- [176] M. Gallinaro et al., *Beyond the Standard Model in Vector Boson Scattering Signatures*, 5, 2020. [[arXiv:2005.09889](#)].
- [177] P. Agrawal, M. Mitra, S. Niyogi, S. Shil, and M. Spannowsky, *Probing the Type-II Seesaw Mechanism through the Production of Higgs Bosons at a Lepton Collider*, *Phys. Rev. D* **98** (2018), no. 1 015024, [[arXiv:1803.00677](#)].
- [178] P. Fileviez Perez, T. Han, G.-y. Huang, T. Li, and K. Wang, *Neutrino Masses and the CERN LHC: Testing Type II Seesaw*, *Phys. Rev.* **D78** (2008) 015018, [[arXiv:0805.3536](#)].
- [179] G. Moulhaka and M. C. Peyranère, *Vacuum Stability Conditions for Higgs Potentials with $SU(2)_L$ Triplets*, , [[arXiv:2012.13947](#)].
- [180] J. Garayoa and T. Schwetz, *Neutrino mass hierarchy and Majorana CP phases within the Higgs triplet model at the LHC*, *JHEP* **03** (2008) 009, [[arXiv:0712.1453](#)].
- [181] W. Dekens and D. Boer, *Viability of minimal left–right models with discrete symmetries*, *Nucl. Phys. B* **889** (2014) 727–756, [[arXiv:1409.4052](#)].

- [182] G. Bambhaniya, J. Chakraborty, J. Gluza, T. Jelinski, and R. Szafron, *Search for doubly charged Higgs bosons through vector boson fusion at the LHC and beyond*, *Phys. Rev. D* **92** (2015), no. 1 015016, [[arXiv:1504.03999](#)].
- [183] G. Bambhaniya, J. Chakraborty, S. Goswami, and P. Konar, *Generation of neutrino mass from new physics at TeV scale and multilepton signatures at the LHC*, *Phys. Rev.* **D88** (2013), no. 7 075006, [[arXiv:1305.2795](#)].
- [184] J. Pumplin, D. Stump, J. Huston, H. Lai, P. M. Nadolsky, and W. Tung, *New generation of parton distributions with uncertainties from global QCD analysis*, *JHEP* **07** (2002) 012, [[hep-ph/0201195](#)].
- [185] T.-J. Hou et al., *New CTEQ global analysis of quantum chromodynamics with high-precision data from the LHC*, , [[arXiv:1912.10053](#)].
- [186] M. Cacciari, S. Frixione, M. L. Mangano, P. Nason, and G. Ridolfi, *Updated predictions for the total production cross sections of top and of heavier quark pairs at the Tevatron and at the LHC*, *JHEP* **09** (2008) 127, [[arXiv:0804.2800](#)].
- [187] J. Alwall, R. Frederix, S. Frixione, V. Hirschi, F. Maltoni, O. Mattelaer, H. S. Shao, T. Stelzer, P. Torrielli, and M. Zaro, *The automated computation of tree-level and next-to-leading order differential cross sections, and their matching to parton shower simulations*, *JHEP* **07** (2014) 079, [[arXiv:1405.0301](#)].
- [188] M. Chiesa, C. Oleari, and E. Re, *NLO QCD+NLO EW corrections to diboson production matched to parton shower*, *Eur. Phys. J. C* **80** (2020), no. 9 849, [[arXiv:2005.12146](#)].
- [189] FCC Collaboration, A. Abada et al., *FCC-hh: The Hadron Collider: Future Circular Collider Conceptual Design Report Volume 3*, *Eur. Phys. J. ST* **228** (2019), no. 4 755–1107.
- [190] A. Arhrib, R. Benbrik, M. Chabab, G. Moulhaka, M. C. Peyranere, L. Rahili, and J. Ramadan, *The Higgs Potential in the Type II Seesaw Model*, *Phys. Rev.* **D84** (2011) 095005, [[arXiv:1105.1925](#)].
- [191] J. F. Gunion, R. Vega, and J. Wudka, *Higgs triplets in the standard model*, *Phys. Rev.* **D42** (1990) 1673–1691.
- [192] P. Dey, A. Kundu, and B. Mukhopadhyaya, *Some consequences of a Higgs triplet*, *J. Phys.* **G36** (2009) 025002, [[arXiv:0802.2510](#)].
- [193] H. M. Georgi, S. L. Glashow, and S. Nussinov, *Unconventional Model of Neutrino Masses*, *Nucl. Phys.* **B193** (1981) 297–316.
- [194] A. Melfo, M. Nemevsek, F. Nesti, G. Senjanovic, and Y. Zhang, *Type II Seesaw at LHC: The Roadmap*, *Phys. Rev.* **D85** (2012) 055018, [[arXiv:1108.4416](#)].
- [195] S. Kanemura and K. Yagyu, *Radiative corrections to electroweak parameters in the Higgs triplet model and implication with the recent Higgs boson searches*, *Phys. Rev.* **D85** (2012) 115009, [[arXiv:1201.6287](#)].
- [196] K. S. Babu and S. Jana, *Probing Doubly Charged Higgs Bosons at the LHC through Photon Initiated Processes*, *Phys. Rev.* **D95** (2017), no. 5 055020, [[arXiv:1612.09224](#)].
- [197] R. N. Mohapatra and G. Senjanovic, *Neutrino Masses and Mixings in Gauge Models with Spontaneous Parity Violation*, *Phys. Rev. D* **23** (1981) 165.
- [198] J. Gunion, J. Grifols, A. Mendez, B. Kayser, and F. I. Olness, *Higgs Bosons in Left-Right Symmetric Models*, *Phys. Rev. D* **40** (1989) 1546.
- [199] N. Deshpande, J. Gunion, B. Kayser, and F. I. Olness, *Left-right symmetric electroweak models with triplet Higgs*, *Phys. Rev. D* **44** (1991) 837–858.
- [200] J. Gluza and M. Zralek, *Feynman rules for Majorana neutrino interactions*, *Phys. Rev. D* **45** (1992) 1693–1700.

- [201] J. Gluza and M. Zralek, *Inverse neutrinoless double beta decay in gauge theories with CP violation*, *Phys. Rev.* **D52** (1995) 6238–6248, [[hep-ph/9502284](#)].
- [202] J. Gluza, *On teraelectronvolt Majorana neutrinos*, *Acta Phys. Polon.* **B33** (2002) 1735–1746, [[hep-ph/0201002](#)].
- [203] M. Kakizaki, Y. Ogura, and F. Shima, *Lepton flavor violation in the triplet Higgs model*, *Phys. Lett.* **B566** (2003) 210–216, [[hep-ph/0304254](#)].
- [204] R. Kitano, M. Koike, and Y. Okada, *Detailed calculation of lepton flavor violating muon electron conversion rate for various nuclei*, *Phys. Rev. D* **66** (2002) 096002, [[hep-ph/0203110](#)]. [Erratum: *Phys.Rev.D* 76, 059902 (2007)].
- [205] J. P. Leveille, *The Second Order Weak Correction to $(g - 2)$ of the Muon in Arbitrary Gauge Models*, *Nucl. Phys.* **B137** (1978) 63–76.
- [206] S. R. Moore, K. Whisnant, and B.-L. Young, *Second Order Corrections to the Muon Anomalous Magnetic Moment in Alternative Electroweak Models*, *Phys. Rev.* **D31** (1985) 105.